Functional characterisation of SLy2 as a novel regulator of the actin cytoskeleton

Inaugural Dissertation

zur

Erlangung des Doktorgrades der

Mathematisch-Naturwissenschaftlichen Fakultät

der Albertus-Magnus Universität zu Köln

vorgelegt von

Max v. Holleben

geboren in München

November 2008

aus dem Institut für Genetik
der Albertus-Magnus Universität zu Köln

Gedruckt mit Genehmigung der
mathematisch-naturwissenschaftlichen Fakultät
der Albertus-Magnus Universität zu Köln

Berichterstatter: Prof. Dr. Jens Brüning
Prof. Dr. Klaus Pfeffer

Tag der mündlichen Prüfung: 03.02.2009

Index

Figure index

Table index

Abbreviation index

°C	Degree centigrade
Aa	Amino acid
APC	Antigen presenting cell
ATP	Adenosine tri-phosphat
BAC	Bacterial artificial chromosome
BCR	B cell receptor
Bp	Base pair
BrdU	Bromo-desoxy-uridine
BSA	Bovine serum albumine
CA	Central acidic domain (of WASP proteins)
cDNA	DNA copy of an mRNA
cSMAC	Central supramolecular activation cluster
Δ	Deletion mutant
DEPC	Diethylpyrocarbonate
DMSO	Dimethylsulfoxide
DNA	Desoxyribonucleic acid
dNTP	Desoxyribonucleids (dATP, dCTP, dGTP, dTTP)
E(x)	Day (x) of embryonic development (mice)
EDTA	Ethylendiaminetetraacetic acid
FA	Focal adhesion
FACS	Fluorescence activated cell sorting
F-actin	Filamentous actin
FH1	Formin homology domain 1
FH2	Formin homology domain 2
G-actin	Globular actin
GBD	GTPase binding domain
GFP	Green fluorescent protein
H	Hour(s)
HACS1	Hematopoietic adapter containing SH3 and SAM domains 1
HS1	Hematopoietic cell specific protein 1
HSV-tk	Herpes simplex virus thymidine kinase
IP	Immunoprecipitation
IS	Immunological synapse
ITAM	Immunoreceptor based activation motif
kb	Kilo basepairs
kDa	Kilo dalton
ko	Knock out
M	Molar
MACS	Magnetic cell sorting
min	Minutes
ml	Milliliter

MTOC	Microtubule organising center
µl	Microliter
µm	Micromolar
NASH	NLS, SAM, SH3 domain containing protein
neoR	Neomycine phosphotransferase gene
NLS	Nuclear localisation sequence
nm	Nano molar
NPF	Nucleation promoting factor
NTA	N-terminal acidic domain
ORF	Open reading frame
PCR	Polymerase chain reaction
PDBU	Phorbol 12,13 dibutyrate
PFA	Paraformaldehyde
pSMAC	Peripheral supramolecular activation cluster
RACE	Rapid amplification of cDNA ends
RNA	Ribonucleic acid
Rpm	Rounds per minute
RT	Room temperature
(non-) RTK	(non-) Receptor tyrosine kinase
SASH1	SAM domain SH3 domain containing 1
SAM	Sterile α-motif
SH2	Src homology 2
SH3	Src homology 3
SLy	SH3 protein expressed in lymphocytes
SLy2	SH3 protein expressed in lymphocytes 2
TCR	T cell receptor
Tg	Transgenic
V domain	Verprolin homology domain
WAS	Wiskott Aldrich Syndrome
WASP	Wiskott Aldrich Syndrome protein
WAVE	WASP family, Verproline Homologue
WH1	WASP homology domain 1
WH2	WASP homology domain 2
WIP	WASP interacting protein
Wt	Wildtype

Abstract

This thesis encompasses the first molecular characterisation of *SH3 protein expressed in lymphocytes 2* (SLy2), a novel member of the recently described SLy family of adapter proteins. SLy2 was previously identified as *hematopoietic adapter containing SH3 and SAM domains 1* (HACS1) on the basis of its deregulated expression in different hematopoietic cancer cell lines (Claudio et al., 2001). Database analysis defined an identical modular organisation of SLy and SLy2, with an N-terminal NLS-, a central SH3- and a C-terminal SAM domain.

SLy2 is expressed throughout the hematopoietic tissues, but also in muscle, heart, brain and colon. *In vivo* overexpression in B cells of a transgenic mouse line established a role for SLy2 in the initial spreading and contraction of B cells in response to contact with antigen containing surfaces. *In vitro* overexpression of wildtype SLy2 protein in HeLa cells resulted in the prominent and robust induction of branched F-actin structures like lamellipodia and peripheral ruffles, to which SLy2 also specifically localised. This primary effect was accompanied by markedly enhanced spreading and correlated with diminished proliferation, most probably due to defective cytokinesis in SLy2 overexpressing cells. A detailed analysis of HeLa cells overexpressing different SLy2 deletion mutants could define the impact of the various domains on the function of SLy2 and especially demonstrated the importance of the SH3 domain. Furthermore, the conserved serine residue 23 could be identified as a potential switch for regulating SLy2 activity.

Overexpression studies with different point mutants of Rac1 suggested a direct role for this small GTPase in the SLy2 induced F-actin structures, as dominant negative Rac1N17 abrogated the F-actin inducing effects of SLy2, whereas constitutively active Rac1V12 even enhanced this phenotype.

Ultimately, the members of the cortactin family of nucleation promoting factors (NPFs), cortactin and its lymphocyte homologue HS1 could be identified as interaction partners of SLy2. As their role in the induction of lamellipodia and immunological synapses (IS) has been clearly established before, they are highly likely to represent the downstream effectors of SLy2 activity.

With the generation of gene targeted SLy2 deficient mice, an in-depth analysis of this novel regulator of branched F-actin structures *in vivo* is now possible.

1. Introduction

1.1. Adapter proteins in cell signalling

Signal transduction is enabled by the concerted actions of modifying enzymes, such as kinases, phosphatases, proteases, ubiquitinases etc., their target proteins and a distinctive set of adapter proteins that serve as molecular scaffolds for the former to assemble and interact. Given the abundance of many signalling proteins and the high degree of redundancy between different signalling pathways, the spatial organisation of interactions is of pivotal importance to ensure the specificity of the transduced signal. This specificity is frequently brought up by the action of adapter proteins that consist of multiple protein-protein interaction domains, bringing the target proteins into close vicinity. In addition, many adapter proteins contain domains that mediate binding to lipid motifs, thereby locating the signalling complexes to the plasma membrane.

Src homology 2 (SH2) and Src homology 3 (SH3) domains belong to the most highly abundant and best known protein-protein interaction domains. Both were first described in the non receptor tyrosine kinase (non-RTK) Src (Hidaka et al., 1991; Koch et al., 1991). SH2 domains bind highly specific to phosphorylated tyrosine residues and thus imply the capacity to integrate the activational status into a binding decision. Well established is the binding of two SH2 domains to the two phosphorylated tyrosine residues in immunoreceptor tyrosine based activation motifs (ITAM), that are present in many intracellular domains of different immune receptors, such as Igα and Igβ (Underhill and Goodridge, 2007). Also SH3 domains are widely distributed across the proteom and mediate binding to evolutionary conserved proline rich sequences that display the consensus sequence *pxxp*, where p stands for proline and x for any amino acid (Feng et al., 1994). Worth mentioning, also an interaction with ubiquitin-containing structures has been reported recently (He et al., 2007). In contrast to the phospho-tyrosine binding SH2 domains, the binding of SH3 domains to their target sequences is not intrinsically regulated but rather controlled by the accessibility of the binding regions. The issue of specificity is obvious in adapter protein – target protein binding and indeed, SH3 domains show a high degree of promiscuity when analysed in *in vitro* binding assays. Apparently, the amino acid composition of the close vicinity of the proline rich sequence or the SH3 domain is of major importance here.

Sterile-alpha-motif (SAM) domains were first described in the yeast *Saccharomyces cerevesiae* and the fruit fly *Drosophila melanogaster* and named according to their

abundance in sex determining proteins and high content of α-helices. They are abundant throughout the whole mammalian genome, yet their function is still not completely elucidated, and even high sequence identity between two SAM domains can not necessarily predict similar functions. SAM domains are involved in protein-protein interactions through their ability to homodimerise. However, also differing protein domains can be bound in a heterologous fashion. Additionally, they have been described to bind RNA molecules, e.g. in the case of the protein Smaug from *D. melanogaster* (Qiao and Bowie, 2005).

1.1.1. The SLy protein family

In 2001, two reports described the identification of novel and homologous proteins, characterised by the presence of two protein-protein binding domains (an SH3 and a SAM domain) and a nuclear localisation signal (NLS) (Claudio et al., 2001; Beer et al., 2001). Beer and coworkers termed the protein *SH3 protein expressed in lymphocytes* (SLy), whereas Claudio *et al.* emphasized the less restricted expression pattern of a homologous protein with the name *hematopoietic adapter containing SH3 and SAM domains* (HACS1). As HACS1 is also called SLy2, the identification of these proteins marked the discovery of an as yet unknown protein family of putative adapter proteins. A third report, published later that same year, described the (re-)identification of SLy2 as a nuclear protein, containing a SH3 and a SAM domain, being preferentially expressed in mast cells and thus termed *Nuclear protein containing SAM and SH3 domains* (NASH) (Uchida et al., 2001).

Both SLy-proteins show a strikingly similar molecular organisation. Aligning the amino acid sequences of both proteins reveals a sequence identity of close to 43% (Figure 1). Yet, the identical regions are not evenly distributed across the proteins, but seem to cluster. The two sections with the highest degree of sequence identity comprise the amino acids 170-231 (72%) and 251-315 (63%). An additional region of high identity is located at the N-terminus from amino acid 1-28 (62%).

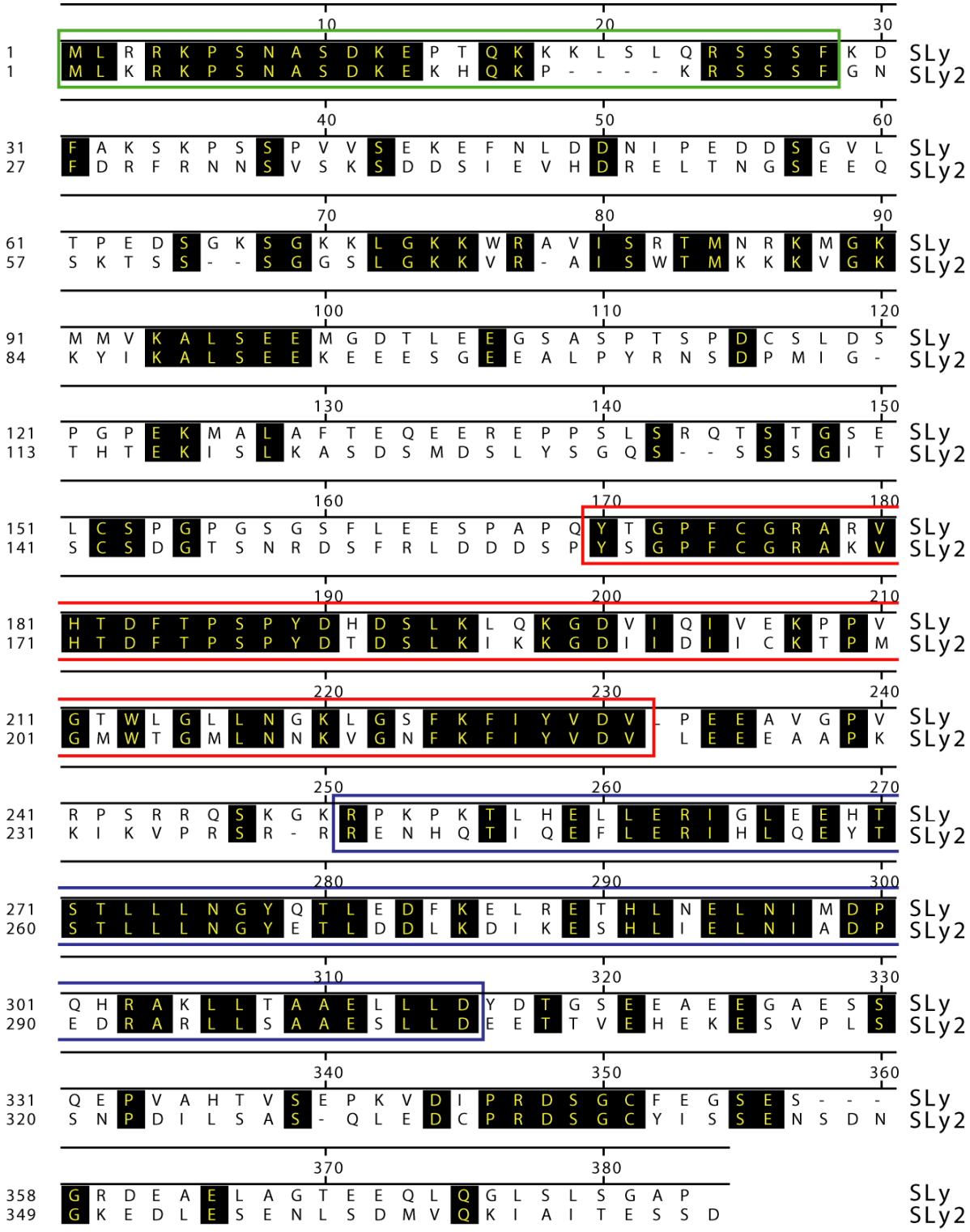

Figure 1: Amino acid sequence alignment of murine SLy and SLy2. Identical amino acids in both sequences are indicated in black. The N-terminus, the SH3 and the SAM domains are indicated with a green, red and blue frame, respectively. The sequences were aligned with Clustal W, using DNASTAR_MegAlign.

Astoul *et al*. demonstrated that SLy is phosphorylated on the serine residue 27 upon T cell receptor (TCR) signalling (Astoul et al., 2003). In agreement with this and the exclusively lymphoid occurrence of SLy, gene-targeted mice expressing only a truncated protein lacking the NLS and Ser27 ($SLy^{\Delta/\Delta}$), display defects in various lymphocyte functions. The proliferative responses of $SLy^{\Delta/\Delta}$ T and B cells upon activation are diminished and the marked reduction in the marginal zone B cell compartment is in agreement with lowered Ig serum levels (Beer et al., 2005; Scheikl et al., 2008). Interestingly, the phenotype of mice with a complete deletion of SLy ($SLy^{-/-}$) shows no difference to those expressing the truncated form. In addition to the defects in peripheral lymphocyte function, also the thymic development of $SLy^{\Delta/\Delta}$ and $SLy^{-/-}$ cells is defective (Reis *et al.*, submitted). All mentioned defects accumulate in the finding of impaired rejection of semi-allograft transplants in $SLy^{\Delta/\Delta}$ mice (Beer et al., 2005). Although there is evidence for elevated apoptosis induction in SLy deficient thymocytes, until now, the molecular mechanism of the effects of the SLy truncation remains ill-explained, which is partially due to the still unresolved issue of interaction partners of this adapter protein. With respect to a molecular mechanism it is of high interest, that one apparent defect of the truncated SLy protein from the $SLy^{\Delta/\Delta}$ mice is the inability to translocate to the nucleus what the wildtype protein readily does (Beer et al., 2005).

The genomic region around the *sly2*-locus (21q11.2) is frequently targeted by translocation events in hematopoietic malignancies (Mitelman et al., 1997). This is interesting since SLy2/HACS1 was initially discovered in a transcriptional study on multiple myelomas, in which this novel protein was shown to be overexpressed (Claudio et al., 2001). Both findings led to a first hypothesis of SLy2 being a novel signalling component in potentially cancer related pathways. Some time later, intriguing evidence on the role of SLy2 in B lymphocyte differentiation was reported (Zhu et al., 2004). As also shown in this report, Zhu *et al.* found that the expression of SLy2 in B cells is elevated upon activation of the cells by differentiation inducing stimuli. Consistently, they could show that the overexpression of SLy2 in splenic B cells leads to the differentiation towards a plasma cell fate. Despite these interesting data it has to be noted that until now, the experimental evidence explaining SLy2 function from a mechanistical point of view remains fragmentary.

The third member of the SLy family, *SAM and SH3 domain containing 1* (SASH1) shares the high structural similarity of the other SLy proteins. SASH1 was first described by Zeller *et al*., who identified it in a comparative screen for genes downregulated in breast cancer cells,

which stands in marked contrast to the above mentioned SLy2 overexpression. This led to the classification of SASH1 as a potential tumour suppressor (Zeller et al., 2003). Klaus-Peter Janssen and his group could demonstrate that SASH1 is also significantly downregulated in other malignant tissues, such as liver and colon. Decreased SASH1 expression levels correlated with the formation of metastases and statistical analyses have established the lowered protein levels as an independent negative prognostic parameter for patient survival (Rimkus et al., 2006). The pronounced discrepancies to the potentially oncogenic role of SLy2 clearly await further analysis.

SASH1 has twice the size of SLy or SLy2 and thus contains additional domains. A coiled-coil domain is located in the N-terminus, whereas a second SAM domain resides within the C-terminus of the protein. The middle part of the protein shows the highest sequence identity with SLy and SLy2. Deduced from its occurrence in arthropods, SASH1 probably represents the founding member of the family, as the other ones are only found in the vertebrate phylum. Accordingly, the additional domains in the N- and the C-terminus must have been deleted during the gene duplications that led to the generation of SLy and SLy2.

1.2. Cytoskeletal structures in eukaryotic cells

Three pillars make up for the cellular skeleton, intermediate filaments, microtubule and actin filaments. Their combined activity provides the essential forces to regulate cell shape, adhesion and migration, vesicle transport, secretion, phagocytosis and mitosis to name but a few functions. Its important role in cell function is impressively illustrated by the fact that proteins involved in assembly and regulation of the cytoskeleton represent almost 3% of all human genes (Venter et al., 2001).

The least is known about the intermediate filaments that are assembled from different families of proteins depending on the cell type. Among the many participating families are various keratins, vimentins, nexins and also the lamins of the nuclear envelope. Their name is based on the finding that their diameter (10-12 nm) is located between that of microtubules (25 nm) and actin-filaments (5-8 nm). They form a dense network crossing the cell and thus serve different functions, from offering a signalling scaffold to the mechanical transduction of forces generated by movements at the cell membrane. Also, they have been implicated in the maintenance of cellular integrity, for example during the extravasation of lymphocytes, as they are endowed with a surprising flexibility towards externally applied forces. It has been shown that they assemble from monomeric subunits into the extended filaments crossing the cytosol; however, the molecular mechanisms

remain elusive. In contrast to microtubules and actin filaments, intermediate filaments do not elongate by treadmilling, which is the hallmark of the former two (reviewed in (Helfand et al., 2004; Goldman et al., 2008)).

Microtubules represent the largest cytoskeletal compound and are assembled from heterodimers of α and β tubulin. Their formation is controlled by the activity of the microtubule organising centre (MTOC) and other accessory proteins (Luders and Stearns, 2007). They elongate by addition of new monomers to the ends of existing filaments, whereas new tubulin monomers are provided by depolymerisation from the other end of the filament, a process known as treadmilling. Motorproteins such as kinesins associate with the microtubular network and mediate transport of e.g. vesicles along these filaments (Lakamper and Meyhofer, 2006). Geiger and coworkers already established more than 20 years ago that the MTOC of cytotoxic T cells reorients towards the contact site of T cell and target cell (Geiger et al., 1982). Accordingly, they carry out a crucial role in secretion and thus lymphocyte effector functions (reviewed in (Huse et al., 2008)). In addition, microtubules have been described to support actin cytoskeletal structures, e.g. in the maintenance of an immunological synapse (IS) (Bunnell et al., 2001). Of note, small GTPases from the Rho family are involved in the regulation of the microtubular network. Thus, there is intensive cross talk between the actin and the tubulin cytoskeleton, which is essential e.g. in cell migration (Watanabe et al., 2005). Yet, the most prominent function of the microtubular network is clearly its role in cell division, where the MTOC turns into the spindle body, which organises the retraction of the chromosome connected microtubules and thus mediates the distribution of the sister chromatids to the newly forming daughter cells (reviewed in (Cuschieri et al., 2007)).

The third, and best described, component of the cytoskeletal structures is the actin filament network. It is assembled from monomeric β-actin molecules, each with a molecular weight of 42kDa. Polymerisation of these monomers into the filamentous polymers is mediated by a plethora of different nucleation and elongation factors, which are assisted by capping proteins whose activity restricts filament growth. Depolymerising factors such as cofilin mediate the degradation of filaments and thus replenish the pool of monomeric actin (Ono, 2007). Actin filaments are not symmetrical but display two diverse ends, a slow growing so called pointed end and a fast growing barbed end. Like microtubules, also actin filaments grow by treadmilling. Compared with the other two cytoskeletal systems, the actin network shows the highest degree of complexity, due to its ability to form linear as well as branched filaments, depending on the accessory factors. Given its inherent flexibility and evolutionary conservation it is not surprising that the actin

network is involved in almost all aspects of cellular life (for review see (Welch and Mullins, 2002).

1.2.1. From G- to F-actin

The formation of mulitmeric actin filaments from monomeric subunits has been a matter of intensive research for decades (reviewed in (Pollard et al., 2000). The molecular concentration of globular (G-) actin inside a cell is approximately 100 µM and most molecules of this pool are present in an ATP bound form. This is remarkable, as the critical concentration needed for filamentous (F-) actin polymerisation in *in vitro* systems represents approximately 0.1 µM and a 100 µM pool of ATP bound actin polymerises to F-actin in a matter of seconds, leaving only 0.1 µM G-actin behind (Pollard, 1983; Pollard, 1986). Thus, the question is apparent how the cell maintains such a high concentration of monomeric actin avoiding immediate and constant polymerisation. This issue is tackled from two sides: First, G-actin is constantly bound by either one of two small proteins, thymosin-β4 (43 amino acids) or profilin (125-139 amino acids) and binding of the former to ATP bound G-actin completely inhibits polymerisation (Pantaloni and Carlier, 1993; Perelroizen et al., 1994). Given the finding that the cellular concentration of thymosin-β4 is even higher than that of G-actin, it accounts for the bulk amount of unpolymerised actin (Cassimeris et al., 1992). Profilin competes with thymosin-β4 for actin binding and the exchange of actin between these two proteins is rapid. Profilin binding interferes with actin filament nucleation but allows the elongation of existing filaments (Goldschmidt-Clermont et al., 1992). However, its affinity for F-actin is low, as the profilin target binding motif in actin is masked in assembled filaments. Profilin adds a further level of regulation to actin polymerisation, as it binds to nucleation factors, such as Arp2/3 complex, WASP and formins and thus leads to the controlled delivery of new monomers to the growing barbed end of the filament. Furthermore, it mediates the exchange of ADP to ATP on the actin monomer, which leads to the re-activation of the previously disassembled monomers (Perelroizen et al., 1996). The second mechanism employed to prevent uncontrolled actin polymerisation is the blocking of barbed ends by accessory proteins, such as gelsolin or capping protein. These molecules display a nanomolar affinity for barbed ends. Given their micromolar concentration in the cytoplasm, most barbed ends will be present in a capped conformation and are thus not prone to further elongation. Capping proteins bind polyphosphoinositides, which reduces their affinity to barbed ends, thus connecting an enhanced activational status of the cell with F-actin elongation (Schafer et al., 1996).

1.2.2. Assembly factors promote *de novo* actin polymerisation

The de-novo nucleation of G-actin monomers into oligomeric complexes is an energetically unfavorable process (Chhabra and Higgs, 2007). Thus, to facilitate efficient and regulated polymerisation, different assembly factors are employed.

1.2.2.1. The Arp2/3 complex

The Arp2/3 complex represents a seven subunit multimeric assembly of ARPC1-5, Arp2 and Arp3. Both latter proteins resemble actin (*actin related proteins*) and cooperatively mimic the barbed end of a preformed actin dimer (Pollard, 2007). Due to the strong elongatory capacity of the barbed end (10-fold stronger than that of the pointed end) this structure favours the attachment of further G-actin molecules, and thus nucleates new filaments. Since the Arp2/3 complex shows a high affinity for the pointed end of actin filaments it remains bound to this end of the filament, serving as capping protein at the same time. Most importantly, the Arp2/3 complex contains the ability to bind to the sides of existing filaments, where it nucleates polymerisation of new filaments with the exact angle of 70° and thus induces the generation of the branched actin networks (Figure 2). Being the only assembly factor with the ability to induce branching of actin filaments, Arp2/3 was shown to be essential for the formation of lamellipodia and other broad F-actin structures and is thus indispensable for the generation of a leading edge in moving cells (Mullins et al., 1998; Bailly et al., 2001). As the intrinsic nucleation activity of the Arp2/3 complex is relatively low, this complex needs to be activated and assisted by nucleation promoting factors (NPFs) to exert its full nucleation capacity (see below).

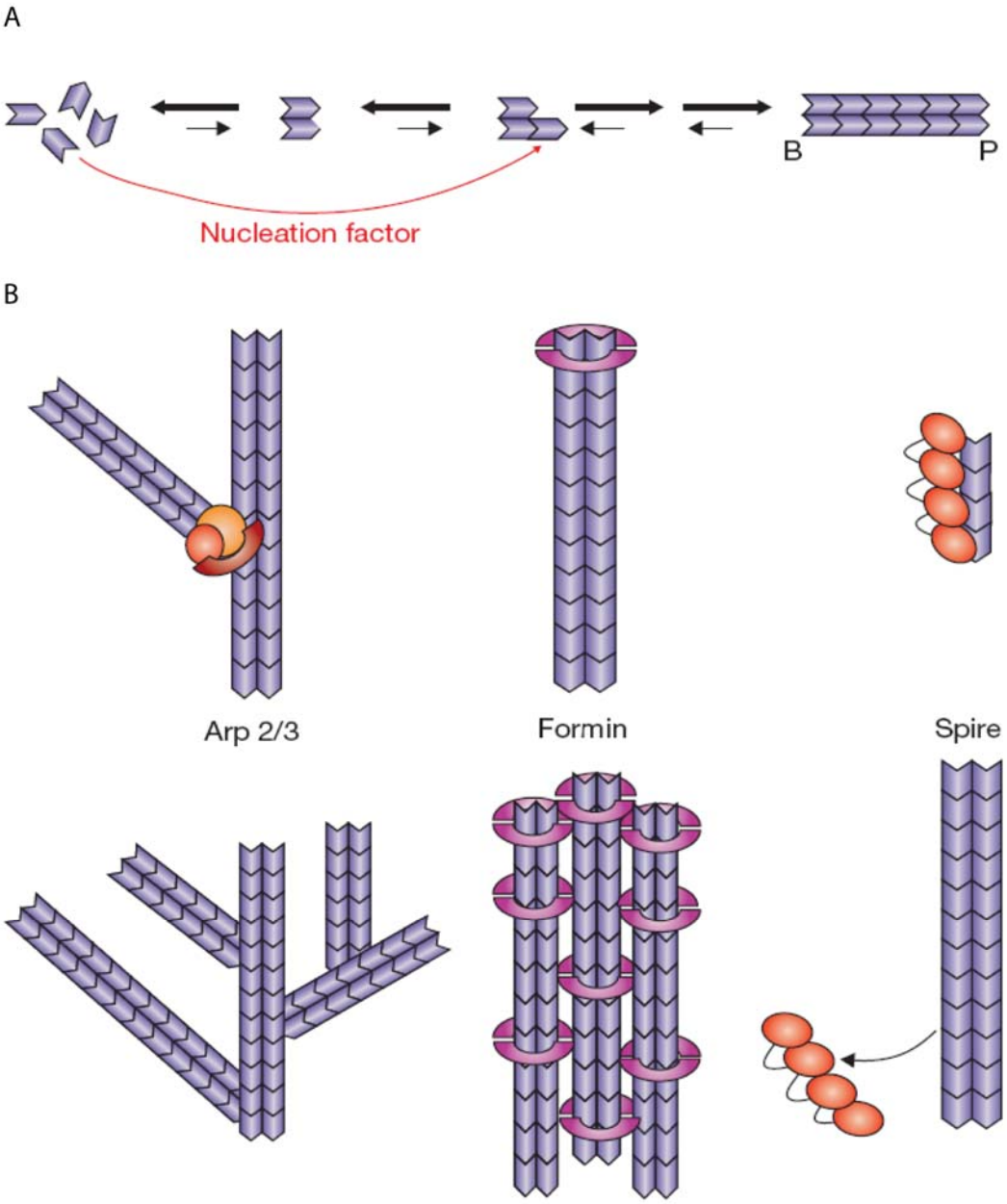

Figure 2: The first steps of actin nucleation are mediated by assembly factors. (A) The first oligomerisation steps from actin monomers to trimers are energetically unfavored, and are therefore unlikely to occur without external assistance (B=barbed end; P=pointed end). (B) Different assembly factors provide a molecular scaffold, which facilitates the nucleation of oligomeric actin complexes. Arp2/3 binds to existing filaments and therefore induces the generation of branched, dendritic F-actin networks. Assembly factors from the formin family and the spire proteins both mediate the formation of linear F-actin filaments, which can be further bundled into higher order complexes (picture taken from (Chhabra and Higgs, 2007)).

1.2.2.2. Formin proteins

As opposed to the already mentioned Arp2/3 complex, formins occur and function as homodimeric protein complexes that are bound to the barbed end of actin filaments (reviewed in (Goode and Eck, 2007)). They mediate elongation by preventing the binding of capping proteins to the barbed end and move together with the growing filament, a process called "processive capping". As a second mechanism of action, they recruit profilin (bound to actin-ATP) to the barbed end of the filament. As deduced from this mode of action it is obvious, that formins only mediate the formation of linear actin filaments. But at least some of the 15 members of the mammalian formin family mediate the bundling of parallel actin polymers, thus facilitating the formation of higher ordered F-actin complexes (Figure 2). Their function is facilitated by two essential domains, the formin homology 1 (FH1) and the formin homology 2 (FH2) domain (Pruyne et al., 2002). While the FH2 domain mediates the homodimerisation of the protein and the binding to F-actin, the FH1 domain is responsible for the recruitment of the profilin-actin dimers (Watanabe et al., 1997; Higgs, 2005). Being activated by small GTPases from the Rho family, the formins reside rather upstream in the signalling cascades leading to F-actin assembly. The importance of the formin mDIA1 in T cell function was recently shown in *mdia1* deficient mice, whose thymocytes and T cells displayed severe problems in egression from the thymus and trafficking to secondary lymphoid organs, respectively (Sakata et al., 2007).

1.2.2.3. Spire

A third and completely different mechanism of nucleation is employed by the protein spire as initially discovered in *D. melanogaster* (Quinlan et al., 2005). This protein is highly conserved up to the vertrebrate phylum and contains an array of four consecutive Wasp homology 2 (WH2) domains (Figure 2). As these domains mediate binding of monomeric actin this molecular structure results in the formation of an actin tetramer, which serves as nucleation platform for further assembly, whereas the first WH2 domain at the same time carries out capping functions to prevent disassembly of the newly forming actin filament (Baum and Kunda, 2005).

1.2.3.Two classes of NPFs facilitate network formation

In order for a cell to reorganise its actin cytoskeleton in response to external stimuli or changed environmental conditions, these diverse signals have to be integrated and transmitted towards the assembly factors, to promote their activation and subsequent F-actin formation. This function is carried out by different NPFs, which roughly cluster into two different groups. The first group comprises the well described *Wiskott-Aldrich-*

Syndrome proteins (WASP and neural-(N-)WASP) and the related *WASP family-verprolin homologous proteins* (WAVE 1-3). The second group represents the novel, non-canonical factors cortactin and its homologous protein HS1, which is restricted to lymphocytes (for reviews, see (Weed and Parsons, 2001; Takenawa and Miki, 2001)).

1.2.3.1. NPF I: WASP, N-WASP and WAVE proteins

WASP is the founding member of this family of proteins (Derry et al., 1994). Its mutated form is responsible for the human immune disorder it is named after (see 1.2.3.), which is marked by defective actin cytoskeletal organisation in leukocytes and platelets. The proteins from the WASP and WAVE families are large multidomain scaffold proteins that integrate various signals towards F-actin formation at the membrane. WASP and N-WASP show a very similar structure, but display different expression patterns. While WASP is expressed only in the hematopoietic system (thus explaining the syndrome it was named after), N-WASP was identified initially in neural tissues, but is expressed also in a wide variety of other organs. Of the WAVE family, WAVE2 is expressed ubiquitously whereas WAVE 1 and 3 are enriched in the brain, but are also found in other tissues. All proteins in these two families share common domains. As they mediate their effects on F-actin formation by activation of the Arp2/3 complex, all WASP and WAVE proteins contain an Arp2/3 interaction motif, the CA (central acidic) domain in the C-terminus, which is essential for their function. The other indispensable motif is the V domain (verprolin homology), which lies N-terminally adjacent and is responsible for the binding of G-actin (Takenawa and Miki, 2001). The N-terminus of the WASP proteins is formed by the WASP-homology 1 domain (WH1), which does not occur in WAVE proteins. It mediates the constitutive binding to the adapter protein WASP-interacting protein (WIP), which has been, amongst other functions, implicated in maintaining the stability of WASP to such an extent, that WIP deficient cells show also severely diminished WASP levels (de la Fuente et al., 2007). Indeed, the WH1 domain is a hot-spot, which is targeted by approximately 50% of WASP mutations found in WAS patients (Rong and Vihinen, 2000).

To conclude, this suggests a mechanism of F-actin nucleation through the WASP mediated recruitment of G-actin monomers to the Arp2/3 complex. This leads to the complex formation between one G-actin molecule and the two structurally related Arp domains, which mimics the trimeric actin complex needed to nucleate polymerisation (Blanchoin et al., 2000), and thus increases the nucleation capacity of Arp2/3.

WASP family proteins are activated by different means and therefore facilitate the integration of multiple signalling pathways to F-actin formation (Takenawa and Suetsugu,

2007). As the proteins are present in an auto-inhibited state in unstimulated cells, the main mechanism of activation is the release of the intramolecular binding of the VCA domain to the central region. Phosphorylation of a central tyrosine residue by Src family kinases inhibits this intramolecular complex, assisted by the binding of phosphatidyl-inositol (4,5) biphosphate (PIP_2) (Rohatgi et al., 1999; Cory et al., 2002). Accordingly, this leads to the activation of WASP downstream of antigen and growth factor receptors. The third mechanism mediating activation of WASP proteins is the binding of active (=GTP bound) Cdc42 to the central GTPase binding domain (GBD) (Rohatgi et al., 1999). The sequential action of Cdc42 and WASP mediated Arp2/3 activation finally leads to the generation of filopodia and the induction of cell movement.

Also the WAVE proteins 1-3 are activated through Rho family GTPases, namely Rac1. Yet, WAVE proteins do not contain a GBD and consistently no direct binding of Rac1 to WAVE could be shown. Instead, proteins of the WAVE family employ adapter proteins that mediate an indirect interaction with Rac1. The protein IRSp53, initially identified as an insulin receptor substrate, was shown to bind to the proline rich stretch in WAVE2 by virtue of its C-terminal SH3 domain, and proved to be essential for Rac induced membrane ruffling. As IRSp53 binds active Rac1 with its N-terminus this leads to the formation of a trimeric complex that finally yields the activation of WAVE2 (Miki et al., 2000). In addition to IRSp53 a cluster of proteins assembled around WAVE is essential for its function. This tetrameric complex comprises the proteins Sra-1, Abi1, Nap and HSPC300 and is constitutively bound to WAVE, which essentially mediates binding to activated Rac (Steffen et al., 2004; Innocenti et al., 2004). WAVE is responsible for the bulk of branched actin formation in lamellipodial structures and accordingly it has also been shown to be of pivotal importance in the formation of an IS and the subsequent activation of the T cell (Suetsugu et al., 2003; Nolz et al., 2006). This explains at least partially the inhibitory effect of dominant negative Rac1 on T cell activation and the dispensability of WASP for T cell-APC synapse formation and initial T cell activation (Cantrell, 2003; Cannon and Burkhardt, 2004).

1.2.3.2. NPF II: Cortactin and HS1

The second class of nucleation promoting factors comprises only two proteins, cortactin and its lymphocyte homologue HS1. The former was identified in a screen for phosphorylated targets of Src kinases, where it represented the most prominently phosphorylated protein (Kanner et al., 1990). Cortactin has been implicated in various processes which are all governed by dynamic branched F-actin cytoskeletal structures

associated with membranes. Amongst others are the formation and movement of the leading edge in migration, the growth of axons, invadopodia formation during metastasis of cancer cells and endocytosis (Kinnunen et al., 1998; Bowden et al., 1999; Cao et al., 2003; Bryce et al., 2005). Consistent with the participation in invadopodia formation, upregulation of cortactin expression is reported for many malignant tissues and correlates with poor prognosis (Weaver, 2008).

HS1 was identified by Kitamura and colleagues as a potential transcription factor (what later proved wrong) and raised interest due to its expression pattern, which was completely restricted to all cells of hematopoietic origin (Kitamura et al., 1989). Common knowledge on cortactin is much broader than on HS1, yet given the high degree of sequence identity, structural homology and the mutual exclusive expression, similar functions for both proteins are proposed. They represent cytoplasmic multi-domain adapter proteins that contain several repeats of a 37 amino acid motif (6.5 x in cortactin and 3.5 x in HS1) (Figure 3). This cortactin repeat mediates the binding of F-actin (Wu et al., 1991; Weed and Parsons, 2001). In addition to the unique repeats, both proteins contain an N-terminal acidic domain (NTA), which mediates binding of the Arp2/3 complex (Uruno et al., 2001) and both, the cortactin repeats and the NTA domain are essential for localisation of cortactin to lamellopodia (Weed et al., 2000). With the NTA domain and the adjacent cortactin repeats, the N-terminal half clearly serves the binding of the effector molecules. Further C-terminally resides a proline, serine, threonine and tyrosine rich stretch, which is targeted by different kinases and SH3 domain containing proteins and is thus probably involved in regulatory mechanisms. Ultimately, the C-terminal SH3 domain of cortactin is responsible for the interaction with various proteins, the most prominent being WASP, N-WASP and WIP, which further increases the integratory capacity (Mizutani et al., 2002; Kinley et al., 2003; Martinez-Quiles et al., 2004).

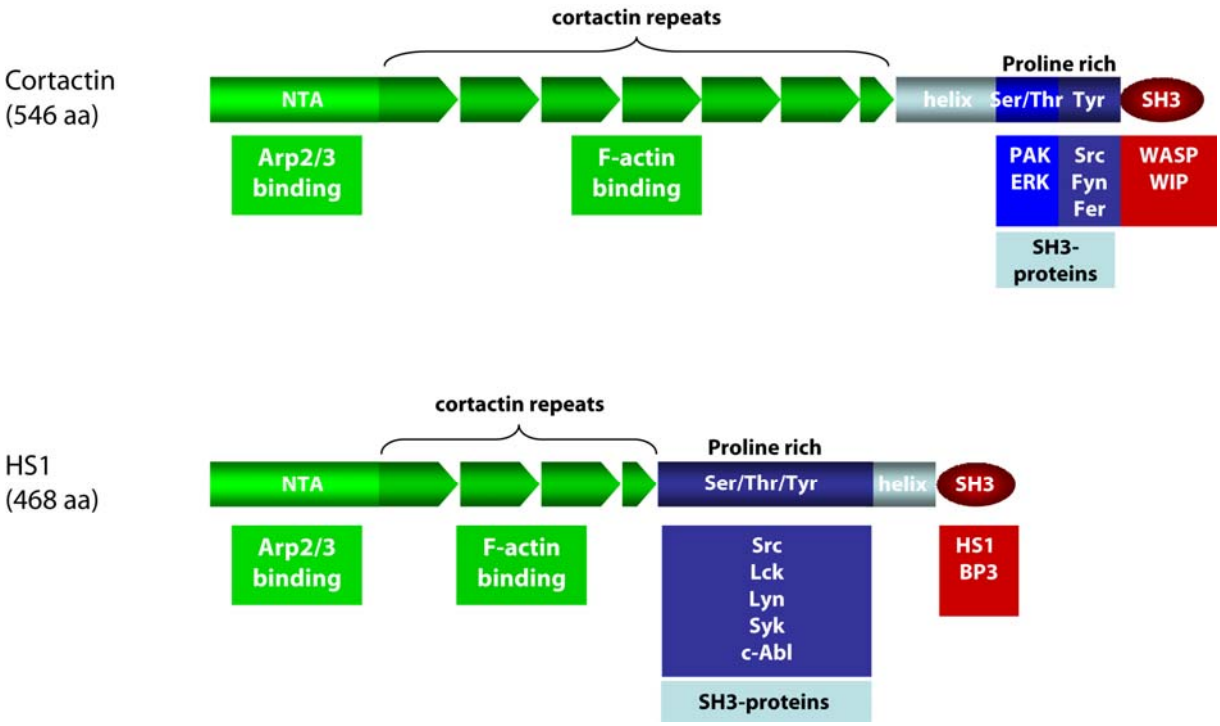

Figure 3: Domain structure and functions of NPFs II cortactin and HS1. Depicted are both proteins of the cortactin family. The Arp2/3 and F-actin binding domains are displayed in green. The regulatory domain is painted in blue. The respective interaction partners of each domain are shown below the depicted molecules. Adapted from (Cosen-Binker and Kapus, 2006) and (Weed and Parsons, 2001).

Ser/Thr-phosphorylation of cortactin by the active-rac binding kinase p21 activated kinase (PAK) and ERK increases the F-actin binding and inducing activity, while Tyr-phosphorylation through Src and Fyn downregulates both effects (Martinez-Quiles et al., 2004). This suggests an equilibrium model, where Ser/Thr phosphorylation leads to the activation of cortactin and the subsequent induction of branched F-actin structures, while Tyr-phosphorylation frees cortactin from old filaments and thus replenishes the pool (Fan et al., 2004). Such sophisticated regulatory mechanisms identify cortactin as a central switch in Arp2/3 activation that has the ability to integrate signals from a wide variety of internal and external stimuli.

Cortactin binds to the Arp3 subunit and this binding leads to the activation of the Arp2/3 complex. The cortactin repeats mediate simultaneous binding to F-actin, which together with the Arp3 binding stabilises and thus extends the life span of the branch points in the dendritic F-actin meshwork, which ultimately increases the net amount of cellular branched F-actin (Weaver et al., 2001; Uruno et al., 2003). As cortactin and WASP bind to different domains of Arp2/3, a ternary complex is possible and even supported through the binding of the cortactin SH3 domain to N-WASP or WIP. Consistently, this complex

results in the synergistically increased induction of Arp2/3 mediated F-actin formation (Uruno et al., 2001). To conclude, cortactin positively influences the formation of branched F-actin networks first via assisting in WASP mediated activation of Arp2/3 and second via the stabilisation of already formed complexes.

Like cortactin, also HS1 binds the Arp2/3 complex and F-actin, suggesting a similar mode of action. However, in marked contrast to cortactin and the WASP proteins, HS1 is not activated through Rho family GTPases but was shown to be Tyr-phosphorylated cooperatively by Syk and Lyn kinases upon antigen receptor crosslinking (Yamanashi et al., 1997). The mutation of two conserved Tyr-residues, Tyr378 and Tyr397 to alanine, interfered with lymphocyte activation by disruption of IS formation. This was due to impaired binding and thus diminished localisation of the SH2 domain containing Rac activator Vav1 at the IS (Gomez et al., 2006). Given the prominent role of Rac2 in lymphocyte function, this might be the main mechanism of HS1 to drive actin polymerisation (see below). A very refined analysis is presented by Butler and colleagues, which proposes a switch capacity for HS1, at least in NK cells (Butler et al., 2008). Depending on the differential phosphorylation of the tyrosine residues 378 and 397, HS1 activity in NK cells is either inducing ICAM dependent adhesion and subsequent killing of target cells or chemotactic migration.

With respect to cortactin function, it is as yet unclear if HS1 also binds to WASP and WAVE proteins to increase branched F-actin network formation. Albeit it was recently shown that HS1 is bound and phosphorylated by c-Abl and that this kinase additionally interacts with WAVE2 in T cells (Huang et al., 2008).

The implication of HS1 in actin dynamics in various lymphocyte species is consistent with its restricted expression pattern. Analysis of RNAi mediated knock down of HS1 in T cells determined its role in antigen induced formation of an IS and the resulting T cell activation and proliferation (Gomez et al., 2006). Along the same lines, HS1 deficient mice display severely impaired B cell function, resulting in defective clonal expansion and a reduced induction of T-independent immune responses (Taniuchi et al., 1995).

In conclusion, cortactin and HS1 both bind to Arp2/3 and F-actin and thus stabilise branched F-actin meshworks. The additional mechanisms of action and the regulatory circuits are partially different for these non-canonical NPFs, yet they show parallels in that they recruit prominent actin regulatory factors to the branch points.

1.2.4.Small GTPases of the Rho family in F-actin regulation

The first and name giving member of the *Ras homology* (Rho) family was identified in 1985 by virtue of its homology to the then recently found Ras oncogenes. Although being initially discovered in the genome of the sea slug *aplysia*, three orthologues in the human system were found soon and named RhoA, RhoB and RhoC (Madaule and Axel, 1985). In the following years, the other members of the family, the Rac proteins and Cdc42 were described, and the group was established as a Ras independent signalling entity (Didsbury et al., 1989; Bender and Pringle, 1989). Like Ras, all Rho family proteins represent small GTPases of approximately 21kDa. As all other GTPases, they occur in two different states, GTP-bound or GDP-bound and accordingly they can function as molecular switches. It is common knowledge that the GTP binding activates Rho proteins. The activity of these proteins is thus positively regulated by cofactors which mediate the exchange of GDP to GTP, so called guanine nucleotide exchange factors (GEFs). Being activated downstream of many cell surface receptors, they mediate the signal transduction of external stimuli to Rho family GTPases. Since the intrinsic GTPase activity of the Rho proteins is low, they need the assistance of GTPase activating proteins (GAPs). Hydrolysation of GTP to GDP renders the GTPase inactive. For all members of the Rho family, a plethora of different GEFs and GAPs has been described (reviewed in (Moon and Zheng, 2003; Rossman et al., 2005)). Concluding, the Rho GTPases are crucial for the signal transduction from a multitude of cell surface receptors to the cytoskeleton.

1.2.4.1. Rho

Due to its homology to Ras, Rho was initially believed to also be endowed with an oncogenic capacity. Only some time later it turned out, that this small GTPase had a strong effect on the induction of F-actin structures (and none on oncogenic processes) (Figure 4 C and (Ridley and Hall, 1992)). Microinjection of the Rho-protein into Swiss-3T3 murine fibroblasts rapidly induced the formation of stress fibres, intracellular cables composed of bundled linear F-actin complexed with myosin. In a mechanism similar to that of the muscle-cell actin-myosin network, stress fibres control cell contractility. To transduce the contractile forces to the membrane, the fibres are connected to membrane associated focal adhesions (FA) at their distal poles. FAs consist of densely clustered integrin molecules, which are connected to the actin cytoskeleton via intracellular adapter proteins. Accordingly they are crucial for cell adhesion to the substratum and thus carry out essential functions in spreading and migration as they provide the necessary traction and anchor points to focus the contractile forces (reviewed in (Campbell, 2008)).

Consistently, also the formation of FA was shown to be drastically increased upon Rho signalling (Figure 4 D and (Ridley and Hall, 1992)). GTP-bound Rho activates two downstream effectors that are crucially involved in stress fibre formation. Rho-GTP binds and activates the formin mDIA1. As described above, formins represent actin assembly factors, the activity of which leads to the formation of linear F-actin filaments (Figure 2) (Kovar, 2006). Interestingly, mDIA1 localises to FAs and subsequently leads to actin polymerisation and stress fibre growth (Butler et al., 2006). As formins remain at the fast growing barbed end of the actin filament, the stress fibre will grow as long as mDIA1 is attached. The second important Rho target in stress fibre formation is Rho kinase (ROK) which is activated upon binding Rho-GTP. This Ser/Thr kinase phosphorylates important downstream targets, among which is the myosin light chain 2 (MLC2) and several myosin regulatory factors. Their ROK mediated phosphorylation increases the contractility of the cells. In addition, ROK activity leads to pronounced stress fibre formation (Leung et al., 1996). However it has to be mentioned that only the activity of both, mDIA1 as well as ROK is sufficient to mimic Rho activity with respect to functional stress fibre assembly (Hotulainen and Lappalainen, 2006).

1.2.4.2. Rac

As Rac and Rho proteins share a highly identical sequence it is surprising how different their impact on the cytoskeleton is. As established in Alan Hall's laboratory at the beginning of the 1990s, Rac microinjection into murine fibroblasts resulted in the prominent induction of lamellipodia (Figure 4 E and (Ridley et al., 1992)). As opposed to stress fibres, lamellipodia are composed of branched F-actin filaments, without the addition of myosin. Accordingly, they are not involved in cell contractility but rather provide the scaffold and the protruding force needed in forward movement at the leading edge of a migrating cell. As such, the lamellipodium makes up for the most distal 1-5 µm of the cellular rim with a thickness of approximately 200 nm (Small and Resch, 2005). As the lamellipodium is composed of diagonally arranged F-actin filaments and the leading edge is pushed forward by laterally moving filaments, prominent branching of F-actin has to occur. The necessity of this Rac dependent formation of branched F-actin structures is impressively illustrated by the fatal phenotype of Rac-deficient mice. The $Rac^{-/-}$ embryos die already during gestation (E9.5) due to failures in germ layer arrangement caused by defective migration of the embryonic cells (Sugihara et al., 1998). The Arp2/3 complex is of essential importance in this respect, as no other assembly factor can induce branched filaments. This hypothesis is supported by RNAi studies proving the essential role of this

assembly complex in lamellipodia formation. In the same publication, Steffen and coworkers also determined the indispensability of the WAVE complex in this respect (Steffen et al., 2006). However, WAVE is not the only target of activated Rac protein, as shown by the later time point of embryonic lethality in WAVE2 deficient mice (E12.5) (Yan et al., 2003). A second mechanism to induce the formation of branched F-actin structures is initiated by the Rac-GTP dependent activation of PAK. As mentioned before, this serine/threonine kinase phosphorylates the NPF II cortactin at a crucial serine residue, resulting in its activation (Vidal et al., 2002; Martinez-Quiles et al., 2004).

As will be discussed later, lamellipodial structures in lymphocytes are of great importance e.g. in the establishment of an IS. Accordingly, Rac1 and Rac2 carry out important roles in different aspects of lymphocyte function (Gomez et al., 2001; Arana et al., 2008).

Finally it has to be mentioned that there is also intensive cross talk between Rho and Rac mediated pathways. For example, to induce cell migration it is crucial not only to push forward the leading edge, but also to disrupt FAs, whose foci of clustered integrins mediate strong adhesion to the substrate. Also, the Rho mediated increase in contractility would rather have inhibitory effects on the migration of cells. Consistently, active PAK counteracts the formation of FAs and stress fibres (Manser et al., 1997). The minimal adhesion needed to provide traction for migration is brought about by focal complexes that also contain clusters of integrin and whose formation is induced by Rac dependent activation of PAK (Figure 4 F and (Sells et al., 1997)). Yet, the regulatory circuits are probably more complex as sequential activation of Cdc42 and Rac has also been shown to lead to the subsequent activation of Rho (Nobes and Hall, 1995), a process that could be important in migration due to the Rho dependent retraction of the rear end of a cell, which marks the last step of the migration process.

Many of the functional analyses of Rac mediated processes have been facilitated by two point mutants (Ridley et al., 1992). Rac1V12, carrying a valin at amino acid position 12 is constantly bound to GTP and thus permanently activated. In contrast, Rac1N17, containing an asparagin residue in position 17, displays a high affinity towards GDP and accordingly remains inactive. Both mutants have been generated analogous to previously characterised mutations in the small GTPase Ras.

1.2.4.3. Cdc42

The third prominent member of the Rho family is the GTPase Cdc42, which was initially discovered in yeast (Johnson and Pringle, 1990). The implication of Cdc42 in F-actin regulation in mammalian cells was characterised in Alan Hall's laboratory. The microinjection of Cdc42 in murine fibroblasts resulted in the marked induction of filopodia all around the cells (Figure 4 G). Filopodia are thin, finger like protrusions emanating from the peripheral branched F-actin network in the lamellipodium at the leading edge. In contrast to the latter, they are composed of linear F-actin filaments, organised into higher order complexes by the F-actin bundling protein fascin (reviewed in (Chhabra and Higgs, 2007)). Interestingly, to visualise optimal filopodia formation, the cells had to be coinjected with dominant negative Rac1N17. Otherwise, the initial filopodia quickly reorganised into lamellipodia due to the activating effect of Cdc42 on Rac (Nobes and Hall, 1995). Along the same lines, as apparent in Figure 4 G, Cdc42 induced filopodia originate in the lamellipodium surrounding the whole cell. This reveals a first hint towards filopodia function: to probe the surrounding environment before migration is initiated; accordingly, filopodia are important for chemotaxis.

With respect to the factors involved in filopodia regulation, much remains elusive until now. The binding and activation of N-WASP through Cdc42 suggests filopodia induction via the Arp2/3 complex (Miki et al., 1998). However, N-WASP deficiency or RNAi mediated knock down of Arp2/3 does not abrogate filopodia induction by Cdc42 (Lommel et al., 2001; Steffen et al., 2006). In contrast, Cdc42 was found to interact with and activate the formin mDIA2 (Peng et al., 2003). For several reasons formins are likely to be the Cdc42 effectors in filopodia formation: first they are known to induce linear F-actin formation, and localise specifically to the tips of growing filopodia. Second and most strikingly, the knock down of mDIA2 results in the abrogation of filopodia formation and the opposite is caused by overexpression of constitutively active mDIA2 (Yang et al., 2007; Block et al., 2008).

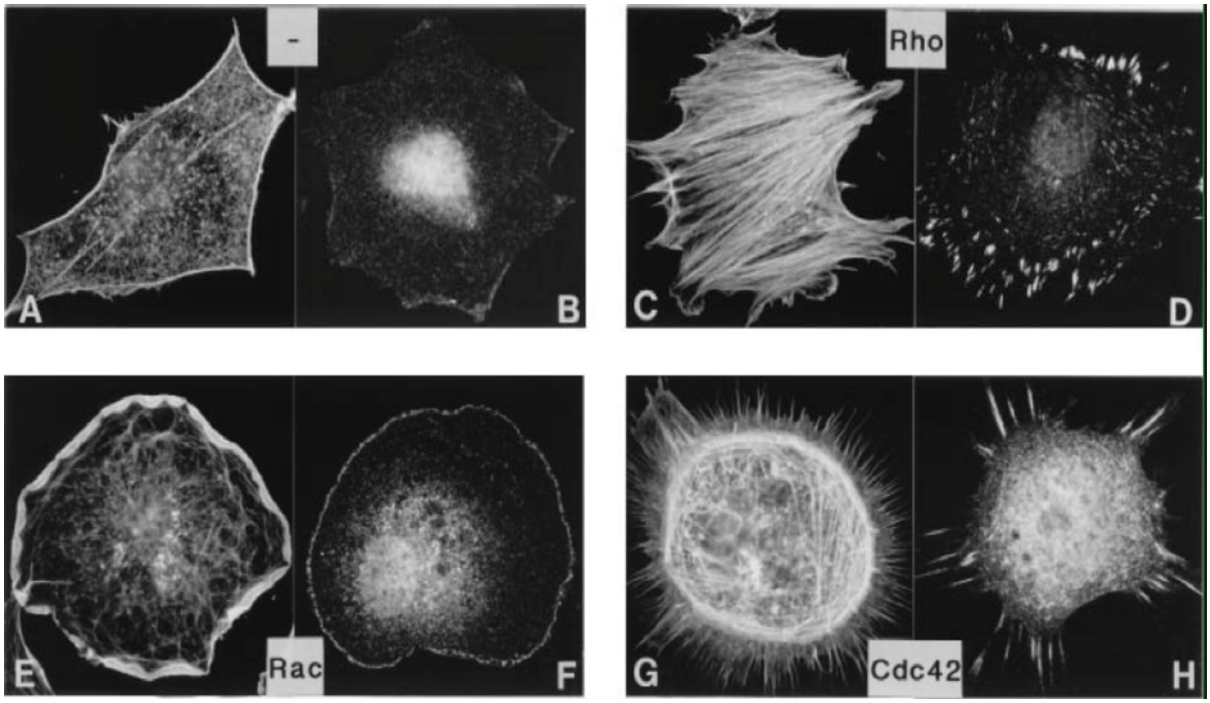

Figure 4: Rho family GTPases exert distinct effects on the F-actin cytoskeleton. Murine Swiss 3T3 fibroblasts were treated to activate Rho, Rac or Cdc42. Cells were either stained for F-actin with phalloidine (A, C, E and G) or with α-vinculin to mark FAs (B, D, F and H). The following stimuli were applied: A+B, untreated; C+D, LPA to activate Rho; E+F, microinjection of constitutively active Rac1V12; G+H microinjection of the Cdc42-GEF FGD1 resulting in activation of Cdc42. The induction of stress fibres and FAs (C+D), lamellipodia (E+F) and filopodia (G+H) is obvious (Picture taken from (Hall, 1998)).

1.2.5. The actin cytoskeleton in lymphocyte activation

The life threatening severity of the Wiskott-Aldrich-Syndrome impressively illustrates the importance of F-actin cytoskeletal reorganisations for hematopoietic cell function (Notarangelo et al., 2008). The analysis of T cells from WAS patients proved defective proliferative responses upon stimulation with α-CD3 (Molina et al., 1993). A more detailed analysis, facilitated by WASP deficient mice argues against a role of WASP in TCR proximal signalling but rather in the subsequent actin polymerisation dependent sustained activation of the T cells (Zhang et al., 1999). Consistently, WASP deficient T cells show impaired exo- and endocytosis, resulting in diminished levels of IL-2. Surprisingly, it was shown recently that WASP deficient T cells can form and maintain an intact IS, suggesting that the IL2 defect is caused by an IS-independent function of WASP (Cannon and Burkhardt, 2004). In contrast, RNAi mediated knock down of WAVE2 in T cells completely abrogates the formation of the F-actin rich platform between T cells and APC, which serves as a scaffold for the IS. Accordingly, the WAVE2 depleted cells show a diminished Ca^{2+} release in response to TCR ligation and display markedly lowered transcription from the *il2*-locus (Nolz et al., 2006).

The IS was initially described by Kupfer and coworkers, when they analysed the polarisation of T cells interacting with APCs or cytotoxic T cells with target cells (Kupfer and Dennert, 1984; Kupfer and Singer, 1988). The hallmark of the IS is the so called bull's eye structure, formed by a ring of integrins clustered around a central focus of TCR molecules. These regions carry out different functions and are referred to as peripheral supramolecular activation cluster (pSMAC) and central supramolecular activation cluster (cSMAC), respectively. The integrin (mostly LFA-1) rich pSMAC mediates the adhesion to the APC, while the cluster of TCRs in the cSMAC accounts for sustained signalling. This assembly is mirrored on the APC side by a ring of ICAM1 organised around peptide loaded MHC molecules. A plethora of accessory signalling and structural proteins localise specifically to either one of the two structures and accordingly ensure correct T cell activation. In addition the secluded area between the two cells allows the spatially highly restricted release of cytokines or cytotoxic agents, minimising side effects or collateral damage (reviewed in (Huse et al., 2008; Dustin, 2008)). In the meantime, multiple different IS have been described, differing largely by the cells connected by them (e.g. regulatory synapses between regulatory T cells and target T cells or cytotoxic synapses between CTLs and target cells).

Actin reorganisation plays an essential role in the formation of an IS, as treatment of the cells with inhibitors of actin polymerisation completely abrogates polarisation of the cell (Bunnell et al., 2001). Interestingly, also interference with the microtubular cytoskeleton affects the IS, however only at a later time point, rather suggesting a function in the maintenance of this complex structure. Being dependent on WAVE2, Rac and Arp2/3 complex signalling, the IS is largely understood as a lamellipodial structure. In agreement with this hypothesis, also HS1 was shown to be of pivotal importance for intact F-actin polarisation at the IS. Knock down of HS1 resulted in impaired T cell-APC conjugate formation and ultimately led to diminished IL2 production. This effect was mainly mediated by the abrogated recruitment of the Rac-GEF Vav1 to the IS (Gomez et al., 2006).

With respect to the amount of research being done on the T cell IS, surprisingly little is known about the IS formed by B cells. Batista and coworkers have shown that B cells form an IS with antigen containing membranes and that also in the B cell synapse a ring of LFA-1 surrounds the antigen receptor enriched cSMAC (Carrasco et al., 2004). However, in marked contrast to T cells, B cells display a biphasic response to membrane bound antigen. The pronounced morphological changes are represented by an initial spreading phase, in which the B cell engages as many BCRs as possible with the cognate antigen. The subsequent retraction gathers the collected antigen and concentrates it into the cSMAC

(Figure 5 A+B). Of note, both actin polymerisation as well as cognate antigen binding are mandatory for these processes to occur (Fleire et al., 2006; Lin et al., 2008). This choreography was shown to be supported by the Rac2 dependent increase of integrin binding downstream of BCR signalling, subsequent adhesion to the antigen containing membrane and the concomitant reorganisation of F-actin (Arana et al., 2008), for an actual review see (Harwood and Batista, 2008).

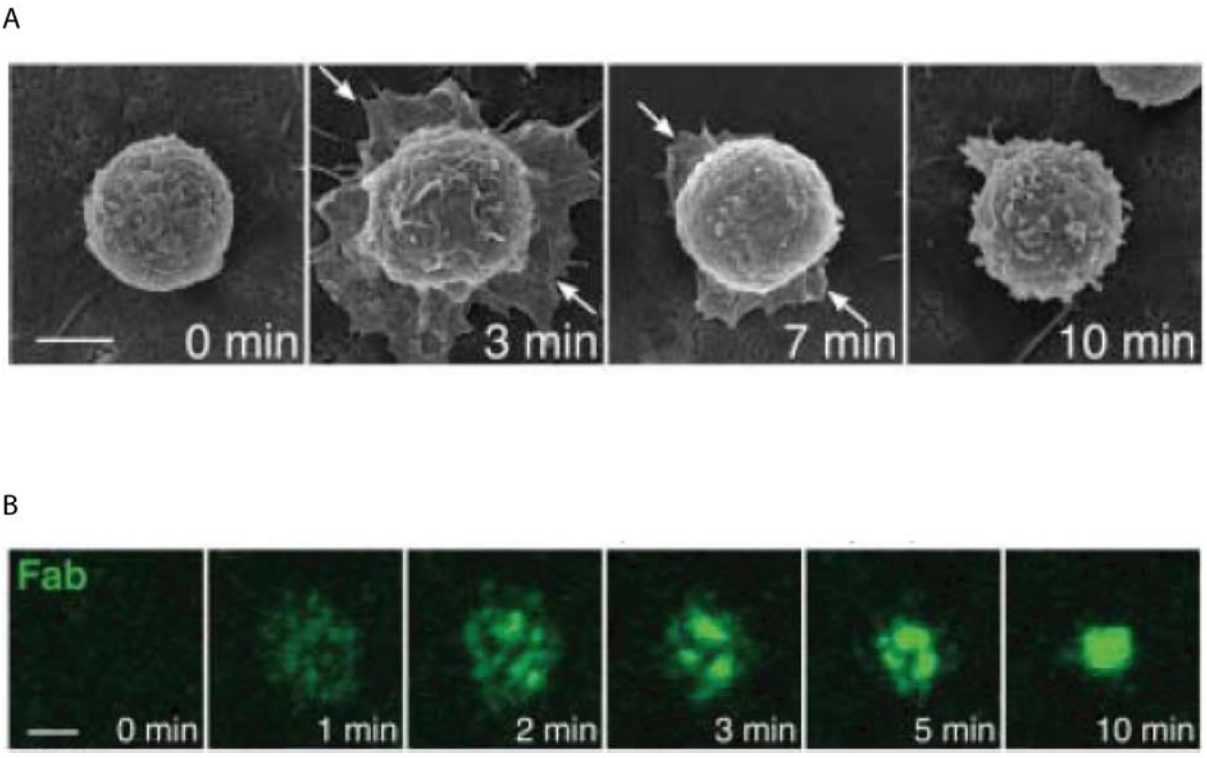

Figure 5: B cell spreading on antigen containing membranes. (A) Scanning electron microscope (SEM) pictures of a transgenic MD4-B cell interacting with COS-7 cells expressing a membrane bound form of HEL-GFP as the cognate antigen. (B) Confocal laser microscopic pictures of a transgenic MD4-B cell interacting with a planar bilayer containing *henn egg lysozyme* (HEL) linked to fluorescently labelled Fab molecules as cognate antigen for the transgenic BCR. Pictures taken from (Fleire et al., 2006).

In contrast to the well-defined function of HS1 in T cell IS formation, its implications in B cell spreading and contraction in response to antigen remain poorly understood. Only recently HS1 has been identified as a central player in the mediation of cytolytic synapse organisation and subsequent target cell killing in NK cells (Butler et al., 2008).

1.3. Objective

Adapter proteins play pivotal roles in the transduction of intracellular signals. They facilitate the formation of multi-protein complexes and thus organise the tempo-spatially regulated interaction of signalling proteins. The SLy family comprises three members, all of which are putative adapter proteins due to their decisive domain structure. The founding member of the family, SLy, was shown to be phosphorylated upon TCR ligation and was thus believed to be involved in the subsequent signalling cascades (Astoul et al., 2003; Beer et al., 2005).

Due to the remarkable degree of structure and sequence-related identity between SLy and its closest relative SLy2, there was specific interest in the role of SLy2 in intracellular signalling processes. As the latter is expressed in a much broader range of tissues than its lymphocyte restricted homologue SLy, it was one objective of this thesis to unravel SLy2 function and its impact in different cell types.

In the beginning of the work on this thesis, the molecular knowledge about this putative adapter protein was extremely poor and accordingly the main task was to define the molecular properties of SLy2. Subsequent *in vitro* analyses in different cell lines should help to define pathways and conditions where SLy2 exerts its activity. Furthermore, due to the characteristic domain structure of SLy2, a comprehensive analysis on the participation of the individual domains in the different functions of SLy2 should be performed. Of special interest in this respect were the NLS and the serine residue 23 since the deletion of these features in the SLy protein had a deleterious effect on SLy function, as established in the SLy-mutant mouse strain (Beer et al., 2005). Finally, the intracellular localisation of SLy2 was also in the focus of attention, with respect to a potential recruitment to specific subcelluar structures.

On the basis of the thus generated *in vitro* results, SLy2 function in different mouse models should be assessed. Therefore, gene-targeted SLy2 deficient and SLy2 overexpressing transgenic mice were to be generated concomitantly. Their phenotypic analysis would thus lead to an extensive elucidation of this novel adapter protein.

2. Materials and methods

2.1. Materials

2.1.1. Chemicals

Chemicals	Supplier
Aceton	Merck, Darmstadt
Agarose	Biozym, Hamburg
Ampicilin, sodium salt	Sigma-Aldrich, Taufkirchen
Ammoniumchloride	Merck, Darmstadt
Ammoniumperoxodisulfate (APS)	Sigma Taufkirchen
Bactoagar	BD Biosciences, Heidelberg
BES	Roth, Karlsruhe
β-mercaptoethanol	Gibco, Karlsruhe
BrdU	Sigma-Aldrich, Taufkirchen
Bromphenolblue	Merck, Darmstadt
BSA (Bovine Serum Albumine)	Sigma-Aldrich, Taufkirchen
Calcium Ionophore	Sigma-Aldrich, Taufkirchen
Calyculin	Sigma-Aldrich, Taufkirchen
Chloroform	Roth, Karlsruhe
Complete Mini Protease Inhibitor Cocktail, EDTA free	Roche, Mannheim
DAPI	Invitrogen, Karlsruhe
Desoxyribonucleids (dATP, dCTP, dGTP, dTTP)	MBI Fermentas, St. Leon-Rot
Dextransulfate	Amersham Biosciences, Braunschweig
Diethylpyrocarbonate (DEPC)	Roth, Karlsruhe
Digitonin	Calbiochem, USA
N,N'-Dimethylformamide	Merck, Darmstadt
Dithiothreitol (DTT)	Invitrogen, Karlsruhe
Dimethylsulfoxide (DMSO)	Sigma-Aldrich, Taufkirchen
DMSO	Sigma-Aldrich, Taufkirchen
DNA standard	Fermentas, St. Leon-Rot
ECL	GE Healthcare, Munich
EDTA	Sigma-Aldrich, Taufkirchen
Ethanol	Merck, Darmstadt

Ethidium bromide	Merck, Darmstadt
Fluoromount-G	Northern Biotech, Birmingham, USA
Formaldehyde	Roth, Karlsruhe
FuGENE 6 Transfection reagent	Roche, Mannheim
Ganciclovir (Cymeven)	Syntex, Aachen
Gelatine	Sigma-Aldrich, Taufkirchen
Geneticin (G418)	Gibco, Eggenstein
Glacial acetic acid	Merck, Darmstadt
Glycerine	Merck, Darmstadt
HCG	Intervet, Unterschleißheim
HEPES buffer	Invitrogen, Karlsruhe
Hypochloric acid	Roth, Karlsruhe
IGEPAL (NP-40)	Sigma-Aldrich, Taufkirchen
Isopropanol	Merck, Darmstadt
L-glutamine	Biochrom, Berlin
Glycerine	Sigma-Aldrich, Taufkirchen
Kanamycine	Sigma-Aldrich, Taufkirchen
LB-Agar	Roth, Karlsruhe
LB-Medium	Roth, Karlsruhe
LPS	Sigma-Aldrich, Taufkirchen
Methanol	Merck, Darmstadt
mIL-2	R&D Systems GmbH, Wiesbaden
mIL-4	R&D Systems GmbH, Wiesbaden
Mineral oil	Sigma-Aldrich, Taufkirchen
Mitomycine C	Sigma-Aldrich, Taufkirchen
MOPS	Sigma-Aldrich, Taufkirchen
N-lauryl sarcosine	Sigma-Aldrich, Taufkirchen
Paraformaldehyde	Merck, Darmstadt
PBS	Invitrogen, Karlsruhe
PDBU (Phorbol 12,13-Dibutyrat)	Sigma-Aldrich, Taufkirchen
PDGF	Sigma-Aldrich, Taufkirchen
Penicilline/streptomycine	Biochrom, Berlin

Phalloidin, TRITC	Sigma-Aldrich, Taufkirchen
Phalloidin, Alexa-633	Invitrogen, Karlsruhe
Phenol	Roth, Karlsruhe
PMA (Phorbol 12-myristate 13-acetate)	Sigma-Aldrich, Taufkirchen
PMSG (pregnant mare serum gonadotropin)	Intervet, Unterschleißheim
PMSF (Phenylmethanolsulfonylfluoride)	Sigma-Aldrich, Taufkirchen
Protease inhibitor cocktail	Sigma-Aldrich, Taufkirchen
Saponine	Sigma-Aldrich, Taufkirchen
Skim milk powder	Oxoid, Hampshire, Great Britain
Sodium azide	Sigma, Taufkirchen
Sodium chloride	Roth, Karlsruhe
Sodium citrate	Roth, Karlsruhe
SDS (sodium dodecyl sulfate)	Schuchart, Hohenbrunn
Sodium hydroxide	Merck, Darmstadt
TEMED (N,N,N'N'-Tetraethylmethylendiamine)	Sigma-Aldrich,Taufkirchen
Triton-X-100	Merck, Darmstadt
Trypan blue solution in PBS	Sigma-Aldrich, Taufkirchen
Trypsin/EDTA	Invitrogen, Karlsruhe
Trypton	Roth, Karlsruhe
Tween 20	Merck, Darmstadt
Yeast extract	Roth, Karlsruhe

2.1.2. Radiochemicals

5'-[α-^{32}P]-d-CTP redivue, specific activity ~3000 Ci/mmol

[^{32}P]-Orthophosphate, specific activity ~3000 Ci/mmol

[Methyl-^{3}H]-Thymidine, specific activity 5.0 Ci/mmol

[^{35}S]-Methionine, cysteine, specific activity ~1000 Ci/mmol

All radiochemicals were purchased from GE-Healthcare, Munich and used during the first half-life period.

2.1.3. Antibodies

All antibodies used in flow cytometry were purchased from Becton&Dickinson, Heidelberg, if not otherwise stated. All secondary antibodies used in western blot analyses originated from Dianova, Hamburg. A polyclonal α-SLy2 antibody was generated by Eurogentec, Belgium. It was purified and tested for specificity prior to usage in this study. The oligopeptide used for its generation was RELTNGSEEQSKTSS.

Table 1: Additionally used antibodies

Description	Species/label	Application	Supplier
Primary antibodies			
α-actin	Mouse	Western blot	Sigma-Aldrich, Taufkirchen
α-BrdU	PE	Flow cytometry	Dianova, Hamburg
α-cortactin	Rabbit	Western blot, immunofluorescence	Cell signalling, USA
α-GAPDH	Mouse	Western blot	Hytest, Finnland
α-HA	Mouse/rabbit	Western blot, immunofluorescence, IP	Sigma-Aldrich, Taufkirchen
α-lamin A/C	Mouse	Western blot	Cell signalling, USA
α-myc	Mouse	Western blot, IP	Dianova, Hamburg
α-rac1	Mouse	Western blot	Pierce, USA
Secondary antibodies			
α-rabbit	Alexa 633	Immunofluorescence	Invitrogen, Karlsruhe
α-mouse	Alexa 633	Immunofluorescence	Invitrogen, Karlsruhe
α-rabbit	Cy3	Immunofluorescence	Jackson ImmunoResearch, Suffolk, UK
α-mouse	Cy3	Immunofluorescence	Jackson ImmunoResearch, Suffolk, UK

2.1.4. Enzymes	Supplier
MMLV, reverse transcriptase	Invitrogen, Karlsruhe
Mung bean nuclease	New England Biolabs, Frankfurt
PFU, Polymerase	Stratagene, La Jolla, USA
Polynucleotide kinase	Roche, Mannheim

Pronase E	Sigma-Aldrich, Taufkirchen
Proteinase K	Roche, Mannheim
Restriction enzymes	New England Biolabs, Frankfurt Roche, Mannheim Fermentas, St. Leon-Rot
RNase A	Sigma-Aldrich, Taufkirchen
SAP (Shrimp alkaline phosphatase)	Biolabs, New England
T4-DNA-ligase	Fermentas, St. Leon-Rot
Taq-polymerase	Roche, Mannheim

2.1.5. Reagents

Reagents	Supplier
BCA Protein Assay	Pierce, Rockford, USA
$CD90^+/B220^+$ MACS beads	Miltenyi, Bergisch Gladbach
Cell strainers (50 µm, 70 µm, 100 µm)	Falcon, New Jersey, USA
Cover glasses	Hecht KG, Sondheim
DIG easy Hyb, Northern Blot kit	Roche, Mannheim
Dispenser tips	Brand GmbH, Wertheim
ExpressHyb hybridisation solution	Clontech-Takara, France
Films, hyperfilm™-ECL	GE Healthcare, Munich
Films, autoradiography, Biochrom	Kodak, Cologne
Lympholyte M, blood cell isolation kit	Cedarlanes, USA
Microspin S-200 HR columns	GE Healthcare, Munich
Nylonmembrane, Gene Screen Plus	NEN® Research products, USA
Nylonmembrane, Hybond N+	GE Healthcare, Munich
Nylonmembrane, Protran BA 85, Cellulose nitrate	Schleicher&Schuell BioScience, Dassel
Object slides	Engelbrecht GmbH, Edermünde
Paper, Whatman 3MM	VWR, Darmstadt
Parafilm M	American National Can™, Chicago, USA
pGEM T easy, PCR cloning kit	Promega

Pipette tips	Starlab, Ahrensburg
Plastics for cell culture	Corning, New York, USA
	Falcon, New Jersey, USA
	Greiner, Solingen
	Nunc, Wiesbaden
Protein Standard for Western blotting	GE Healthcare, Munich
QIAGEN Plasmid Isolation kits	QIAGEN, Hilden
Quick & Easy BAC Modification kit	Gene Bridges, Dresden
QuickChange site directed mutagenesis kit	Clontech-Takara, France
Reagent tubes	Eppendorf, Wesseling-Berzdorf
RNA Isolation kit (Fluka)	Sigma-Aldrich, Taufkirchen
SMART™-RACE cDNA amplification kit	Clontech-Takara, France
Sterile filters	Sartorius, Göttingen
TA cloning kit	Invitrogen, Karlsruhe
Takara Ladderman labelling kit	Takara, France
Ultracentrifuge Tubes	Beckman-Coulter, Krefeld

2.1.6. Electronic devices

	Supplier
β-Counter LKB Wallac	Perkin Elmer, USA
Centrifuges, table top	
Biofuge fresco	Heraeus, Hanau
Megafuge 1.0 R	Heraeus, Hanau
Centrifuges, cooling	
Sorvall® RC 26 PLUS	Heraeus, Hanau
Megafuge 1.0, Rotor 2250	Heraeus, Hanau
Omnifuge 2.0 RS	Heraeus, Hanau
Confocal microscope, LSM510	Zeiss, Jena
Developer machine Curix 60	Agfa, Cologne
DNA-crosslinker BIO-LINK BLX	Biometra, Göttingen
Electrophoresis chambers for DNA and RNA	Hoefer, Amstetten
Electroporation device Gene Pulser II	Biorad, Munich
ELISA Reader Sunrise	Tecan, Crailsheim

FACSCanto	Becton Dickinson GmbH, Heidelberg
Gel documentation system	BioDoc Analyze, Biometra, Göttingen
Gel dryer	Biorad, Munich
Hybridisation oven OV3	Biometra, Göttingen
Incubator BBD 6220	Heraeus, Hanau
Microscope Axiovert 25	Zeiss, Jena
PCR machines	
T3 Thermoblock	Biometra, Göttingen
T1 Thermoblock	Biometra, Göttingen
TGradient	Biometra, Göttingen
Photometer Gene Quant	Pharmacia Biotech
Phosphoimager, Typhoon 8600	GE Healthcare, Munich
Shaker for bacterial cultures, 3015	GFL, Burgwedel
Sterile work bench, Hera Safe	Heraeus, Hanau
Thermomixer	
Termomixer Compact	Eppendorf, Wesseling-Berzdorf
DRI Block	Techne, Jahnsdorf
Ultracentrifuge L60	Beckman Coulter, Krefeld
Ultracentrifuge rotor SW55Ti and corresponding buckets	Beckman Coulter, Krefeld
Ultra-sonifier, Branson-Sonifier 450	G.Heinemann, Schwäbisch Gmünd
Ultra-Turrax, T25 basic	IKA Werke GmbH, Staufen
Waterbaths:	
WNB22	Memmert, Schwabach
1092	GFL, Burgwedel
E100	Lauda, Lauda-Königshofen

2.2. Buffers and media

2.2.1. Stock solutions and buffers

Description	Composition
Actin-stabilisation buffer	100 mM PIPES, pH 6.9 30% glycerol 5% DMSO 1 mM $MgSO_4$
DEPC treated H_2O for RNA treatment	1ml DEPC per 1l H_2O Stirred over night, then autoclaved
dNTP-Mix	1 mM dATP 1 mM dCTP 1 mM dTTP 1 mM dGTP
FACS staining buffer	PBS 2%FCS 0.02% Na-azide
FACS staining buffer (thymocytes)	DMEM 2%FCS 0.02% Na-azide
Fixing solution for radiolabelled gels	40% methanol 10% glacial acetic acid
Loading dye, DNA, (10x)	0.05% bromphenol blue 0.05% xylene Cyanol FF 50% glycerol

Loading dye, protein, (5x)	30 mM Tris, pH 6.8 10% SDS 45% glycerol 25% β-mercaptoethanol 0.05% bromphenol blue
Lysis buffer (protein samples)	1% NP – 40 1% Laurylmaltosid 10 mM NaF 1 mM Na_3VO_4 1 mM PMSF 10 mM EDTA 170 mM NaCl 50 mM Tris, pH 7.5 1 Protease Inhibitor Cocktail tablet per 10 ml
Lysis buffer (whole organ lysates and IP)	140 mM NaCl 5 mM $MgCl_2$ 20 mM Tris, pH 7.6 2 mM NaF 1% Digitonin or NP-40 1 Protease Inhibitor Cocktail tablet per 10 ml
Lysis buffer (ES cells)	10 mM NaCl 10 mM Tris, pH 7.5 10 mM EDTA 0.5 % N-Lauryl-Sarcosine 400µg/ml Proteinase K
Lysis buffer (Erythrocytes)	155 mM NH_4Cl 10 mM $KHCO_3$ 100 mM EDTA

MACS-buffer	PBS 0.5% BSA 2.5 mM EDTA degassed and filtered stored at 4°C
Maleic acid buffer	100 mM maleic acid 150 mM NaCl pH 7.5
MEN buffer for northern blot (10x)	200 mM MOPS 50 mM Na-Acetate 10 mM EDTA pH 7.0 DEPC treated H_2O stored in the dark
PBS	13.7 mM NaCl 2.7 mM KCl 80.9 mM Na_2HPO_4 1.5 mM KH_2PO_4 pH 7.4
PCR buffer (10x)	500 mM KCl 100 mM Tris-HCl, pH 8.3 15-25 mM $MgCl_2$ 0.1% gelatine
Pronase E	10 mg/ml 10 mM Tris, pH 8.0 10 mM NaCl selfdigest 1h at 37°C
Proteinase K	10 mg/ml in H_2O_{bidest}

Running buffer (Western Blot) (1x)	50 mM MOPS 50 mM Tris base 0.1% (w/v) SDS 1 mM EDTA, pH 7.7
SSC 20x	3 M NaCl 0.3 M tri-sodium citrate
Solution I (Alcalic lysis)	50 mM glucose 25 mM Tris 10 mM EDTA
Solution II (Alcalic lysis)	0.2 M NaOH 1% (w/v) SDS
Solution III (Alcalic lysis)	60.0% Potassium acetate 11.5% glacial acetic acid 28.5% H_2O_{bidest}
TAE buffer for electrophoresis	40 mM Tris, pH 8.0 20 mM glacial acetic acid 2 mM EDTA
TBS-T (20 x)	200 mM Tris/HCL, pH 7,4 3M NaCl 0.01% Tween
TE-Puffer	10 mM Tris, pH 8.0 1 mM EDTA, pH 8.0
TNE buffer for mouse tail biopsies	10 mM Tris, pH 8.0 100 mM NaCl 1 mM EDTA, pH 8.0

Transfer buffer (Western Blot)(20 x)	25 mM Bicine 25 mM Bis Tris 1 mM EDTA
Wash B (IP, low salt)	150 mM NaCl 10 mM Tris pH 7.6 0.2 % digitonin or NP-40 1 Protease inhibitor cocktail tablet per 10ml
Wash C (IP, high salt)	500 mM NaCl 10 mM Tris, pH 7.6 0.2 % digitonin/NP-40 1 Protease inhibitor cocktail tablet per 10ml
Wash buffer I (Southern Blot)	2x SSC 0.05% SDS
Wash buffer II (Southern Blot)	1x SSC 0.1% SDS

2.2.2. Bacteria culture media

Bacteria were generally cultivated in autoclaved Luria-Bertani (LB) complete media

Table 2: Composition of bacteria culture media

Description	Composition	Amount per litre
LB	Tryptone	10g
	Yeast extract	5g
	NaCl	10g
	H_2O_{dest}	ad 1l
	pH 7. 2	

Solid media were generated by addition of 15g agar/litre LB media. Liquid bacterial cultures were shaked at 37°C over night; dishes were incubated overnight at 37°C without shaking.

Bacterial dishes with colonies were sealed with parafilm and stored for a maximum of 4 weeks at 4°C. For long term storage, the cultures were mixed with 50% sterile glycerine and kept at -80°C.

2.2.3. Cell culture media

All media used during this study were purchased from Invitrogen, Karlsruhe. Leukemia inhibiting factor (LIF) was generated as supernatant of the LIF producing clone CHO-LIF-D.

Table 3: Media and additives for eucaryotic cell culture

	ES	**EF**	**EL-4**	**Jurkat**	**293 FT**	**HeLa**	**Primary lympho-cytes**
Basic media	DMEM (high glucose)	DMEM (high glucose)	RPMI	RPMI	DMEM	DMEM	RPMI
Additives							
FCS	10%	5%	10%	10%	10%	10%	10%
Penicilline (U/ml)	100	100	100	100	100	100	100
Strepto-mycine (µg/ml)	100	100	100	100	100	100	100
L-glutamine	2 mM	2 mM	2 mM	2 mM	2 mM	2 mM	2 mM
β-ME (mM)	0.05	0.05					0.05
LIF	1%						
Treatment							
Trypsine	0.05% 10 min	0.05% 5 min			0.05% 5 min	0.05% 5 min	
Mitomycine C		10µg/ml for 2.5 hours					
Freezing medium	10%DMSO 20% FCS 70%DMEM	10%DMSO 20% FCS 70%DMEM	10%DMSO 20% FCS 70%RPMI	10%DMSO 20% FCS 70%RPMI	10%DMSO 20% FCS 70%DMEM	10%DMSO 20% FCS 70%DMEM	

2.2.4. Antibiotics

To positively select for bacteria carrying plasmids, the culture media were supplemented with ampicilline, kanamycine, chloramphenicole or tetracycline. Transgenic ES cells after electroporation were selected with neomycine and ganciclovir.

Table 4: Procaryotic and eucaryotic antibiotics

Substance	Stock solution	Working concentration
Ampicilline	100 mg/ml in H_2O_{bidest}, sterilised	100 µg/ml
Kanamycine	100 mg/ml in H_2O_{bidest}, sterilised	100 µg/ml
Substance	**Stock solution**	**Working concentration**
Chloramphenicole	25 mg/ml in isopropanol	12.5 µg/ml
Tetracycline	100mg/ml in H_2O_{bidest}, sterilised	20µg/ml
Neomycine	Stock solution with 100 mg/ml active substance in media	200 µg/ml
Ganciclovir	Stock solution 2 mg/ml in sterile H_2O_{bidest}; 128 µl in 500 ml media	2 µM

2.3. Bacteria, cell lines and animals

2.3.1. Bacteria

Two different lines of bacteria were used to propagate plasmid vectors.

Table 5: Bacterial lines used during this study

Bacterial line	Genotype	Reference
E. coli XL1-blue	endA1, hsdR17, thi-1, supE44, recA1, relA1, gyrA96, Δ(lac), (F'proAB), lacIqZΔM15, Tn10 (TetR)	Stratagene, USA
E. coli DH5α	supE44, ΔlacU169, (Φ80lacZΔM15), hsdR17, recA1, endA1, gyrA96, thi-1, relA1	(Hanahan, 1983)

2.3.2.Cells and cell lines

Table 6: Cells and cell lines used during this study

Cell/Cell line	Description	Reference
Jurkat	human T-lymphoma cells	ATCC
Jurkat SLy2-wt-HA	Jurkat cells, lentivirally transduced with pWPI-SLy2-wt-HA	generated during this study
Jurkat SLy2-ΔNLS-HA	Jurkat cells, lentivirally transduced with pWPI-SLy2-ΔNLS-HA	generated during this study
Jurkat SLy2-S23A-HA	Jurkat cells, lentivirally transduced with pWPI-SLy2-S23A-HA	generated during this study
Jurkat SLy2-ΔSH3-HA	Jurkat cells, lentivirally transduced with pWPI-SLy2-ΔSH3-HA	generated during this study
Jurkat SLy2-ΔSAM-HA	Jurkat cells, lentivirally transduced with pWPI-SLy2-ΔSAM -HA	generated during this study
Jurkat GFP	Jurkat cells, lentivirally transduced with pWPI	generated during this study
HeLa	human epithelial cell line	ATCC
HeLa SLy2-wt-HA	HeLa cells, lentivirally transduced with pWPI-SLy2-wt-HA	generated during this study
HeLa SLy2-ΔNLS-HA	HeLa cells, lentivirally transduced with pWPI-SLy2-ΔNLS-HA	generated during this study
HeLa SLy2-S23A-HA	HeLa cells, lentivirally transduced with pWPI-SLy2-S23A-HA	generated during this study
HeLA SLy2-ΔSH3-HA	HeLa cells, lentivirally transduced with pWPI-SLy2-ΔSH3-HA	generated during this study
HeLa SLy2-ΔSAM-HA	HeLa cells, lentivirally transduced with pWPI-SLy2-ΔSAM -HA	generated during this study
HeLa GFP	HeLa cells, lentivirally transduced with pWPI	generated during this study
293FT	Derived from 293T. Used to maximize the production of lentiviral particles	(Naldini et al., 1996)
ES cells E14.1	Murine embyonic stem cells generated from the mouse line 129/SvJ Ola	(Kuhn et al., 1991)
EF cells	Embryonic fibroblasts, generated from d14.5 *post coitum* CD1 mouse embryos	Prepared continuously
Thymocytes/ splenocytes	Primary cells, cultivated after organ homogenation	Prepared continuously

2.3.3. Animals

All animals used during this study were kept in the animal house of the Heinrich-Heine-University, Düsseldorf. Blastocysts, needed for the generation of gene-targeted mice were prepared from C57BL/6 mice. Female CD1 mice served as foster mothers. The SLy2 locus was inactivated in 129/Ola SvJ stem cells and backcrossed to C57BL/6 to yield SLy2$^{-/-}$ mice of MHC haplotype H-2b. The transgenic SLy2 overexpressing mice were generated by Miltenyi Biotech, Bergisch Gladbach, on 129/Ola SvJ background. Also these mice were backcrossed continuously to C57BL/6 during this study.

2.4. Primers

All primers used during this study were purchased from Metabion (Martinsried).

Table 7: Primers

Name	Sequence	Application
Type_SLy2-ko_for	GGATCTCATTGTGATTCCGTGG	5′ primer for typing of SLy2 gene-targeted mice
Type_SLy2-ko_wt rev	GACTTGGAGCTGTCAATGTAAC	3′ wt primer for typing of SLy2 gene-targeted mice
Screen_SLy2-ko_ko rev	GAGAATAGGAACTTCGGAATAGG	3′ ko primer for typing of SLy2 gene-targeted mice
Screen_SLy2-tg_for	CTGAAGGAGACTGTGGTTGAGTGGTGG	5′ primer for typing of SLy2 transgenic mice
Screen_SLy2-tg_rev	CGTAATCTGGAACATCGTATG	3′ primer for typing of SLy2 transgenic mice
SLy2_LA_for	TCCCCCGGGAGACAAGGAGAAACACCAAAAACC	Amplification of the long arm of homology
SLy2_LA_rev	AAATATGCGGCCGCAAAGTATATVTCGTVGTGTATCTGG	Amplification of the long arm of homology
SLy2_SA_for_XhoI	CCGCTCGAGGCCCTTGGCTACGTTTACAGC	Amplification of the short arm of

Name	Sequence	Application
		homology
SLy2_SA_rev_SalI	ACGCGTCGACGAGGCATTGGATGGCTTCCT	Amplification of the short arm of homology
Neo_hom-rec_for	CGCAGCAGCAGTTTTGGGAATTTTGACCGTTTTCGGAATAA TTCCGTATCGCCTTAACGTTGGAAAAGCTG	Amplification of the neo-gene for the fosmid based targeting construct
Neo_hom-rec_rev	CTCTTCTCCTGCTTCTGGGGACCTTTATCTTCTTAGGAGCTG CTTCCTCTTCCGATCGCCTAGGGGTAACC	Amplification of the neo-gene for the fosmid based targeting construct
TK_hom-rec_for	GGATCCCCGGGTACCGAGCTCGAATTCGCCCTATAGTGAG TCGTATTACAATCGAGCAGTGTGGTTTTGC	Amplification of the TK-cassette for the fosmid based targeting construct
TK_hom-rec_rev	GGTAACGCCAGGGTTTTCCCAGTCACGACGTTGTAAAACG ACGGCCAGTGAAGGTCATGAGATTATCAAAAAGG	Amplification of the TK-cassette for the fosmid based targeting construct
SLy2_5′ probe_for	GTTAACTGAGAACCACCCAG	Amplification of the 5′ flanking probe
SLy2_5′probe_rev	ACCTACCTTTCAATTTCATTGC	Amplification of the 5′ flanking probe
SLy2_3′probe_for	GCCTAAGACCAGAACTTCTAGC	Amplification of the 3′ flanking probe
SLy2_3′probe_rev	CCAGGCTGGCTTCTTCATGC	Amplification of the 3′ flanking probe
SLy2_cDNA_for_SwaI	ATTTAAATACCATGCTAAAGAGGAAGCCATCC	Amplification of the SLy2 cDNA
SLy2_cDNA_rev_PacI	TTAATTAATCACGCGTAATCTGGAACATCGTATGGGTAGTC ACT-GGATTCTGTGATGGC	Amplification of the SLy2 cDNA
SLy2_dNLS_for	ATCAAAGCTCTTTCTGAGGAAAAAG	Generation of a

Name	Sequence	Application
		NLS deficient SLy2 species
SLy2_dNLS_rev	TAGACTTCCTCCACTGCTTGAAG	Generation of a NLS deficient SLy2 species
SLy2_S23A-mut_for	CCGAAGCGCAGCGCTTTTGGGAATTTTGAC	Mutates the serine 23 to alanine
SLy2_S23A-mut_rev	GTCAAAATTCCCAAAAGCGCTGCTGCGCTTCGG	Mutates the serine 23 to alanine
SLy2_dSH3_for	TTAGAAGAGGAAGCAGCTCCT	Generation of a SH3 deficient SLy2 species
SLy2_dSH3_rev	GCCACAGAATGGCCCTGAGT	Generation of a SH3 deficient SLy2 species
SLy2_dSAM_for	GAAACCACTGTAGAACATGAAAAG	Generation of a SAM deficient SLy2 species
SLy2_dSAM_rev	TCTTCTCCTGCTTCTGGGGAC	Generation of a SAM deficient SLy2 species
SLy2-cDNA-hum_for_SwaI	AAAATTTAAATACCATGCTCAAGAGAAAGCCATCC	Cloning of the human SLy2 cDNA
SLy2-cDNA-hum_rev_PacI	AAATTAATTAATCACGCGTAATCTGGAACATCGTATGGGTA GTCACTTGGCTCTGTGATAATAATC	Cloning of the human SLy2 cDNA
Exon 5 rev	GTAGGGGCTGTCATCATCCAGTCG	Identification of upstream cDNA sequences in a RACE PCR (GSP-1)
Cortactin_cDNA-for	AAAGCTAGCACCATGTGGAAAGCCTCTGCAGG	Cloning
Cortactin_cDNA-rev	TTTCTCGAGCTGCCGCAGCTCCACATAG	Cloning
CD2-IC_cDNA-for	AAAGCTAGCACCATGTGCAAGAGGAGAAAACGGAACAGG	Cloning
CD2-IC_cDNA-rev	TTTCTCGAGATTAGGGGGCGGCAGTGAAACAC	Cloning
RhoA-GTPase_cDNA-for	AAAGCTAGCACCATGGCTGCCATCAGGAAGAAAC	Cloning
RhoA-GTPase_cDNA-rev	TTTCTCGAGCAAGATGAGGCACCCAGAC	Cloning
Cdc42-GTPase_cDNA-for	AAAGCTAGCACCATGCAGACAATTAAGTGTGTTG	Cloning

Name	Sequence	Application
Cdc42-GTPase_cDNA-rev	TTTCTCGAGTAGCAGCACACACCTGCGG	Cloning
Rac1-GTPase_cDNA-for	AAAGCTAGCACCATGCAGGCCATCAAGTGTGTG	Cloning
Rac1-GTPase_cDNA-rev	TTTCTCGAGCAACAGCAGGCATTTTCTCTTC	Cloning
3BP2_cDNA-for	AAAGCTAGCACCATGGCGGCTGAGGAGATGCAG	Cloning
3BP2_cDNA-rev	TTTCTCGAGCCTGGGCCCAGCGTAGCCG	Cloning
Cbl-b_cDNA-for	AAAGCTAGCACCATGGCCGGCAACGTGAAGAA	Cloning
Cbl-b_cDNA-rev	AAACTCGAGGGTGGCTACGTGAGCAGGAG	Cloning
CD34-IC_cDNA-for	AAAGCTAGCACCATGAACCGTCGCAGTTGAG	Cloning
CD34-IC_cDNA-rev	AAAGTGGAGCAGTTCTGTGTCAGCCACCA	Cloning
C3G-cDNA-for	AAAGCTAGCACCATGAGCAGCGGCCTCGGCCT	Cloning
C3G-cDNA-rev	AAACTCGAGGGTCTTCTCTTCGCGGTCTG	Cloning
DAB2_cDNA-for	AAAGCTAGCACCATGTCTAACGAAGTAGAAACAAGC	Cloning
DAB2_cDNA-rev	AAATCTAGACTAGGCAAAAGGATTTCCGA	Cloning
SLP65_cDNA-for	AAAGCTAGCACCATGGACAAGCTGAATAAGATAAC	Cloning
SLP65_cDNA-rev	ACACTGGAGTGAAACCTTCACAGCATATTTC	Cloning
SLP76_cDNA-for	AAAGCTAGCACCATGGCCTTGAAGAATGTCC	Cloning
SLP76_cDNA-rev	ACACTCGAGCAGACAGCCTGCAGC	Cloning
Gab1_cDNA-for	AAAGCTAGCACCATGAGCGGCGGCGAAGTGGTTTGCT	Cloning
Gab1_cDNA-rev	ACACTCGAGCTTCACATTCTTGGT	Cloning
RN-tre_cDNA-for	AAAGCTAGCACCATGATTCAAGTCTTGCAGCTTG	Cloning
RN-tre_cDNA-rev	AAACTCGAGCAGCAACACTGATTCCTGCA	Cloning

2.5. Plasmid vectors

2.5.1. Original vectors

Different original vectors, some of them commercially available, were used in the generation of plasmid constructs.

Table 8: Original vectors used to generate all constructs during this study

Description	Properties	Reference
pBluescript II KS +	AmpR, KanR, f1 ori, Col E1 ori, lac-Promotor, lacZ-Fragment, rop-	Stratagene, USA
pCR II-TOPO	Allows the direct cloning of PCR products by T/A cloning. AmpR, KanR, f1 ori, Col E1 ori, lac-Promoter, lacZ-Fragment	Invitrogen, Karlsruhe
pBS neo	pGK *neoR* poly A in pBluescript	K. Pfeffer, Düsseldorf
pGEM7 TK	Contains the thymidine kinase gene from Herplex Simplex Virus	K. Pfeffer, Düsseldorf
pWPI	Lentiviral, bicistronic expression	(Zufferey et al., 1998) und http://tronolab.epfl.ch

Description	Properties	Reference
	construct, containing the pEF2α promoter and an IRES controlled GFP gene.	
Rac1V12	Contains a GFP-tagged constitutively active form of rac1	(Ridley et al., 1992)
Rac1N17	Contains a GFP-tagged dominant negative form of rac1	(Ridley et al., 1992)
pEPIFos+SLy2 genomic sequences clone WI1-1784F7	ChloramphR, Basis for fosmid constructs	www.bacpac.chori.org
pBAD	Bacterial expression plasmid coding for λ-recombinases Redα and Redβ	Gene Bridges, Dresden
pSEC Tag	Expression of myc-tagged proteins	Invitrogen, Karlsruhe
p1026x	Contains a bipartite promoter with the lck-proximal promoter and the IgH enhancer	(Iritani et al., 1997)

2.5.2. Constructs generated during this study

Table 9 depicts all constructs which were cloned during this study, originating from the previously mentioned original vectors.

Table 9: Vectors generated during this study

Description	Original vector	Insert	Properties
Target vector (conventional cloning)	pBluescript II KS +	Short arm of homology, Long arm of homology, *neoR* and HSV-tk cassettes	Targeting constructs for homologous recombination in ES cells
Target vector (fosmid based cloning)	pEPIfos+SLy2 genomic sequences	*neoR* and HSV-tk cassettes	Targeting construct for the homologous recombination in ES cells
5' flanking probe	pCR II-TOPO	5'flanking probe (1000bp)	Contains the 5'flanking probe for the targeting of the SLy2 locus
3' flanking probe	pCR II-TOPO	3'flanking probe (1000bp)	Contains the 3'flanking probe for the targeting of the SLy2 locus
pWPI-SLy2-wt-HA	pWPI	SLy2-cDNA fused to an HA tag	Lentiviral SLy2 expression vector

Description	Original vector	Insert	Properties
pWPI-SLy2-ΔNLS-HA	pWPI	SLy2-ΔNLS-cDNA fused to an HA tag	Lentiviral SLy2 expression vector
pWPI-SLy2-S23A	pWPI	SLy2-S23A-cDNA fused to an HA tag	Lentiviral SLy2 expression vector
pWPI-SLy2-ΔSH3-HA	pWPI	SLy2-ΔSH3-cDNA fused to an HA tag	Lentiviral SLy2 expression vector
pWPI-SLy2-ΔSAM-HA	pWPI	SLy2-ΔSAMcDNA fused to an HA tag	Lentiviral SLy2 expression vector
Rac1V12+mCherry	Rac1V12	mCherry, red fluorescent protein, derivative of DS red	Eucaryontic expression vector for the simultaneous expression of Rac1V12 and Cherry
Rac1N17+mCherry	Rac1N17	mCherry, red fluorescent protein, derivative of DS red	Eucaryontic expression vector for the simultaneous expression of Rac1N17 and Cherry
pSEC Tag+cortactin	pSEC Tag	Cortactin cDNA	Expression of myc-tagged cortactin
pSEC Tag+CD2_IC	pSEC Tag	CD2_intracellular domain cDNA	Expression of myc-tagged CD2-intracellular domain
pSEC Tag+RhoA	pSEC Tag	RhoA cDNA	Expression of myc-tagged RhoA
pSEC Tag+Cdc42	pSEC Tag	Cdc42 cDNA	Expression of myc-tagged Cdc42
pSEC Tag+Rac1	pSEC Tag	Rac1 cDNA	Expression of myc-tagged Rac1
pSEC Tag+3BP2	pSEC Tag	3BP2 cDNA	Expression of myc-tagged 3BP2
pSEC Tag+Cbl-b	pSEC Tag	Cbl-b cDNA	Expression of myc-tagged Cbl-b
pSEC Tag+CD34_IC	pSEC Tag	CD34_intracellular domain cDNA	Expression of myc-tagged CD34 intracell. domain
pSEC Tag+C3G	pSEC Tag	C3G cDNA	Expression of myc-tagged C3G
pSEC Tag+DAB2	pSEC Tag	DAB2 cDNA	Expression of myc-tagged Dab2
pSEC Tag+SLP65	pSEC Tag	SLP65 cDNA	Expression of myc-tagged SLP65
pSEC Tag+SLP76	pSEC Tag	SLP76 cDNA	Expression of myc-tagged SLP76

Description	Original vector	Insert	Properties
pSEC Tag+Gab1	pSEC Tag	Gab1 cDNA	Expression of myc-tagged Gab1
pSEC Tag+RN-tre	pSEC Tag	RN-tre cDNA	Expression of myc-tagged RN-tre

2.6. Methods

2.6.1.Generation of mice

The gene-targeted mice described in this study were generated following standard protocols. The transgenic SLy2 overexpressing mouse line was generated by Miltenyi Biotech, Bergisch Gladbach.

2.6.1.1. Gene-targeted mice

The two following paragraphs describe the generation of the targeting constructs by two different methods. Both constructs were used to electroporate ES cells to obtain homologously recombined gene-targeted cells.

Conventional cloning strategy

The first targeting construct was generated by cloning of two arms of homology on either side of a neomycine resistance gene (*neoR*) gene. Both arms, the short and the long arm of homology, were obtained by PCR from genomic E14 DNA and cloned into pBluescript by standard cloning techniques. Targeted disruption of the locus was achieved by placing a *neoR*-cassette between both regions of homology that would be inserted into the genomic SLy2 locus upon homologous recombination. To allow negative selection of not homologously recombined clones, a *HSV-TK* cassette was inserted 3' of the long arm.

Fosmid derived cloning strategy

As the frequency of homologous recombination increases with the length of both arms of homology, a new technique was applied to construct the second targeting vector. This method makes use of fosmid vectors, which consist of a long stretch of genomic DNA (~40-60kb) cloned into a plasmid, allowing for propagation in *E.coli* in the presence of chloramphenicole. To generate a targeting construct, a *neoR*-cassette was inserted via homologous recombination (Red/ET cloning system, Gene Bridges, Dresden) into the target site. The first step in an ET cloning reaction was the electroporation of the fosmid carrying *E.coli* with an inducible bacterial expression plasmid (pBAD) for the λ-recombinases Redα and Redβ that contains a temperature-sensitive origin of replication (*oriR101*), allowing propagation of the plasmid only up to 30°C. This rendered the bacteria

chloramphenicole/tetracycline double resistant. These double resistant clones were picked, grown and expression of the recombinase was induced by addition of L-arabinose (20µl of a 1M solution) and incubation of the cells at 37°C. Subsequently, 200ng of the *neoR*-cassette containing short arms (50bp on either side) homologous to the site of insertion, was electroporated into the bacteria. The arms of homology were added to the *neoR*-gene by PCR with the primers shown in chapter 2.4. As the *neoR*-cassette contains a kanamycine resistance gene, it rendered the bacteria harbouring a successful recombination event double resistant against chloramphenicole and kanamycine. Double resistant clones were picked and recombination was assessed by PCR, restriction digest and finally by southern blot. The *HSV-TK* cassette was inserted 3' of the homology region with the same method, using an expression cassette with an additional ampicilline resistance gene.

Culture of murine embryonic fibroblasts (EF) and stem cells (ES)

EF served as feeder cells for ES cell culture, supplying the stem cells with the necessary growth factors. To prevent overgrowth of the ES cells by the EF cells, the latter were mitotically inactivated by treatment with mitomycin C for 2.5 hours at 37°C. Afterwards, the cells were washed twice with PBS and the ES cells were plated on top. For the generation of EF cells, E14.5 mouse embryos were sacrificed and, after removal of head and fetal liver, pushed through a 70 µm cell strainer to obtain single cells. The resulting fibroblasts were propagated for 4 days and storage frozen at $5x10^6$/vial.

The medium for ES cell culture was generally supplemented with LIF, to prevent differentiation of the cells. The undifferentiated state of the ES cell colonies was determined by their morphology. An undifferentiated colony has an elliptic shape, with sharp borders and a shiny appearance. Upon differentiation, the colonies develop pseudopodia and become grey, granulated and dimly coloured.

Electroporation of ES cells

ES cells were transfected by electroporation with one of the SLy2 targeting constructs.

On the day of transfection, the cells were trypsinised and $5x10^7$ were resuspended in 7ml of ES cell medium. 200µg of the linearised targeting construct were solubilised in 1ml PBS and mixed with the cells. 800µl of this mix were transferred to each electroporation cuvette and electroporated in a Biorad Gene pulser II at 340V and 250µF. After 10min incubation on ice, the cells were resuspended in prewarmed ES medium and the content of each cuvette was plated on two EF cell covered 10 cm dishes.

Selection of recombinant ES cells

After electroporation, the ES cells were cultivated for 24h without antibiotics. Thereafter the medium was supplemented with 200µg/ml neomycine and from day 4 on additionally with 2 µM ganciclovir. This double selection favored cells that had incorporated the targeting construct (neomycine-selection), but had done so in a homologously recombined fashion, without incorporation of the *HSV-TK* gene (ganciclovir selection).

Detection of homologously recombined clones

On day 10 after electroporation the surviving colonies were washed twice with PBS, harvested in 20µl PBS with a sterile pipette and each one was transferred to one well of a 96-well plate. The colonies were separated to single cells by trypsinisation and each well was supplemented with EF cells. After two days, two thirds of each well were transferred to an EF covered 48-well plate and the remaining third was further propagated in the 96-well plate. Again two days later, the cells on the 48-well plates were trypsinised, mixed 1:1 with 2x cell-freezing-media and stored at -80°C. The colonies in the 96-well plates split to three gelatine coated flat bottom 96-well plates. After cultivation for another week with a daily change of media, the genomic DNA was prepared and analysed by southern blot for homologously recombined clones.

Superovulation of donor animals

To maximize the number of blastocysts to be harvested from the C57BL/6 donor mice, these were superovulated. On day -6 before injection, the donor mice were injected IP with 100µl PMSG (pregnant mare serum gonadotropin) around 4.00h p.m. Two days later around 2.00h p.m., the same mice were injected IP with 100µl hCG (human chorion gonadotropin) and directly mated to C57BL/6 males. This treatment yielded the E 3.5 blastocysts needed for ES cell injection.

Generation of chimeric mice

The C57BL/6 donor blastocysts were injected each with approximately 20 homologously recombined ES cells and 10-20 of such manipulated blastocysts were implanted into CD1 foster mothers, which had been mated to vasectomised males to confer a state of mock pregnancy. 19 days later the offspring was born. The degree of chimerism could be deduced from the colour pattern of the coat a week later. Upon six weeks of age, the chimeric mice were mated to C57BL/6 animals and the resulting offspring was analysed for germ line transmission of the mutation by analysis of coat colour and subsequently by southern blot and PCR.

Typing of mice with the targeted allele

DNA prepared from tail biopsies served as typing PCR template. The PCR typing strategy applied to identify the gene-targeted animals made use of a three primer multiplex PCR system with one forward primer and two reverse primers, one complementary to the wildtype and the other to the targeted locus. This system yielded a 1000 bp band for the wildtype locus and a 750 bp fragment for the targeted locus.

2.6.1.2. Transgenic mice

Generation of a transgenic, SLy2 overexpressing mouse line

To analyse the effect of a constitutive overexpression of SLy 2 in primary lymphocytes, a transgenic mouse line was established. The mice were generated by Miltenyi Biotech, through pronucleus injection of a SLy2 expression construct into 129/SvJ Ola zygotes. The expression construct contained a SLy2 cDNA cloned behind a chimeric promoter combining the proximal *lck*-promoter and the *IgH*-enhancer, resulting in a robust expression in T and B cells (Iritani et al., 1997).

Typing of transgenic mice

Transgenic mice were identified by a PCR, amplifying a 650bp fragment from inside the transgenic expression construct. Mice carrying two transgenic alleles were identified by real time PCR with the following primers and probe set. A PCR for INFβ served as internal control.

Table 10: Primers and probes used in typing of homozygous transgenic animals

Gene	Forward primer	Reverse primer	Probe sequence
SLy2 transgenic allele	aatacatcaaagctctttctgagga	tgggatcactgttccgatatg	ggagagga, Probe #55
INFβ	caggcaacctttaagcatcag	cctttgacctttcaaatgcag	ctgggact, Probe #95

2.6.2. Generation and maintenance of transgenic cell lines

2.6.2.1. General maintenance

Splitting and passaging

Adherent cells were passaged every second day. The cells were washed once with PBS and trypsinised at 37°C until detached from the plate. The trypsin was inhibited by addition of medium, the cells were centrifuged and 1/10 was seeded again. Cells growing in suspension were split 1 to 5 every second day.

Freezing and thawing

Adherent cells were trypsinised, centrifuged and resuspended in 1x freezing medium. Suspension cells were harvested, centrifuged and resuspended in 1x freezing medium. To ensure a slow cooling process, the filled freezing vials were first stored at -20°C for 30 min and then transferred to -80°C afterwards. For long term storage, the vials were kept in liquid nitrogen.

For thawing, the vials were incubated in a 37°C waterbath and the cells were quickly transferred to prewarmed medium. Washing removed the DMSO and the cells were seeded.

Determination of cell numbers

To determine the concentration of a cell suspension, the cells were mixed with trypane-blue (0.16% in PBS) to stain dead cells, transferred to a Neubauer counting chamber and counted under the microscope.

2.6.2.2. Lentiviral transduction of cells

The lentiviral vectors used during this study are unable to replicate and follow the lentiviral replication cycle only until the integration into the host genome. The lentiviral system applied here was of the second generation, with the genes necessary for virus production being divided to three different plasmids. Transient transfection of 293FT cells with these plasmids resulted in generation of viral particles (Zufferey et al., 1998).

The first plasmid, pWPI (Klages et al., 2000) contained the SLy2 cDNA (wildtype or different mutated forms) under the control of an EF1-α promoter. The cDNA was followed by an IRES (internal ribosome entry site) which preceeded an open reading frame for green fluorescing protein (eGFP). This bicistronic expression construct ensured expression of the SLy2 and eGFP in every transduced cell, allowing the determination of transduction efficiency by flow cytometry. Two sequences important for integration and packaging, the long terminal repeats (LTRs) flanked the expression cassette on either side. The construct contains deletions in the U3 region of the 3' LTR, which serves as template for the 5' LTR during reverse transcription, resulting in deletions in the lentiviral promoter upon integration of the proviral DNA. This disables the transcription and leads to the autoinactivation of the vector. The second plasmid codes for the packaging genes *gag, pol* and *rev*. The vector pCMV-dR8.74psPAX2 used in this study, is deleted for additional viral genes, as *vpr, vif, vpu* or *nef* (Zufferey et al., 1998). The third plasmid contains the cDNA for the G protein of the vesicular stomatitis virus (VSV-G) serving as viral envelope protein.

Production of viral particles

On the day before transfection, 2-3x10^6 293FT cells were seeded onto a 10 cm dish. The next day the cells were transfected by calcium-phosphate. 20µg of the respective pWPI construct were mixed with 15µg of PAX2 and 5µg of VSV-G. The mixture was filled up to 250µl with 2.5 mM HEPES and mixed with 250µl $CaCl_2$. While continuously vortexing, the DNA/$CaCl_2$ mixture was dropwise added to 500µl 2xHEBS and then incubated at RT for 30 min for complex formation. The medium on the 293FT dishes was changed to FCS free DMEM and the DNA mix was added to the cells. After incubation for 5 hours, the FCS free medium was discarded and 6ml of normal 293FT medium were added. The viral particles were harvested 48 hours later by gathering the supernatant of the transfected cells and centrifugation at 1200 rpm for 10 min to remove cell debris. Afterwards, the supernatant was divided to 2ml freezing tubes, snap-frozen in liquid nitrogen and stored at -80°C

Generation of stably transduced cell lines

For the transduction of adherent cells, 1x10^4 cells were seeded into each well of a 24-well plate the day before transduction. The next day, the medium was removed and 500µl of lentiviral supernatant, supplemented with 4µg/ml polybrene, were added to the cells. To enhance the transduction efficiency, the plates were centrifuged for 2 hours at 1200 rpm and 32°C. After centrifugation, the cells were incubated at 37°C for 3-5 hours, after which the supernatant was diluted with 500µl. The cells remained in this diluted supernatant overnight. The transduction procedure for suspension cells was essentially the same, with the exception, that the 1x10^4 cells were harvested on the day of transduction and resuspended in lentiviral supernatant supplemented with 8µg/ml polybrene. As the transduction efficiency of Jurkat cells was somewhat lower than that of HeLa, the former were transduced twice on two following days. This treatment routinely yielded 85%-96% transduced cells, as determined by flow cytometry.

2.6.2.3. Additional transfection methods

Calcium-phosphate transfection

293T and 293FT cells were routinely transfected with Ca-phosphate as described in chapter 2.6.2.2., to perform expression and interaction studies with different SLy2 constructs and additional proteins.

FuGENE 6

To transfect HeLa cells FuGENE 6 (Roche, Mannheim) was used, following the instructions of the manufacturer. Briefly, 7x10^4 cells were seeded into each well of a 6-well plate on the day before transfection. For each well, 8µl of FuGene reagent were mixed with 92µl serum-

free DMEM. After incubation for 5 min at RT, this mixture was added to 4µg of the respective plasmid DNA, followed by 15 min incubation at RT. The transfection mix was added to the cells, which were analysed 24h-48h later.

2.6.3. Cell culture experiments

2.6.3.1. Spreading assay

Transgenic HeLa cells

To determine the spreading capacity of HeLa cells expressing different SLy2 mutants, the cells were detached from the dish by treatment with 0.05 mM EDTA. No trypsine was added, to maintain the integrity of the cellular surface molecules. 2-4x10^4 cells were seeded onto a gelatine coated cover glass. Cells were allowed to adhere for 45 min, washed with PBS once and fixed in 4% PFA for 15 min, followed by staining for filamentous actin (F-actin) and nuclei with phalloidine and DAPI, respectively. The spreading index of each cell was determined as the ratio of cell length and cell width.

Transgenic primary splenocytes

Lymphocytes, activated through their antigen receptors, show a distinct choreography of spreading and contraction at their contact site to an antigen bearing surface.

The spleens of SLy2 transgenic mice and wildtype littermates were isolated semi-sterile. Pushing the organs through 70 µm cell strainers yielded a single cell suspension, which was centrifuged and resuspended in 1ml erythrocyte-lysis buffer per spleen and incubated at RT for 5 min. Lysis was stopped by addition of 10ml PBS and cells were recovered by centrifugation. The cells were MACS separated into $B220^+$ and $CD90^+$ fractions and were stimulated one hour with αCD40 and IL-4 (5µg/ml and 10ng/ml) or αCD3 and CD28 (10µg/ml), respectively. After stimulation, 1x10^6 cells were seeded onto cover glasses coated with αIgM or αCD3 and allowed to adhere on ice for 30 min. To induce spreading, the cells were incubated at 37°C followed by fixing with 4% PFA (37°C/ 8 min) after different timepoints, ranging from 1-30 min. Again, F-actin and nuclei were stained and the spreading index was determined as the size of the area of adherence.

2.6.3.2. Proliferation assay

BrdU pulse-chase

As opposed to the previously described ^{3}H-thymidine incorporation assay, a BrdU pulse-chase experiment allowed the determination of the proliferation rate over a much larger time. The rate of proliferation is deduced from the decline of the BrdU content of the cells. 1x10^5 cells were seeded per well of a 6-well plate. The cells were pulsed by incubation in

BrdU-supplemented medium (10µg/ml) for eight hours, after which they were washed and normal medium was added. To chase, half of the cells of each well were harvested daily, stained for BrdU and analysed by flow cytometry. Staining was performed according to manufacturer's instructions. Briefly, the cells were washed with PBS, resuspended in 70% EtOH and fixed at 4°C for at least 30 min. Histones were extracted by resuspending the cells in 100 mM HCl/0.5% Triton-X-100 and incubation on ice for 10 min. Cells were centrifuged, resuspended in ultrapure H_2O and genomic DNA was denatured at 95°C for 10 min. Thereafter, cells were washed once with PBS/0.5% Triton-X-100 and stained with αBrdU-PE in PBS/1% BSA for 30 min at RT. The percentage of $BrdU^+$ cells was determined by FACS analysis.

2.6.4. Biochemical assays

2.6.4.1. SDS-polyacrylamide gel electrophoresis and Western blotting

SDS-polyacrylamide gel electrophoresis was used to separate proteins according to their molecular weight. The determination of the analysed proteins was facilitated by a simultaneously applied molecular weight standard (GE Healthcare, Braunschweig). After the gel content had been transferred to a nitrocellulose membrane, proteins were detected by specific antibodies and appropriate secondary reagents.

Sample preparation from cultured cells

For lysis, the cells were washed once with PBS, centrifuged and resuspended in lysis buffer, supplemented with various proteinase and phosphatase inhibitors. To maximize the lysis efficiency, the lysates were incubated rotating 15 min at 4°C and cleared by centrifugation at 13000 rpm for 10 min afterwards. Sample loading buffer was added 1:5 to each sample and proteins were denatured at 95°C for 5 min. Samples were stored at -20°C.

Sample preparation from mouse organs and blood

Organs were taken semi-sterile from mice and homogenised in lysis buffer with an ultra-turrax (speedlevel 6, 5-10 sec). After incubation on ice for 15 min the lysates were cleared by centrifugation and the protein concentration was determined by a BCA-assay. Lysates were mixed 1:5 with sample loading buffer and proteins were denatured at 95°C for 5 min.
Blood samples were depleted of erythrocytes prior to lysis. This was achieved by applying lympholyte M solution according to the instructions of the manufacturer. Lysis of the recovered cells was performed as previously described.

Gel electrophoresis, blotting and detection

The protein samples were separated on 4%-12% or 10% polyacrylamide gels. Routinely, pre-cast minigels from Invitrogen were applied. Only IPs of ^{35}S labelled lysates were separated on large, individually cast 10% polyacrylamide gels. For separation, up to 30µg of total protein were loaded into each sample loading pocket and the samples were separated electrophoretically at 100-200V with constant voltage for 1-2 hours.

The proteins were transferred to a nitrocellulose membrane in a wet-blotting-device (Invitrogen, Karlsruhe), according to the manufacturer's instructions. Afterwards the membrane was blocked with 3% skim milk powder in TBS-T for one hour at RT, to prevent unspecific binding of the antibodies. Incubation with the first antibody, specific to the respective protein, was perfomed in 3% skim milk/TBS-T at 4°C overnight. Afterwards, the membrane was washed three times with TBS-T for 5 min each at RT, followed by incubation with the secondary antibody, coupled to peroxidase, again in 3% skim milk/TBS-T for one hour at RT. The membrane was again washed three times with TBS-T for 5 min. Signals were detected with X-ray films, after a one-minute incubation of the membranes in a 1:1 mixture of ECL solutions 1 and 2.

2.6.4.2. Immunoprecipitation (IP)

Immunoprecipitation allows the analysis of physical interactions between proteins in a cell-lysate. The primary protein is bound by a specific antibody and the resulting immuno-complex is precipitated by binding to protein A- or protein G-coupled agarose beads. Analysis of the precipitates by western blotting reveals coimmunoprecipitated interaction partners of the primary protein. In the present study, IPs were mostly performed with αHA antibodies to precipitate different HA-tagged SLy2 species.

The cells were lysed as previously described and the antibody was added to the cleared lysate, followed by a rotating incubation at 4°C overnight. Washed agarose beads were added and again incubated rotating for 1 hour. The beads were washed four times with increasing salt conditions and proteins were eluted in 2.5x sample loading buffer at 95°C for 10 min. The composition of lysis and wash buffers is shown in chapter 2.2.1.

Alternatively an α–HA pre-coupled agarose (Sigma-Aldrich, Taufkirchen) was applied.

Table 11: Antibodies and agarose-species used in IPs

Antibody	Target/epitope	Species	Working concentration	Agarose	Manufacturer
Anti-HA	HA-tag	Rabbit	1:200	Protein-A agarose	Sigma-Aldrich, Taufkirchen
Anti-HA	HA-tag	Mouse	1:200	Protein-G agarose	Sigma-Aldrich, Taufkirchen
Anti-HA agarose	HA-tag	Mouse	1:300		Sigma-Aldrich, Taufkirchen
α-cortactin	Cortactin	Rabbit	1:125	Protein-A agarose	Cell Signalling, USA

2.6.4.3. Separation of G- and F-actin fractions

Actin occurs in two different states inside a cell, either the monomeric, globular (G-) form or the polymeric, filamentous (F-) form. The ratio of the G- to the F-state changes constantly, e.g. upon cell migration or lamellipodia formation and can be influenced by a plethora of stimuli. Many actin associated proteins localise specifically to one or the other fraction inside a cell. To analyse the amount of SLy2 recruited to either the G- or the F-actin fraction, one 10 cm dish of HeLa cells was lysed with 2ml actin-stabilisation-lysis-buffer. Lysates were recovered with a cell scraper and transferred to polyallomer ultra centrifuge tubes (Beckman-Coulter, USA), followed by centrifugation for 20 min at 4°C with 32000 rpm through a glycerol gradient in a Beckman Ultracentrifuge L60 (SW 55 Ti Rotor, and corresponding buckets). This resulted in a pellet fraction (F-actin) and the supernatant, representing the cytosolic G-actin fraction. The latter was recovered and the pellet was resuspended in lysis buffer containing 5 µM Cytochalasin D, stabilising the F-actin. Both fractions were mixed with sample loading buffer and denatured for 10 min at 95°C. The pellet samples were additionally ultrasonified to shear the genomic DNA, thereby reducing the viscosity. Corresponding amounts of each fraction were analysed by western blotting.

2.6.4.4. Identification of binding partners by ^{35}S-labelling

The identification of interaction partners by ^{35}S-labelling essentially relies on immunoprecipitation and allows the highly sensitive analysis of the interaction partners of a protein, without the need for specific antibodies. To radioactively label the cellular proteins, the cells were starved in medium lacking methionine and cysteine for 24 hours

and then supplemented with radioactively labelled species of these aminoacids (Redivue pro mix, GE Healthcare, Munich) for 10 hours. Afterwards, the cells were treated with different stimuli, washed and lysed. HA-tagged SLy2 was precipitated from the lysates and the IPs were separated on polyacrylamide gels. The gels were fixed and dried as described and exposed to X-ray films.

2.6.5. Immunofluorescence and confocal imaging

2.6.5.1. Preparation of samples

Adherent cells were seeded onto gelatine coated cover glasses (Ø=1.3 cm) in a 24-well plate one day before staining, if not otherwise stated. For gelatinisation, the cover glasses were incubated with PBS/0.2% gelatine for at least 30 min at 37°C. If stimuli were used, the cells were treated on the cover glasses, just prior to staining.

2.6.5.2. Staining procedure

The complete staining procedure was performed in the 24-well plate on an orbital shaker at RT in the dark. The cells were washed at least once with PBS and fixed in 4% PFA for 15 min, washed once with PBS and permeabilised in PBS/0.05% saponine for 15 min. To avoid unspecific binding, the samples were blocked with 2% goat serum in PBS with 1/10 permeabilisation solution for 20 min, prior to incubation with the primary antibody in PBS with 1/10 blocking buffer for at least one hour. Unbound antibody was removed by three consecutive washes with 10% permeabilisation buffer, 5 min each. Subsequently, the samples were incubated with the fluorescently labelled secondary antibody and eventually phalloidine, both in 10% blocking buffer for 45 min. Unbound secondary antibody was removed by two PBS washes and nuclei were stained with DAPI for 3 min, followed by two final washing steps. For conservation, the samples were mounted with Fluoromount-G on clean object slides, and left to dry for at least one day prior to microscopic analysis.

Alternative staining protocol

To stain less abundant proteins (cortactin) a slightly modified protocol was applied. After fixation, the cells were permeabilised and blocked in PBS with 5% goat serum and 0.3% Triton-X-100 for one hour. The samples were incubated with the primary antibody at 4°C over night in PBS with 2% BSA and 0.3% Triton-X-100, followed by repeated washing with PBS and incubation with the secondary antibody for 1 hour at RT. Afterwards, the samples were treated identical to the previous protocol.

2.6.5.3. Confocal imaging and analysis

All images were taken with a Zeiss LSM 510 and 40x or 63x objectives.

Table12: Fluorophores used in the study with excitation and emission spectra

Fluorophore	Excitation wave length	Emission wave length	Colour
DAPI	350 nm	470 nm	Blue
GFP	488 nm	509 nm	Green
Cy3	554 nm	568 nm	Orange
TRITC	557 nm	576 nm	Orange
mCherry	587 nm	610 nm	Red
Alexa-633	633 nm	647 nm	Far-red

Cell sizes were determined with the Zeiss LSM Image Browser. The colocalisation studies were performed with ImageJ (NIH) and the plugin "Colocalisation-RGB", with the threshold for each colour set to 50-70 points. Colocalised pixels appear white in the merged images.

2.6.6. Flow cytometry (FACS Analysis)

Flow cytometry is a powerful tool to qualitatively and quantitatively analyse different cell populations. Cells or other particles, marked with a fluorescently labelled antibody, are suspended in PBS and pushed with high pressure through a fine nozzle. This yields a thin stream of droplets, each surrounding a single cell that passes a laser, scattering the laser light. Additionally the fluorescent label is excited and emits light of a specific wavelength. The scattered and the emitted light are detected by so called photo-multipliers. The scattered light delivers information about the size and the granularity of the cells, whereas the emitted light reveals the existence of bound antibodies. Upon permeabilisation of the cell membrane with detergents or alcohol, also intracellular targets can be stained. The application of multiple lasers and detectors facilitates the analysis of multiple fluorescently labelled markers on one cell at the same time, provided non-overlapping emission spectra. All FACS analyses were performed at a FACSCanto flow cytometer (BD, Heidelberg). Data were analysed with FlowJo software.

2.6.6.1. Fluorescent labelling of surface markers

The cells were suspended in FACS staining buffer. Splenocytes, thymocytes and bone marrow cells were incubated with Fc-block for 5 min prior to staining, to prevent unspecific binding of antibodies to the cells. Cells were stained with the primary antibody for 20 min on ice. Unbound antibody was removed by washing with FACS staining buffer and cells were subsequently stained for 20 min on ice with the secondary antibody or fluorescently labelled streptavidin (in case of biotin labelled primary antibodies). Repeated

washing removed unbound antibodies, and the cells were resuspended in FACS staining buffer before analysis.

2.6.6.2. Staining of intracellular epitopes

Intracellular FACS staining was only performed in the BrdU pulse-chase experiments. The staining protocol is described in chapter 2.6.3.2.

2.6.7. Molecular biology

2.6.7.1. Agarose gel electrophoresis

Analytic gel electrophoresis

Agarose gel electrophoresis was used to separate DNA fragments according to their size. The method makes use of the property of DNA to migrate in an electric field from the negative to the positive pole. The size dependent separation is facilitated by the negative correlation of fragment size and migratory speed, the latter being inverse proportional to the logarithm of the molecular weight of the fragment. Added ethidium bromide (EtBr) intercalates into the DNA and thus allows the visualisation of the fragments in UV light.

Agarose gels used ranged from 0.7% to 3% and were prepared by boiling of the respective amount of agarose in TAE buffer until a clear solution was obtained. Upon cooling to ~40°C EtBr (4µg/ml) was added and the mixture was cast into a gel tray containing combs to form pockets for later loading of DNA samples. After setting of the gel, the combs were removed and the gel was transferred to a TAE filled running chamber and an electric current ranging from 30-120 mA was applied after the DNA samples had been loaded to the pockets.

Preparative gel electrophoresis

To isolate fragments of a specific length from a mixture of DNA molecules, the sample was separated on an agarose gel and the respective bands were be excised under UV light with longer wave length (325 nm). The DNA was isolated from the piece of gel using the QIAquick Gel Extraction Kit (Qiagen, Hilden) according to the instructions of the manufacturer.

2.6.7.2. Isolation of plasmid DNA

Qiagen Kits were used for the isolation of plasmid DNA to obtain DNA with the highest possible purity for cloning, transfection and sequencing reactions. Depending on the culture size, Mini or Maxi preparations were carried out. The purification was done according to the manufacturer's instructions.

Alcalic lysis

Alcalic lysis (Birnboim and Doly, 1979; Zufferey et al., 1998) was applied to prepare the plasmid DNA from a large number of clones for subsequent restriction analysis. The bacteria were lysed at 4°C with SDS and NaOH, leading to the denaturation of RNA, DNA and proteins. The subsequent neutralisation step results in the renaturation of the plasmid DNA, but not the much larger genomic DNA molecules. The latter are precipitated by SDS together with RNA and proteins. After clearance, the plasmid DNA can be precipitated from the lysate by addition of ethanol.

Experimental protocol I(conventional plasmid preparation) :

Clones to be analysed were picked into 2ml LB-medium, containing the appropriate selective agent and cultivated shaking over night at 37°C. 1.5ml over-night-culture were pelleted at 13000 rpm the next day and resuspended in 250µl solution I. The addition of 250µl solution II and the subsequent gentle mixing resulted in the lysis of the cells and the previously described denaturation. Renaturation/precipitation was achieved by adding 250µl solution III, mixing and a 5 minute incubation on ice. The lysate was cleared through centrifugation at 13000 rpm for 15 min and transferred to a new reaction tube. Subsequently, 0.8x volumes of isopropanol were added to precipitate the plasmid DNA, which was pelleted by centrifugation (13000 rpm, 30 min). The DNA was washed with 70% ethanol to remove residual salt and solubilised in 50µl TE buffer after drying.

Experiment al protocol II (fosmid preparation):

Due to the large size of the fosmid and BAC vectors, a slightly different purification protocol was applied. The cells of a 500ml overnight culture were pelleted and lysed in 36ml of Buffer I. The addition of equal volumes of buffers II and III lead to the lysis, denaturation and subsequent renaturation of the fosmid DNA. Lysates were cleared by passing through a whatman filter paper and the DNA was precipitated by the addition of an equal amount of isopropanol. Precipitates were collected by centrifuging and solubilised in 10ml of equilibration buffer. This DNA solution was added to a preequilibrated Maxi-prep column and the fosmid DNA was washed, eluted and purified according to the manufacturer's instructions. Because of the low copy number of fosmid vectors, 500ml of bacterial culture yielded only around 100µg of DNA.

2.6.7.3. Preparation of genomic DNA

From ES cells in 96-well plates

To prepare the genomic DNA of ES cells for the subsequent southern blot analysis, the cells were lysed over night at 56°C in a humid chamber with 50µl ES cell lysis buffer/well. After cooling to room temperature, 100µl ethanol were added to each well and incubated for one hour at RT, until white strands of DNA were visible. Three washes with 70% ethanol removed residual salts and the DNA was dried completely before the restriction mix was added.

From ES cells grown in dishes

ES cells from 5-10 cm dishes were harvested by trypsinisation, washed in PBS once and lysed overnight at 56°C in 10ml ES cell lysis buffer/10 cm dish. The lysate was divided to ten 2ml reaction tubes and vortexed together with 1ml of phenol. After centrifugation, the upper phase was recovered and transferred to a new reaction tube. Mixing and vortexing with an equal amount of chloroform removed the residual phenol and again the aqueous phase was transferred to a new tube. The DNA was precipitated with an equal amount of isopropanol. The white DNA strands were recovered with a plastic pipette tip, dipped once into 70% ethanol to remove residual salt and solubilised in at least 200µl TE buffer.

From mouse tail biopsies

The DNA needed for PCR typing of SLy2 ko and SLy2 transgenic mice was gathered from mouse tail biopsies, taken at least 3 weeks after birth. Mouse tails were lysed overnight, shaking at 56°C in 500µl TNE buffer each, supplemented with 100µg/ml Proteinase K. The lysates were cleared by centrifugation at 13000 rpm for 15 min and the supernatant was transferred to a new 1.5 ml reaction tube. The DNA was precipitated by addition of 500µl isopropanol and pelleted by centrifugation at 13000 rpm for 30 min. The pellet was washed in 70% ethanol and 50-150µl TE buffer were added, depending on the size of the pellet. The DNA was solubilised one hour at 56°C and at least 24h at 4°C before used in PCR reactions.

2.6.7.4. Restriction of DNA

The enzymes used for DNA restriction analyses were generally purchased from New England Biolabs (NEB) or MBI Fermentas, and applied according to the instructions of the manufacturer.

Plasmid DNA

Plasmid DNA was digested at the appropriate temperature with 1x buffer and BSA where necessary. At least 5 units of enzyme were used for each µg and digestion was carried out 2 hours or more.

Genomic DNA

Due to the harder accessibility of genomic DNA or the contamination with residual salts, RNAs and proteins, especially in the 96-well DNA preparations, a different digestion protocol was applied for genomic DNAs. In addition to 1x buffer, every reaction contained 1x BSA, 1 mM DTT and RNase A. Samples were digested at least for 4 hours, in case of the 96-well digests over night in a humid chamber.

2.6.7.5. Preparation of total cellular RNA

To avoid RNase contamination, all RNA work was done with a special set of pipettes, tips and tubes and only DEPC treated water was used in all reactions.

RNA from different mouse tissues was isolated with the Fluka RNA isolation kit according to the instructions of the manufacturer. Solid organ samples were homogenised in solution D prior to RNA isolation, whereas blood was lysed completely in solution D, without previous removal of erythrocytes. The concentration of the isolated RNAs was determined photometrically and the samples were stored at -80°C to minimize decay.

2.6.7.6. Polymerase chain reaction (PCR)

PCR uses the property of DNA polymerases to synthesise a new double stranded DNA molecule from a single strand. Repeated denaturation and polymerisation leads to an exponential amplification of a specific DNA sequence (Mullis et al., 1986). To start amplification, the polymerase needs a small double stranded part of DNA, which is generated by a 20-30 bp primer that hybridises complementary to the original strand. This short double stranded stretch is then elongated at the 3' end. As the original (template) strand is denatured to single strands by heat in every cycle, a thermostable enzyme has to be used, which is derived from the bacterium *Thermus aquaticus*. The constant repeats (up to 35) of denaturation, primer annealing and elongation yield the exponential amplification mentioned previously.

Table 13: Composition of a standard PCR reaction

Reagent	Volume
DNA	10ng-200ng
Forward primer (20-100 µM)	1µl
Reverse primer (20-100 µM)	1µl
dNTP	1µl
10x buffer	5µl
Taq-Polymerase (5 units/µl)	1µl
H_20_{bidest}	ad 50µl

The sequences of all primers used in this study are listed in chapter 2.4.

PCR reactions were assembled on ice, the reaction mix was quickly vortexed and centrifuged. The annealing temperature of each primer was deduced from its length and base composition. The elongation time could roughly be estimated as 1 minute per kb.

Table 14 shows a typical PCR program.

Table 14: Standard conditions for PCR reactions

Temperature	Time	Objective	Cycle (replication 30-35 times)
95°C	3 min	Initial denaturation of the DNA	
95°C	20 sec	Denaturation	X
55-68°C	30 sec	Annealing of primers	X
68-72°C	variable	Amplification of the complementary strand	X
4°C	infinite	Pause	

Real Time PCR

Real Time PCR represents a special PCR technique, which allows the quantitative determination of copies of a given sequence inside a complex pool of DNA molecules (e.g. a pool of tissue cDNAs).

The method utilises of a pair of primers yielding the amplification of a small DNA fragment (~70 bp) from the respective sequence. After the heat induced strand separation, an initially quenched, fluorescently labelled DNA probe binds sequence specific to the strand, thereby emitting a light signal. This signal is detected and the quantity of signals for each sample is determined by the light cycler.

During the present study Real Time PCR was applied to differentiate between mice that carried one or two alleles of the SLy2-transgene. The primers and probes are depicted in chapter 2.6.1.2.

Rapid amplification of cDNA ends PCR (RACE PCR)

RACE PCR allows the amplification of cDNA molecules without knowing the specific sequence on both sides of a given stretch of DNA. Accordingly it is used to determine the unknown upstream or downstream sequences of cDNAs. During the present study only 5' RACE was performed, with a special oligonucleotide used as upstream primer in reverse transcription that binds unspecifically, but preferentially to 5' RNA ends. During this study RACE was applied to RNAs isolated from wildtype and gene-targeted mice to determine the nature of the message found in the first SLy2 gene-targeted mouse.

All RACE reactions were conducted using the SMART RACE cDNA amplification kit by Clontech and were done according to the instructions of the manufacturer. The gene specific primers (GSPs) used in reverse transcription and RACE PCR are described in chapter 2.4.

2.6.7.7. Southern blot analysis

Southern blot allows the sequence specific detection of DNA fragments (Southern, 1975), generated by a restriction digest and size-separated by agarose gel electrophoresis. The fragments are blotted to a positively charged nylon membrane and hybridised sequence specific by a radioactively labelled probe. By exposition to an X-ray film the bands can be visualised.

Electrophoresis and blotting

20µg of genomic DNA per sample were restricted as described and subjected to electrophoresis. With respect to the large quantity of different fragments the gels were run over night at a very low voltage (≤40V) to ensure optimal separation also of larger fragments. Subsequently the gels were incubated shaking for 20 min in 0.25 M HCl to partially depurinate the DNA fragments, which resulted in breakage, ameliorating the transfer of larger fragments (>8kb). The following incubation in 0.4M NaOH for 20 min caused the denaturation and separation of the DNA double strands, to facilitate the later hybridisation of the DNA-probe. The DNA transfer from the gel to the membrane occurred through capillary blotting. The capillary blot was assembled as follows:

To begin with, a 10 cm stack of paper towels was placed next to a large tray containing the transfer solution (0.4M NaOH). The following layers were placed on top of the stack, from bottom to top:

- Three layers of 3 mm Whatman paper, drenched in transfer solution
- The nylon-membrane, equilibrated in transfer solution
- The gel
- Two layers of 3 mm Whatman paper, drenched in transfer solution
- A bridge of 3 mM Whatman paper, drenched in transfer solution, whose end tipped into the transfer solution in the tray
- A glass cover plate

All layers were assembled absolutely free of air bubbles, which would interfere with efficient transfer. On top of the glass plate a weight of approximately 0.5 kg was placed, and the blot was incubated over night. The capillary forces of the paper towels draw the blot solution through the assembled stack, transferring the DNA fragments from the gel onto the membrane, where they are bound due to their negative charges. After disassembly of the blot, the membrane was briefly washed in 2xSSC and the membrane was crosslinked by UV, thereby covalently attaching the DNA to the nylon membrane.

Probe labelling

A DNA fragment can be labelled radioactively during an one-step amplification, using random primers for initiation and a nucleotide mix containing radioactively labelled ^{32}P-dCTP (Feinberg and Vogelstein, 1983).

For probe labelling the Takara Ladderman labelling kit was used according to the instructions of the manufacturer. 50µCi ^{32}P-dCTP were used in each labelling reaction. Not incorporated radioactive nucleotides were removed by gelfiltration with Microspin S-200 HR columns.

Hybridisation and detection

The hybridisation leads to the generation of stable double stranded hybrids between the labelled probe and the DNA fragments on the membrane, due to sequence complementarity. These hybrids can later be detected by exposition of the membrane to an X-ray film.

To prevent unspecific binding of the probe, the membrane was incubated in blocking solution (ExpressHyb) for at least one hour prior to addition of the probe. After blocking, the labelled probe was denatured at 95°C for 5 min and allowed to hybridise with the membrane over night. To remove unbound probe, the membranes were washed extensively after hybridisation. Three 10 minute washes at RT of the low stringency wash solution I were followed by 1-2 washes at 50°C with the high stringency wash solution II,

removing essentially all probe fragments not complementary bound. The specifically bound probe was detected by autoradiography.

2.6.7.8. Northern blot analysis

As opposed to Southern blot analyses, Northern blotting is used to detect messenger RNA (mRNA) molecules sequence specifically with a labelled DNA probe. The total cellular RNA is separated under denaturing conditions in an agarose gel, containing formaldehyde and capillary blotted to a positively charged membrane, where hybridisation to a labelled DNA probe and subsequent detection allows the analysis of abundancy and size of the respective mRNA.

Sample preparation and electrophoresis

Total cellular RNA was isolated from cells or tissues as previously described and denatured for 10 min at 70°C in the presence of formaldehyde. The samples were loaded onto 1% agarose gels, containing 10% MOPS and 2% formaldehyde and separated at 80V for 4 hours. A RNA size standard was separated simultaneously to facilitate the determination of RNA sizes.

Blotting procedure and detection

The capillary blot assembly essentially followed the protocol mentioned in chapter 2.6.7.7., with the only exception that 20xSSC was used as transfer buffer. After blotting the RNA size ladder was marked under UV light and the membranes were hybridised with DNA probes for SLy2 and actin as loading control. Probes were labelled with DIG-nucleotides. The DIG Easy Hyb system (Roche, Mannheim) was used for labelling, hybridisation and detection was done according to the instructions of the manufacturer. The hybridised blots were incubated with αDIG antibody overnight and unbound antibody was removed by washing with maleic acid buffer. CDP-Star was used as substrate to visualise the hybridised probe by exposure to X-ray films.

2.6.7.9. Site directed mutagenesis

To generate the SLy2 species containing the point mutations serine to alanine at position 23, the QuickChange site directed mutagenesis kit (Stratagene, USA) was applied according to the manufacturer's instructions. The integrity of the mutation was confirmed by sequencing.

2.6.7.10. Cloning of plasmid vectors

In the generation of all plasmid vectors constructed during the present study, standard cloning techniques were applied.

Restriction of vector and insert

Both the target vector and the insert to be cloned were digested with restriction enzymes as described previously to generate compatible ends, either blunt or with single stranded overhangs.

Dephosphorylation of the vector

To interfere with a self (re-) ligation of the vector backbone in the ligation reaction, the linearised vector fragment was dephosphorylated by treatment with the shrimp alkaline phosphatase (SAP) for one hour at 37°C. As the ligase is dependent on these terminal phosphates, the SAP treatment inhibited the ligation of the vector without the insert fragment, which provided the necessary phosphates.

Ligation of vector and insert

The ligation of vector and insert fragments was mediated by the T4 phage ligase, which catalyses the reaction between the phospho-diester of the 5' phosphate group and the 3' hydroxyl group of the linear fragments. The ligase mediates ligations between blunt ends as well as overhanging ends.

Important for an efficient ligation is a molar ratio of the vector to the insert of approximately 1:3. The reaction was carried out in 20µl with 1x ligation buffer (freshly thawn) and 1-2 units of T4 DNA ligase. Ligation occurred at 16°C for one hour and subsequent incubation at 4°C overnight.

Transformation of *E.coli*

Chemically competent DH5α or XL1 blue *E.coli* were used to propagate the ligated constructs. Competent bacteria (Cohen et al., 1972) were thawn on ice, mixed with the ligation reaction and transformed by a 42°C heatshock for 45 sec. After incubation at 37°C for one hour to allow the expression of the resistance gene, the bacteria were plated onto LB-agar supplemented with the appropriate antibiotics for selection. Picking of bacterial clones and analysis of plasmid construct was performed as described.

3. Results

3.1. SLy2 belongs to the SLy family of adapter proteins

SH3 protein expressed in lymphocytes (SLy) was the first protein of the SLy family to be cloned. It was initially identified as an SH3 and SAM domain containing protein preferentially expressed in lymphocytes (Beer et al., 2001). Subsequently it was shown by Doreen Cantrells group from Dundee, Scotland, that SLy is specifically phosphorylated on Serine 27 upon T cell receptor crosslinking (Astoul et al., 2003).

3.1.1. Properties of the novel SLy family protein SLy2

3.1.1.1. Identical molecular structure as SLy

Analysis of the SLy2 amino acid sequence with the protein database Expasy (*www.expasy.org*) revealed a domain structure that is identical to SLy (Figure 6). The N-termini of the proteins are composed of a bipartite NLS (aa 4-86), whose sub-domains are divided by a 49 amino acid spacer. Located further downstream is the SH3 domain in the middle section of the protein (aa 167-222), which is followed by a C-terminal SAM domain (aa 241-305). Interestingly, the regions of high identity correlated with the SH3 and the SAM domains, indicating that these features are evolutionary conserved. Along the same lines, the N-terminal area of homology contains the first part of the bipartite NLS and the serine 27 of SLy (corresponding to serine 23 in SLy2), which was shown to be phosphorylated upon T cell receptor crosslinking (Astoul et al., 2003).

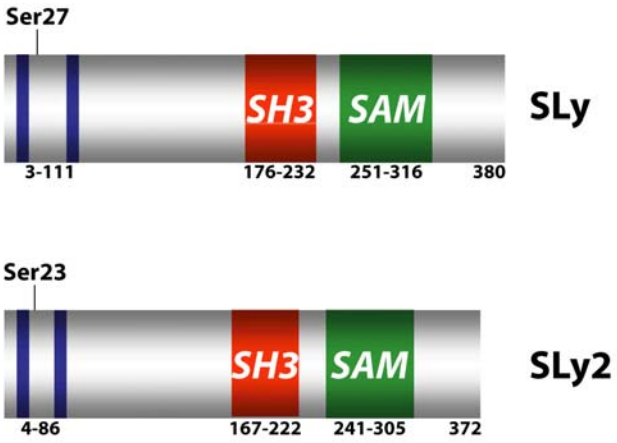

Figure 6: Molecular structure (schematic) of SLy and SLy2 as determined by database analyses. The complete amino acid sequences of SLy and SLy2 were examined by Expasy/Swiss Prot, which yielded the depicted domain structure. The two blue areas in the N-terminus of the protein represent the bipartite nuclear loclisation sequence. The numbers below each protein indicate localisation of each domain with respect to the amino acid sequence.

3.1.1.2. Chromosomal localisation and genomic organisation of the *sly2*-gene

The *sly2*-gene is located on chromosome 21 in the human and on chromosome 16 in the murine genome. In the human genome it resides in the chromosomal segment q11.2. The gene belongs to a cluster whose deregulation is reported for Down-syndrome patients and early-onset forms of inheritable Alzheimer's disease (Groet et al., 1998; Cheon et al., 2003; Kimura et al., 2007).

The *sly2* locus is comprised of eight coding exons, with the start ATG in exon 1 and the stop codon positioned in exon 8 (Figure 7). The complete locus spans a genomic region of 50.5kb. The size of the locus is mainly caused by a huge intron of more than 20kb between exons 1 and 2. Different databases report splice variants for SLy2 including additional exons, yet various RACE and RT-PCR analyses conducted during this thesis could not confirm such predictions (data not shown).

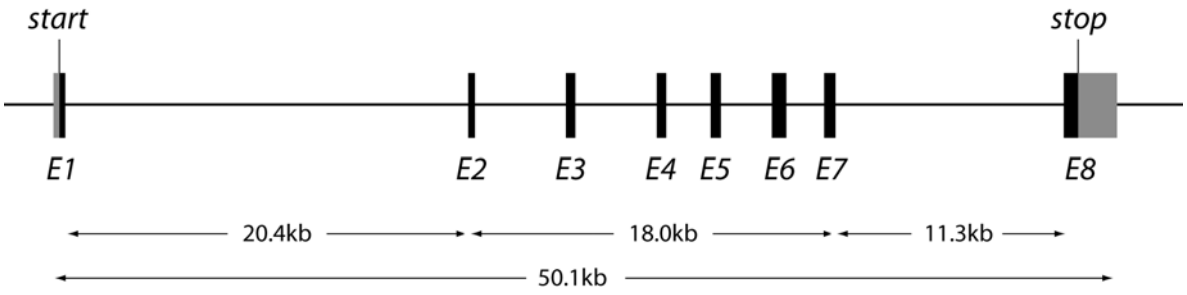

Figure 7: Exon-intron organisation of the murine genomic *sly2*-locus. The start ATG is located in exon 1, the stop codon resides in the 5' end of exon 8, resulting in an open reading frame of 1116 bp. The coding region is marked in black, 5' and 3' UTRs in grey. The sizes of the complete locus, the two largest introns and the central exon cluster are depicted. Organisation of the locus is drawn according to the entry in the Ensembl database (www.ensembl.org).

3.1.1.3. Expression pattern of SLy2

An anti-serum to the murine SLy2 protein was generated to facilitate the determination of SLy2 expression by western blotting. Analysis of lysates from different mouse organs indicated robust expression of SLy2 in spleen and thymus, yet almost none in the bone marrow (Figure 8). Remarkably high protein levels were detected in muscle, brain, heart and colon. No expression was found in liver, kidney and lung (data not shown). The signal obtained from the pancreas sample seemed to migrate somewhat higher, suggesting a different splice variant or posttranslational modification. The former possibility could not be ruled out, but all RT-PCRs conducted during this thesis only yielded a single fragment, argueing in favour of posttranslational modifications (data not shown). The observed expression pattern positions SLy2 between the strictly lymphoid expression of SLy and the ubiquitous occurrence of Sash1, the third member of the SLy family (Zeller et al., 2003).

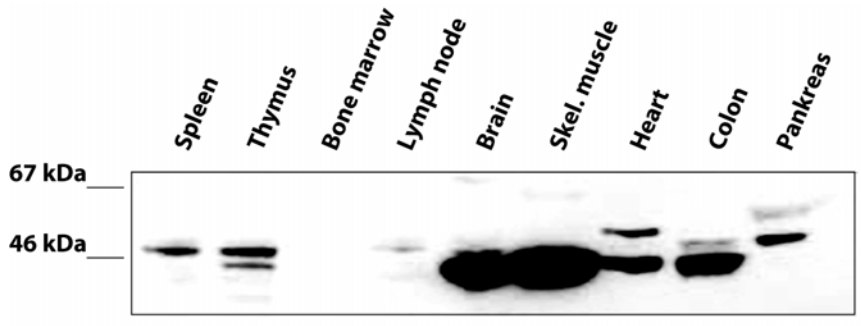

Figure 8: Expression levels of SLy2 in different mouse organs. Organs were lysed as described and the protein concentration of the lysates was determined. 30µg of protein were analysed for each sample. Endogenous levels of protein were detected with a polyclonal SLy2 anti-serum.

3.1.1.4. SLy2 expression is regulated in B cells

To confirm data presented by Zhu *et al.* on the dependency of the expression levels of SLy2 upon various stimuli, splenic B cells were purified by MACS and stimulated with IL-4, IL-4+LPS and IL4+α–CD40 for six and 16 hours (Figure 9 and (Zhu et al., 2004)). A subsequent western blot analysis proved that the expression of SLy2 was upregulated after these proliferation, maturation, and differentiation inducing stimuli. The upregulation was most pronounced upon the addition of LPS and α–CD40 in combination with IL-4.

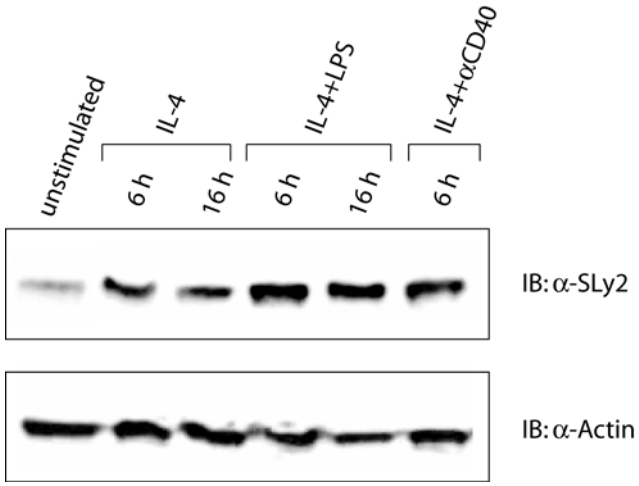

Figure 9: SLy2 expression is regulated in B lymphocytes. Splenic B cells were isolated by MACS and treated with the indicated stimuli. Cells were lysed and SLy2 protein levels were analysed by western blotting with the purified SLy2 anti-serum. Actin served as loading control.

3.1.1.5. Intracellular localisation of SLy2

Due to the predicted bipartite NLS in the N-terminus of the protein, it was intriguing to analyse the distribution of SLy2 between the nucleus and the cytosol. In addition, the phenotype of the $SLy^{\Delta/\Delta}$ mouse documented drastically the importance of nuclear translocation for SLy function (Beer et al., 2005). The separation of cell lysates into nuclear and cytoplasmic fractions proved that the majority of the cellular SLy2 molecules resided in the cytoplasm, and only a small fraction in the nucleus (Figure 10). To analyse the functionality of the predicted NLS in the N-terminus, a deletion mutant was generated, which lacked the C-terminal section of the bipartite NLS (SLy2-ΔNLS). Of note, this deletion resulted in a marked decrease of the nuclear SLy2. The ΔNLS mutant migrates as a double band, which is probably caused by differential phosphorylation (see figure 21 for details).

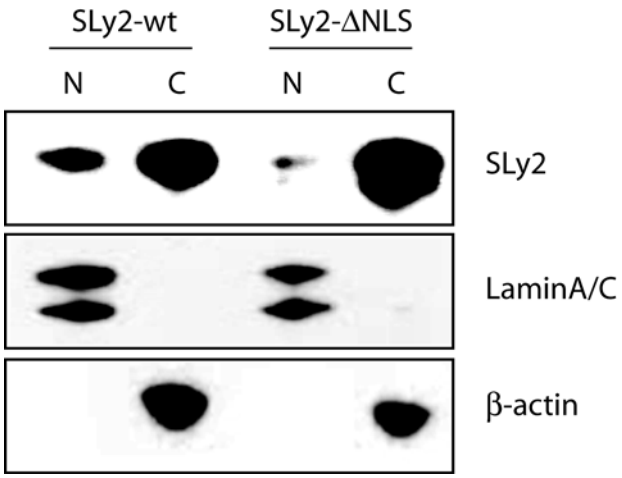

Figure 10: SLy2 contains a functional NLS. SLy2 wildtype or SLy2-ΔNLS expressing HeLa cells were subjected to biochemical separation of the nuclear (N) and the cytoplasmic (C) fraction. The integrity of fractionation was assessed by probing the membrane with α-Lamin A/C and α-GAPDH for the nuclear and the cytoplasmic fraction, respectively.

3.1.1.6. SLy2 is differentially phosphorylated in primary cells and cell lines

As SLy was shown to be phosphorylated upon TCR ligation, it was apparent to also analyse the phosphorylation status of SLy2. In an initial experiment SLy2-HA overexpressing Jurkat (data not shown) or SVEC cells were pulsed with ^{32}P labelled orthophosphate. Subsequently, the cells were stimulated for different time points with PDBU and ionomycin to mimic activation through membrane bound receptors. As apparent, SLy2 was prominently phosphorylated from the beginning and the extent did not change over the time period tested (Figure 11 A). In contrast, when primary, transgenic thymocytes (see 3.2. for details) were subjected to PDBU/ionomycin stimulation, this resulted in a marked and sustained induction of phosphorylation of SLy2 (Figure 11 B). Of note, SLy2 was only phosphorylated at a minimal level prior to stimulation of the cells, which stands in marked contrast to the results obtained from the cell line experiments.

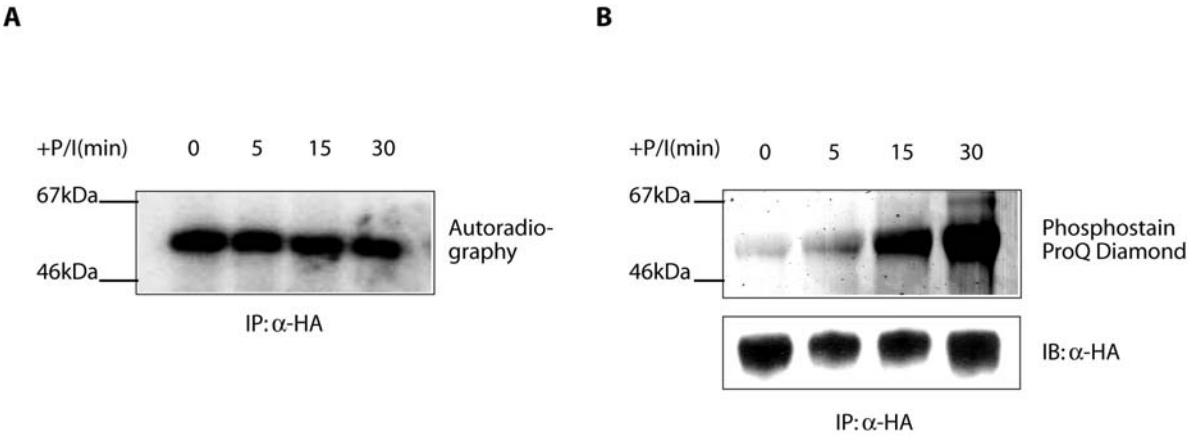

Figure 11: SLy2 is differential phosphorylated in malignant cell lines or primary cells. (A) SLy2-HA expressing SVEC cells were pulsed with ^{32}P-labeled orthophosphate, stimulated with PDBU/ionomycin and SLy2 was immunoprecipitated with α-HA. The IPs were separated on a 10% polyacrylamide gel and the gel was analysed by autoradiography after fixing and drying. (B) Transgenic SLy2-HA expressing thymocytes were stimulated with PDBU/ionomycin for the indicated time points and subsequently SLy2 was immunoprecipitated and IPs were electrophoretically separated. The gels were stained with ProQ diamond phosphostain (Invitrogen) and evaluated in an Amersham Typhoon 8600 phosphoimager.

3.2. SLy2 transgenic mice

3.2.1. Generation and confirmation

To gain insights into the role of this newly identified protein, a transgenic mouse was generated. Transgenic mice are a well established and reliable method to analyse the cellular and systemic effects of the overexpression of a protein. The injection of a eukaryotic expression construct into the pronucleus of a mouse zygote leads to its integration into the genome and the re-implantation of such genetically modified zygotes into the oviduct of a mock-pregnant foster mouse yields several individual founder animals. Breeding of these founders each establishes a transgenic mouse line. It lies in the nature of this technique, that the exact location of the transgene insertion remains stochastic. To rule out the possibility that the phenotype shown by a transgenic mouse is caused by the deletion of a different locus through the insertion, several different transgenic lines have to be analysed in parallel.

The choice of the promoter in the transgenic construct determines the expression pattern of the overexpressed protein. As SLy2 was shown to be highly expressed in hematopoietic cells and especially upregulated in B cells upon activation with various stimuli (Figure 9) its function in the lymphoid lineage should be further elicited. Therefore, a transgenic construct was chosen that contained a chimeric promoter, assembled from the

immunoglobulin heavy chain enhancer (E*μ*) and the proximal promoter of the tec-family kinase Lck (*lck*-prox), resulting in a robust expression in B and T cells respectively (Figure 12 and (Iritani et al., 1997)). The complete SLy2 cDNA together with an HA-tag was cloned behind the chimeric promoter and the integrity of the construct was confirmed by three different restriction digests as shown in Figure 12. The generation of the transgenic mice was accomplished by Miltenyi Biotech (Bergisch-Gladbach).

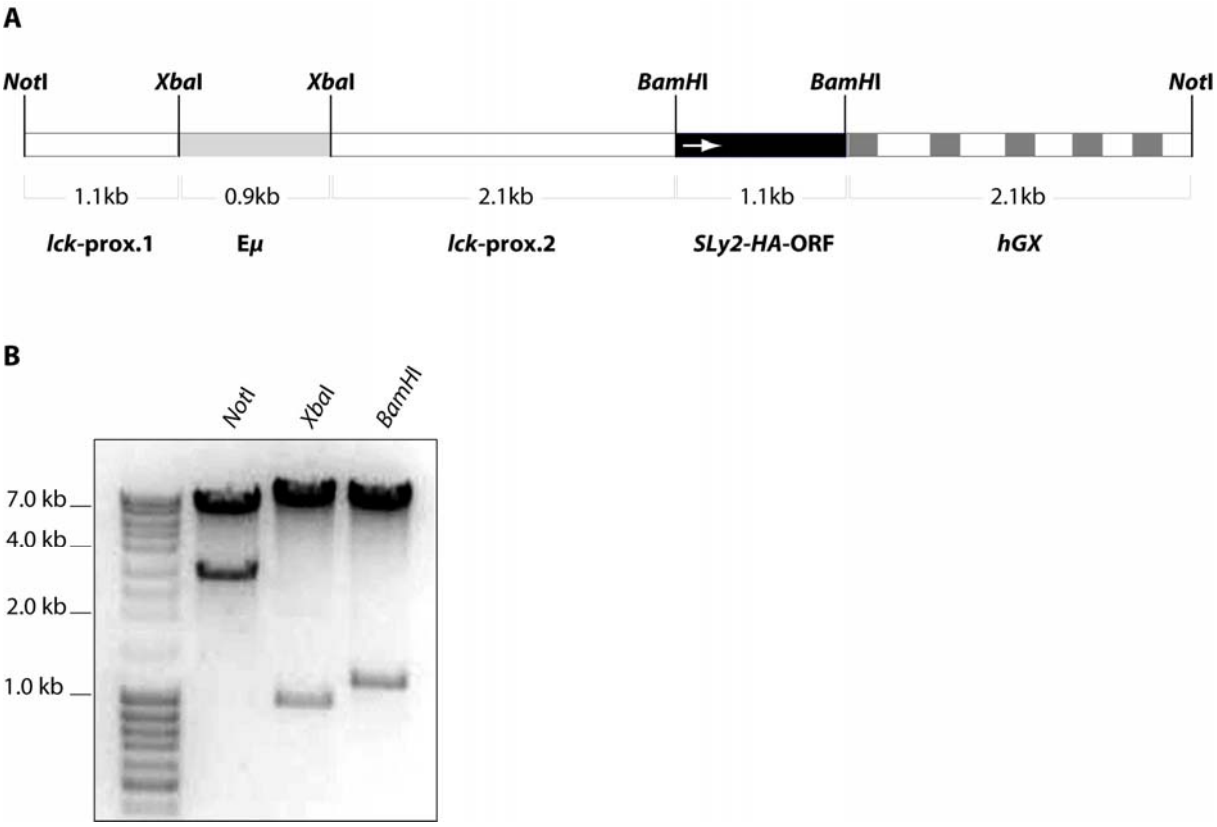

Figure 12: Map of the T and B cell specific expression construct. (A) The complete open reading frame of SLy2 was cloned together with an HA-tag into the BamHI site of p1026x, downstream of the chimeric promoter lck-Eμ. The arrow in the SLy2 ORF indicates the reading direction of the frame. The promoter is assembled from the lck proximal promoter and the IgH enhancer (Eμ). Optimal expression of the SLy2 cDNA was ensured by a spliceable, but non-translatable expression cassette of the human growth hormone (hGX), located 3' of the SLy2 cDNA. (B) p1026x+SLy2-cDNA was digested with BamHI, XbaI and NotI, and analysed on a 1% agarose gel. The signal migrating at 3kb in the *Not*I digest represents the pUC19 backbone of the expression construct, whereas the expression cassette migrates above at 7kb.

Tail biopsies were taken from the 32 founder mice to isolate the genomic DNA. The DNA samples were digested with *BamH*I to yield a 1.1 kb fragment encompassing the complete transgenic SLy2 ORF. The SLy2 cDNA was used as a southern blot probe, identifying five founder mice carrying the transgene: #845, #853, #861, #869 and #871. Since the DNA

concentration of the mouse tail DNA preparations is hardly to determine, the differing signal strength does not necessarily correspond with the copy number harboured by the founder (Figure 13).

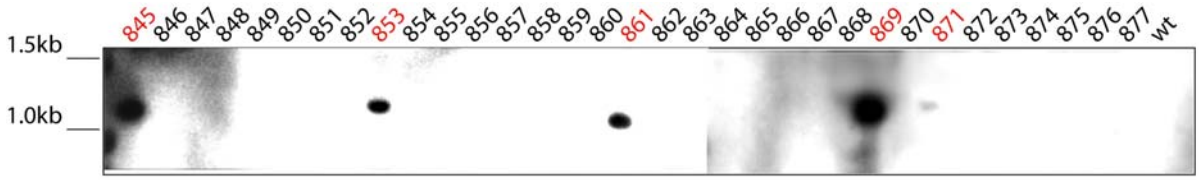

Figure 13: Southern blot analysis of founder animals. The DNA was prepared from mouse tail biopsies, digested with BamHI and separated on 1% agarose gels. Samples were blotted and hybridised with a DNA probe complementary to the complete transgenic expression cassette. Mice carrying the transgene are shown in red numbers.

These mice were bred to C57BL/6 animals to establish five transgenic mouse lines (tg-1 to tg-5). PCR typing of the resulting offspring revealed that #871 was not able to pass on the transgene, so that no line could be established from this founder. To assess the expression of the SLy2-transgene without killing the mice, the F1 daughter generation of the founder animals was bled and total RNA was isolated from the blood samples. Additionally, protein samples were prepared from peripheral blood leukocytes. The RNA was analysed by northern blotting (Figure 14 A), while western blotting was performed with an α-HA antibody to assess the expression on the protein level (Figure 14 B and C). Both methods clearly indicated that transcription as well as translation of the transgene was high and comparable for the transgenic lines SLy2_tg-1 to SLy2_tg-4 (Figure 14). The expression level in $B220^-$ cells appeared to be somewhat higher than in the $B220^+$ fraction. The bone marrow samples showed the lowest expression of the transgene, which could be due to the low abundancy of transgene expressing cells or a lower per-cell expression level in this tissue (Figure 14 C).

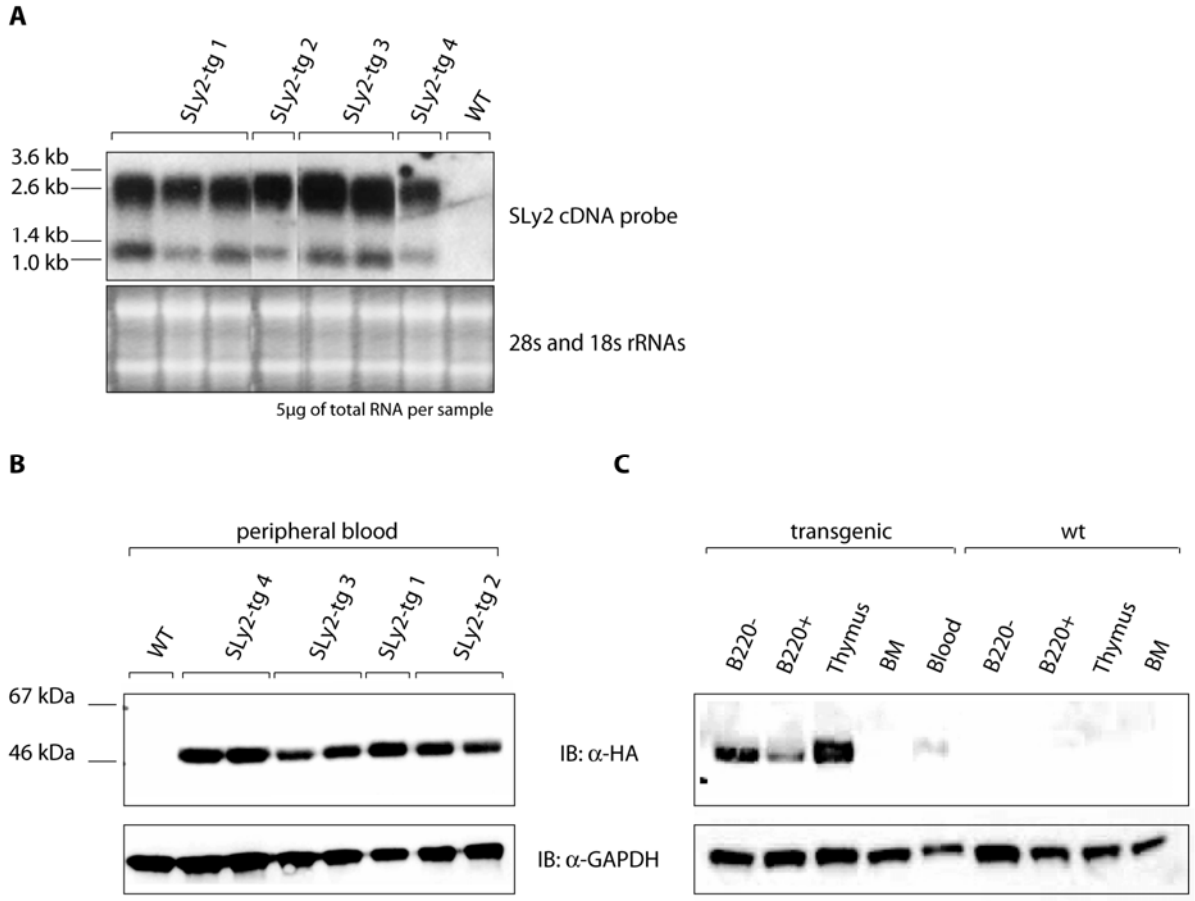

Figure 14: Robust expression of SLy2-HA in transgenic mice. (A) Northern blot analysis of complete RNA from peripheral blood of all four transgenic mouse strains. The SLy2 cDNA was used as a probe. The different sizes originate from different splice variants with respect to the hGX minigene in the 3' end of the construct. The 18s and 24s rRNAs in the gel pictures are shown as loading control beneath the blot. (B) Expression of tg-SLy2 in peripheral blood. Nucleated blood cells were purified as described, lysed and analysed by western blotting. (C) Expression of tg-SLy2 in splenic B and T cells, thymus, bone marrow and blood. Spleen cells from wt and tg animals were separated into $B220^-$ and $B220^+$ fractions, lysed and analysed by western blotting. Blots were probed for GAPDH as loading control.

3.2.2. Unaltered development of lymphoid cell populations

Encouraged by the strong expression of the transgene, its influence on the development of the different lymphoid cell populations was assessed. Therefore, spleens, thymi and bone marrow of transgenic mice and wildtype littermates were isolated and the distribution of the different lymphoid populations was analysed by flow cytometry. The spleens and thymi of wildtype and transgenic animals displayed equal cell numbers (data not shown). With respect to the different T and B cell subpopulations, the analysis comprised double-negative (DN) thymocytes, peripheral T cells, immature and mature peripheral B cells, transitional 1, marginal zone (MZB) and follicular B cells and plasma cells.

All of the analysed populations appeared to be unaltered in spite of the ectopic expression of SLy2 (Figure 15).

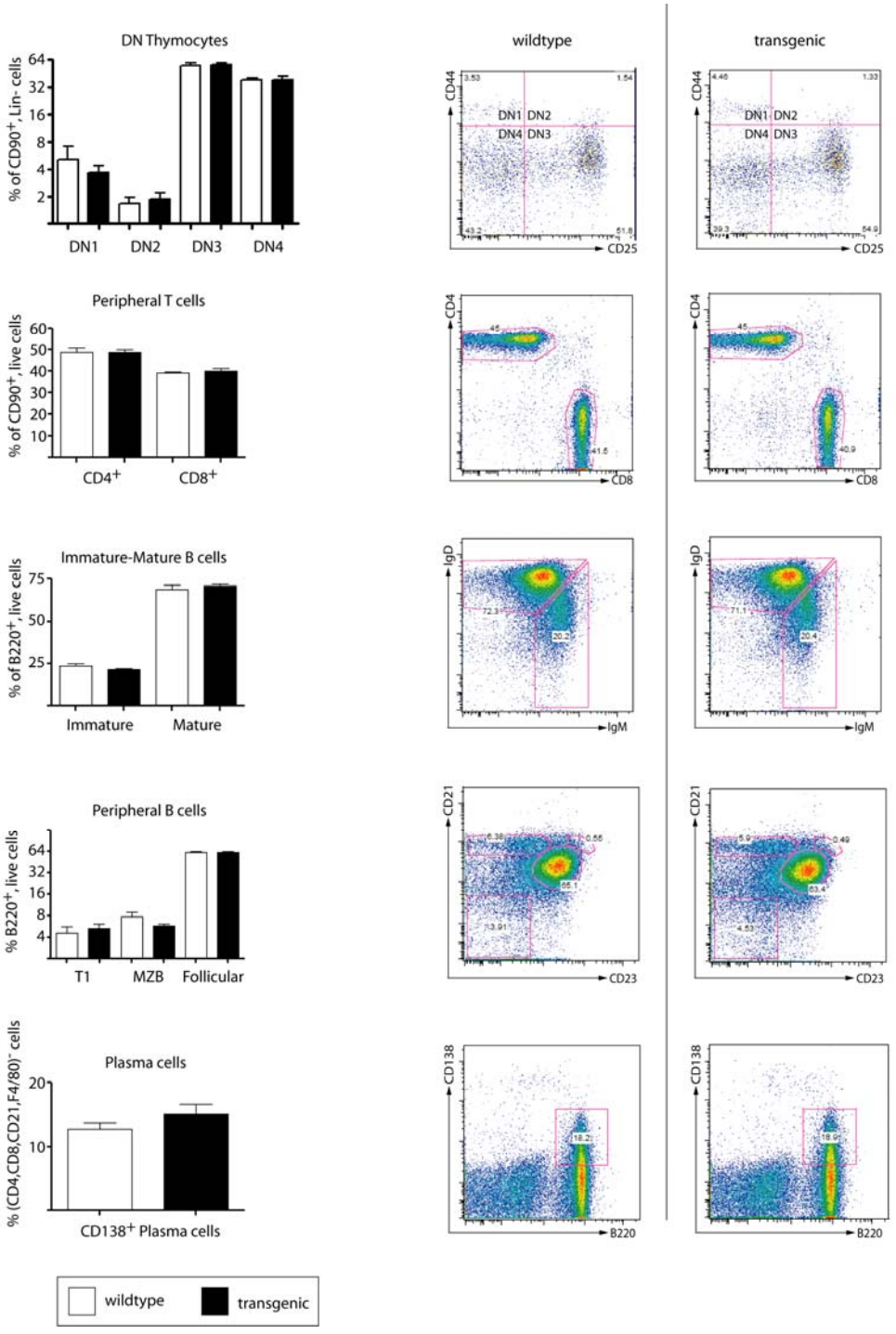

Figure 15: Flow cytometric analysis of lymphoid populations. Thymocytes, splenocytes and bone marrow cells were isolated as described. The cells were stained with the indicated fluorescently labelled antibodies and analysed on a FACS Canto II. The quantifications in the left panels combine the data of three independent experiments (n=10, 5 Tg mice, 5 wt mice). The FACS data were evaluated with FlowJo software.

3.2.3. Impaired spreading of transgenic B cells to α-IgM coated surfaces

As SLy was identified, amongst other findings, by its effect on T cell adhesion, it was interesting to determine wether the overexpression of SLy2 would have a similar effect. Yet, more interesting than mere adhesion would be to analyse the ability of the B cells to spread on α-IgM coated surfaces. It is known that upon contact to a surface bound antigen or target cell, B cells undergo a distinct choreography of spreading and contraction, to maximize the amount of gathered antigen. This behaviour is dependent on the strict spatio-temporal regulation of a complex signalling network and interfering with it (e.g. by blocking actin polymerisation) will lead to defective activation of the B cells (Fleire et al., 2006; Harwood and Batista, 2008).

Wildtype and transgenic $B220^+$ splenocytes were seeded onto cover glasses coated with α-IgM and allowed to adhere and spread. After different timepoints the cells were fixed and stained for F-actin. Determination of the size of the F-actin ring at the contact area between the cells and the substrate revealed that the transgenic B cells had apparent difficulties in the initial spreading phase as opposed to wildtype cells (Figure 16). After two minutes of stimulation, the transgenic cells still did not show any signs of spreading, as opposed to the wildtype cells, which had already reached half of their maximum contact area. Beginning after 5 min, the transgenic cells started to recover, yet their spreading was still impaired at 15 min after onset of stimulation. Indeed, it remained inferior to the wildtype situation over the complete time course and only recovered towards the end of the time course.

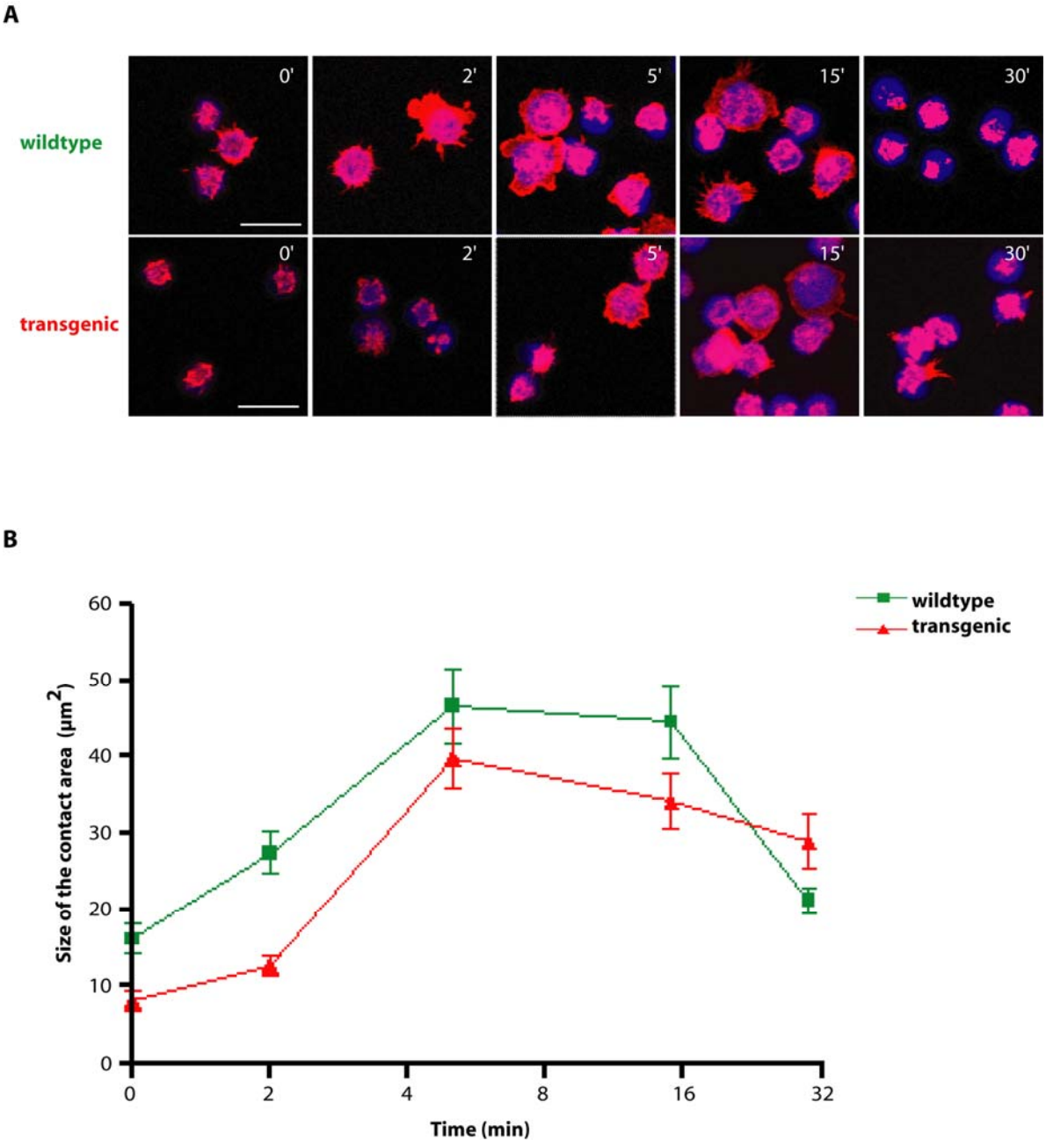

Figure 16: Actin dynamics in B cells interacting with α-IgM coated surfaces. (A) wt and tg splenocytes were purified and MACS sorted for B220 surface expression. Isolated splenic B cells were prestimulated for one hour with α-CD40 and IL-4 and subsequently allowed to adhere to α-IgM coated cover glasses. The cells were fixed in 4% PFA after the indicated time points and stained for F-actin (red) and nuclei (blue) as described (scalebar: 10 µm). (B) Quantitative analysis of (A). The size of the area of interaction was determined for 30-50 cells at each timepoint.

3.3. Effects of SLy2 expression on cellular actin networks

3.3.1. SLy2 overexpression leads to ectopic ruffle formation

Due to the marked influence of SLy2 on lymphoid actin dynamics, it was mandatory to analyse the underlying mechanisms in more detail. As SLy2 was also shown to be expressed in the epithelial cell line HeLa (data not shown), these cells were chosen as experimental system, whose larger size compared to lymphocytes greatly facilitated the analysis of subcelluar structures. Therefore, HeLa cells were transduced with a lentiviral expression construct comprising the complete SLy2 cDNA under the control of the EF2α promoter, resulting in robust and ubiquitous expression. The SLy2 protein was expressed fused to an HA-tag for detection in immuno-fluorescence, as the SLy2 anti-serum did not yield satisfying results in such stainings. From the same construct and promoter GFP was expressed under the control of an internal ribosome entry site (IRES), thus enabling the identification of transduced cells. Control cells were just transduced with the empty IRES-GFP vector, resulting in GFP expression alone.

SLy2-HA expressing and control cells were allowed to grow on gelatine coated cover glasses, immuno-fluorescently stained for F-actin and analysed by confocal microscopy. The pronounced effect of the enhanced SLy2 expression on the actin cytoskeleton was immediately evident (Figure 17 A and B). Compared to control cells (Figure 17 A), SLy2-HA expressing cells virtually lost all cortical actin and were almost completely devoid of visible stress fibres (Figure 17 B left and middle panels). Instead, all their F-actin seemed to cluster to lamellipodial- or ruffle-like structures at the distal poles of the cells. A further finding was the changed appearance of the cells. Whereas the majority of the control cells displayed an even shape, the SLy2-HA expressing cells were marked by the occurrence of many leading edges per cell, often yielding a star or tripod like shape (Figure 17 B). Additionally, many of the SLy2 overexpressing cells produced long cytoplasmic protrusions, evoking a stretched, tubular-like appearance (Figure 17 B, right panel). Frequently, these protrusions seemed to connect two cells, thus rather representing thin cytoplasmic bridges, so called cytonemes.

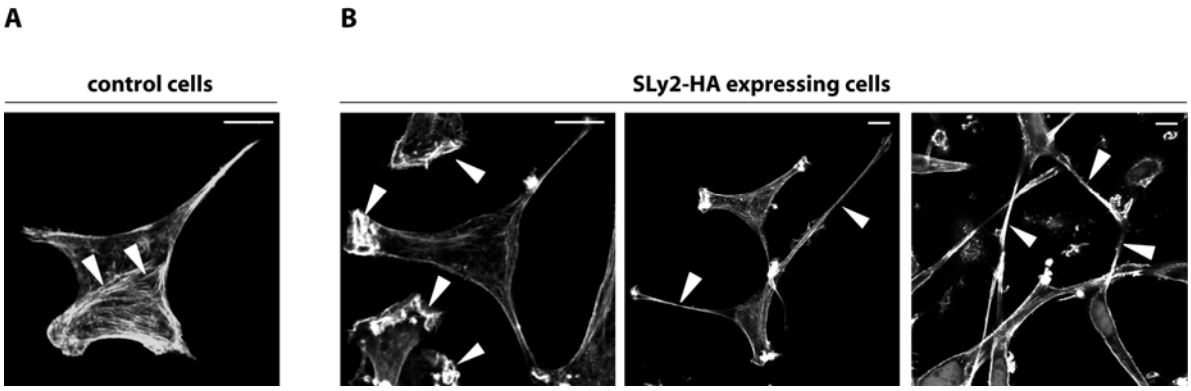

Figure 17: Overexpression of SLy2 in epithelial cells induces membrane ruffling and lamellipodia formation. HeLa cells were transduced with pWPI-SLy2 or a control construct. The cells were seeded onto gelatine-coated cover glasses and allowed to grow overnight. Subsequently the objects were fixed and stained for F-actin. Arrowheads indicate stress fibres (A), distal ruffles and lamellipodia (B, left panel) or cytonemes (B, middle and right panel) (scalebar: 10 µm).

3.3.2. SLy2 colocalises with F-actin in peripheral ruffles

Subsequently, the subcellular localisation of SLy2 was analysed in further detail. Therefore, control and SLy2 expressing HeLa cells were stained with α–HA and phalloidine, to analyse SLy2 and F-actin structures, respectively. Most of the cellular SLy2 molecules resided in the cytoplasm, yet a specific fraction reproducibly located to the remarkable F-actin structures described above (Figure 18). Thus, the ectopic expression of SLy2 not only led to the induction of lamellipodia and ruffles, but the protein also colocalised with F-actin in these structures. Interestingly, SLy2 did not colocalise with the cortical actin in the thin cellular bridge, further underlining the specificity of its appearance in the peripheral ruffles. The images were analysed with ImageJ (NIH) on a per-pixel level and pixels emitting signals from both stainings appear white in the merged image (right panel).

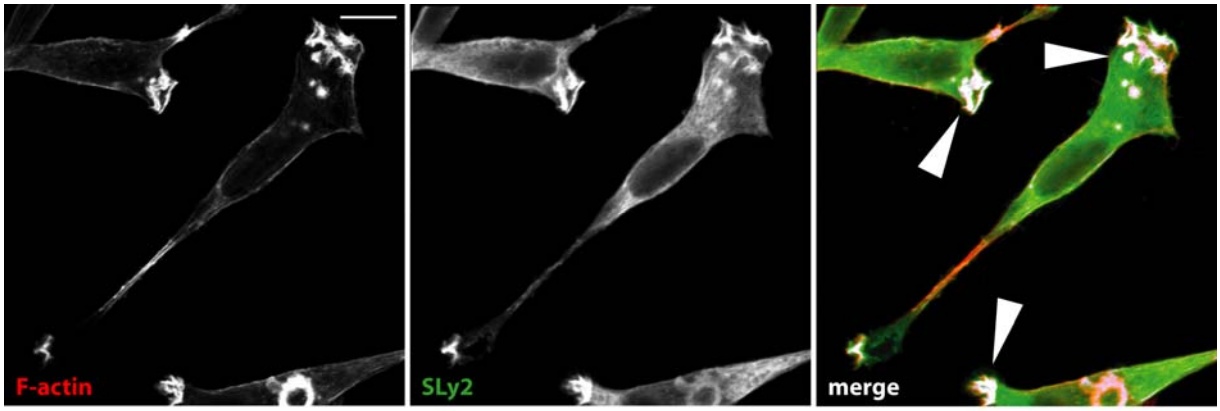

Figure 18: SLy2 colocalises with F-actin in ruffles and lamellipodia. HeLa cells were transduced with a SLy2-HA expression construct and seeded on gelatine coated cover glasses. Cells were stained with phalloidine (red) and α-HA (green) yielding the stainings shown in the left and middle panels, respectively. The right panel shows the merged image. Pixels with colocalising staining are marked white (arrowheads). Images were analysed with ImageJ (scalebar: 10 µm).

3.3.3. Assessing the role of the domains of SLy2 in actin dynamics

Due to the characteristic domain structure of SLy2 it was apparent to ask which domains would be important in mediating the effects on F-actin dynamics. Deletion mutants of SLy2 were generated, lacking the NLS, the SH3 or the SAM domain. In addition, the function of the serine residue 23 was addressed by employing a serine 23 to alanine point mutated SLy2 species (Figure 19). As demonstrated by western blotting with an α–HA antibody, all mutants were expressed correctly. The ΔSAM displayed reduced expression levels, as will be mentioned later. Also remarkable was the strongly differing migration behaviour of the ΔSAM mutant. Although only 8 aa smaller than the ΔSH3 mutant it migrated at only 30kDa. As the sequence of the expression vector was repeatedly sequenced and confirmed, the molecular reason for this size-difference remains to be determined.

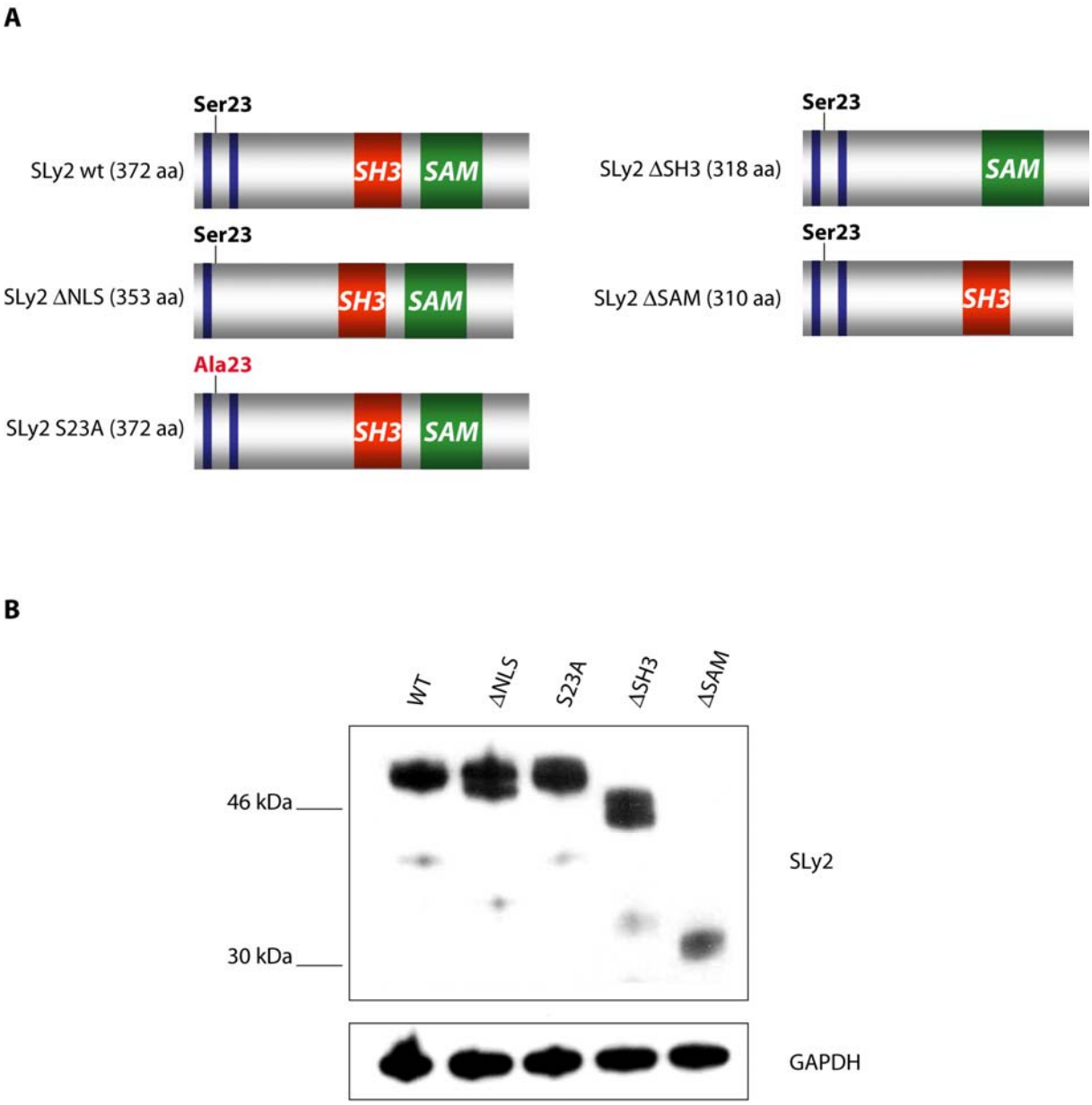

Figure 19: Construction of the different SLy2 deletion mutants. (A) The deletion mutants used in this study were constructed on the basis of the Swiss-Prot database structure prediction. (B) Correct expression of all mutants was assessed by western blotting of HeLa lysates with an α-HA antibody.

Of note, the various SLy2 deletion mutants showed greatly differing effects on the F-actin cytoskeleton. Whereas the S23A mutant retained and even slightly increased the reorganisation of the F-actin network, all other mutants lost this ability to differing extent (Figure 20, A). The mildest loss of function was caused by deletion of the NLS. The induction of the distal ruffles and the effect on cortical actin structures was partially retained, but diminished in quantity as well as quality. Also, these cells never took on the already mentioned tripod like shape, although they did display a much more tubular

morphology compared to control cells. Surprisingly, though still inducing some F-actin reorganisation, the ΔNLS mutant did not colocalise with the phalloidine staining anymore, as indicated clearly by the lack of white areas in the merged image (Figure 20, B).

As already mentioned above, the change of serine 23 to alanine, rather enhanced the phenotype of SLy2 overexpressing cells (Figure 20 A and B). The cells displayed even more ruffles per cell than the wildtype SLy2 expressing cells, yet the overall shape appeared to be more round than the control cells. Unique among all tested SLy2 variants was the subcellular localisation of the S23A mutant, which was more skewed towards the membrane, sometimes even displaying a ring-like distribution along the cell border (Figure 20 A). With respect to the colocalisation with F-actin, the S23A mutant was a phenocopy of the wildtype protein (Figure 20 B).

The loss of the SH3 domain abolished much of the SLy2 effect on actin dynamics (Figure 20, A). The cells regained the natural, less stretched shape of the control sample and also the distal ruffles vanished. This phenotype was accompanied by a reappearance of the cortical F-actin structures, along with stress fibres. It is consistent with this loss of function that the deletion of the SH3 domain also considerably interfered with F-actin colocalisation, although not as much as the deletion of NLS domain (Figure 20 B).

In addition to abolishing the entire effect of SLy2 on the actin cytoskeleton, the deletion of the SAM domain also likely implied a severe impact on the overall stability of the protein (Figure 20 A and B). This was marked by the finding that most of the transduced cells did not show any detectable staining for SLy2-ΔSAM, while FACS analysis of the same cells clearly proved normal expression of the IRES-GFP (data not shown). This notion was confirmed by western blot analysis with α–HA, which proved a severely lowered level of expression compared to the other mutants or the wildtype protein (Figure 19 B). Accordingly, it could not be ruled out, that the overall lowered concentration of the protein accounted for the apparent lack of the SLy2 effect. Nevertheless, when analysing cells with a fairly strong expression of the mutant, these displayed a phenotype most similar to the control cells, without extensive induction of distal ruffles or lamellipodia and no loss of cortical actin or stress fibres (Figure 20 A). Also the subcellular distribution of the protein changed quite drastically from that of the wildtype protein, completely losing all correlation to any F-actin structure. Clearly, this was reflected in the colocalisation study too (Figure 20 B). Due to the low expression level of the ΔSAM mutant, this species was not included in the following analyses, as the missing domain most likely could never solely account for the apparent loss of function.

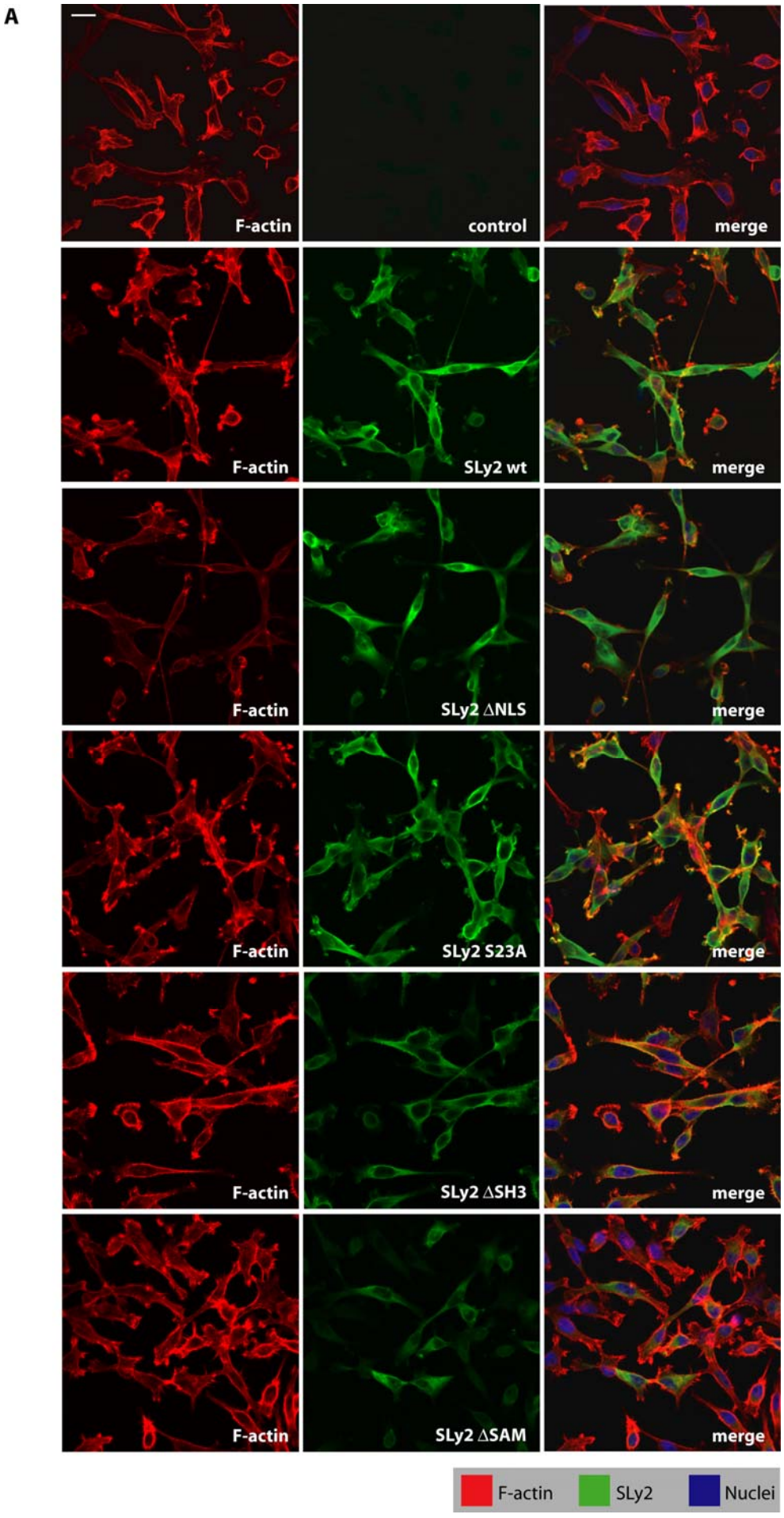
A
F-actin
control
merge
F-actin
SLy2 wt
merge
F-actin
SLy2 ΔNLS
merge
F-actin
SLy2 S23A
merge
F-actin
SLy2 ΔSH3
merge
F-actin
SLy2 ΔSAM
merge
F-actin
SLy2
Nuclei

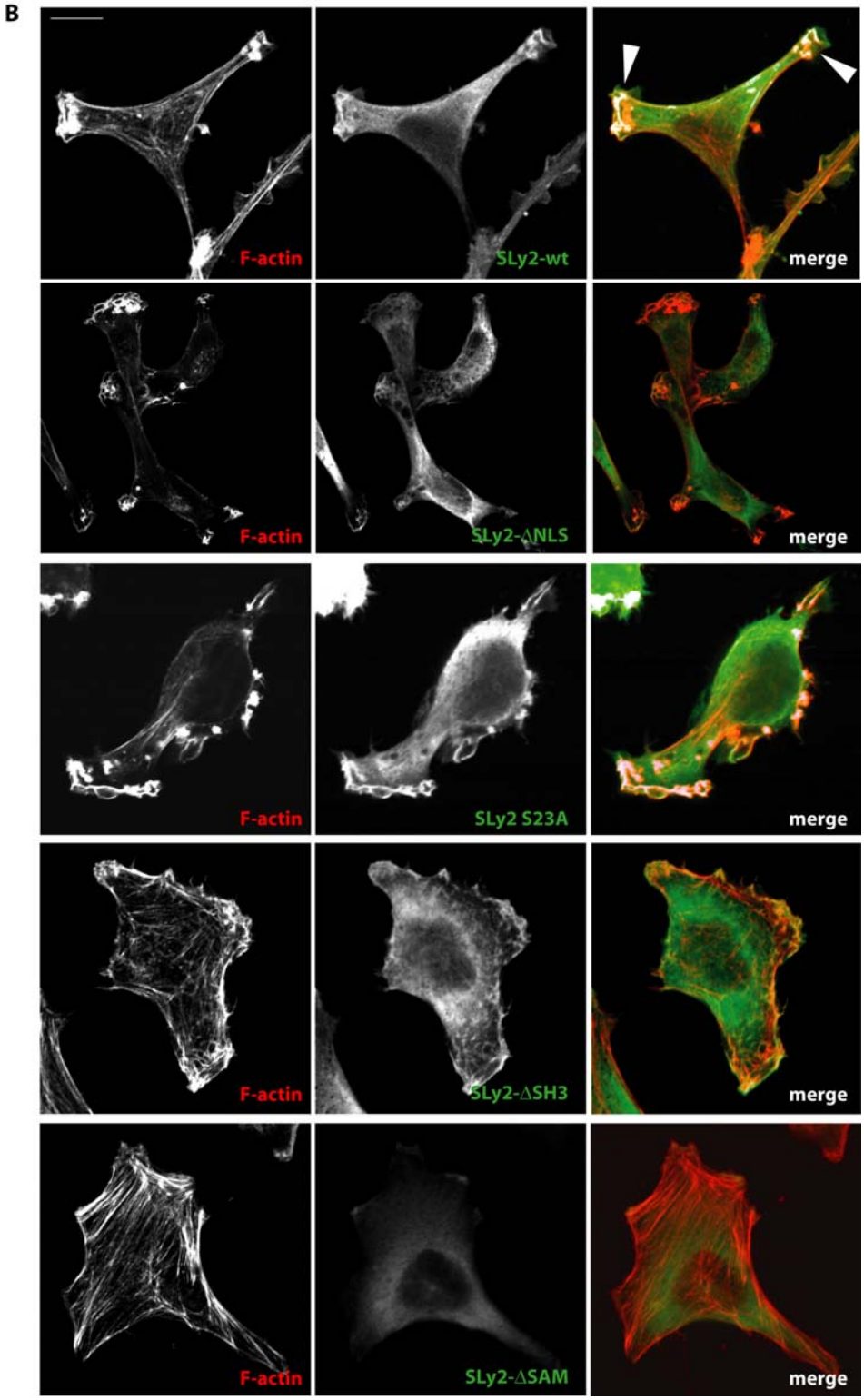

Figure 20: SLy2 colocalises with F-actin structures depending on the NLS or the SH3 domain.

HeLa cells were transduced with the indicated expression constructs and seeded onto gelatine coated cover glasses. After growing for 24h, the cells were fixed and stained with anti-HA for SLy2 (green), with phalloidine for F-actin (red) and with DAPI for nuclei (blue). (A) Overview images (scalebar: 20 µm). (B) Detailed images with a per-pixel colocalisation analysis, conducted with ImageJ and the plugin *colocalization RGB*. Pixels with a colocalisation of both colours are marked white in the merged images (scalebar: 10 µm).

To confirm the findings from the immuno-fluorescence analysis by biochemistry, lysates of the various HeLa cell lines were separated by ultracentrifugation in a glycerine gradient into the F-actin and the G-actin containing fraction. Western blot analysis of the fractionated lysates clearly showed that the distribution of the ΔNLS and the ΔSH3 mutants was skewed towards the G-actin fraction, whereas the wildtype and the S23A species almost exclusively appeared in the F-actin fraction (Figure 21 A), indicating an incorporation into F-actin associated complexes. The ΔNLS and, to a lesser extent, also the ΔSH3 mutants migrated as double bands, which represent most likely differentially phosphorylated species, as treatment of the cells with the protein phosphatase inhibitor calyculin shifted the ratio towards the upper (=more phosphorylated) band (Figure 21 B).

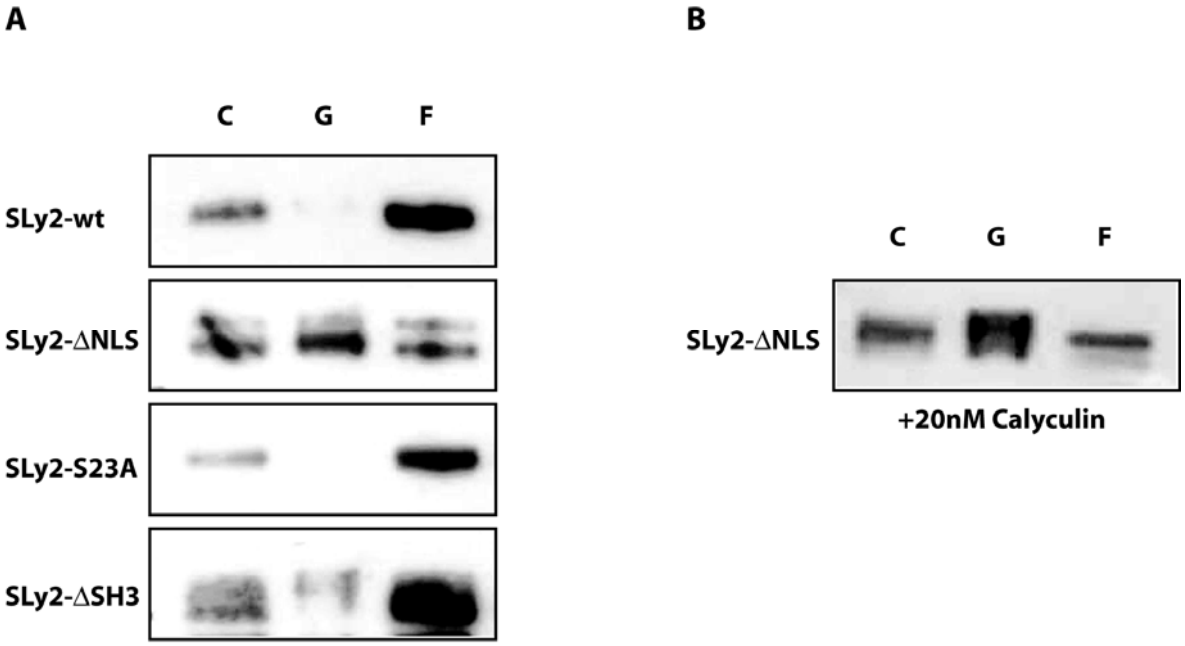

Figure 21: NLS and SH3 mediate the exclusive localisation to the F-actin fraction. (A) HeLa cells expressing the indicated constructs were lysed and lysates were ultracentrifuged in a glycerine gradient to separate G- and F-actin fractions. The complete lysate (C), the G-actin fraction (G) and the F-actin fraction (F) were analysed for the presence of SLy2 by western blotting with an α-HA antibody. (B) The same fractions are shown for the ΔNLS mutant after a 5 min treatment of the cells with the phosphatase inhibitor calyculin prior to lysis.

3.3.4. SLy2 expression enhances the spreading behaviour

To determine the impact of SLy2 on the actin cytoskeleton in a more functional assay, the spreading of the transgenic HeLa cells to gelatine coated surfaces was analysed (Figure 22 A, B and C). Consistent with previous findings concerning the effects on actin dynamics,

the wildtype SLy2 expressing cells had spread to a significantly larger extent than their control counterparts after 45 min and also the S23A mutant expressing cells spread more readily to the gelatine substrate. Surprisingly, the deletion of the NLS or the SH3 domain facilitated spreading to a much larger extent than expected, with a spreading index significantly higher than that displayed by the control cells (Figure 22 A and B). The seemingly diminished spreading activity induced by the SH3 deletion reflects a weakness in the analysis, as the spreading index was determined by the ratio of the length to the width of each cell. Since the ΔSH3 expressing HeLa cells spread in a more even and round fashion, this ratio does not express the effect of this mutant. Yet, if comparing the size of the cell-substrate contact area instead, the ΔSH3 mutants aligned with the other SLy2 species analysed with respect to their spreading behaviour (Figure 22, C). Since the S23A expressing cells showed such a pronounced tripod like shape, also here it was difficult to determine the true width and length of each cell. Accordingly, this HeLa species was additionally analysed by the second method too, proving the strong effect of this mutant protein.

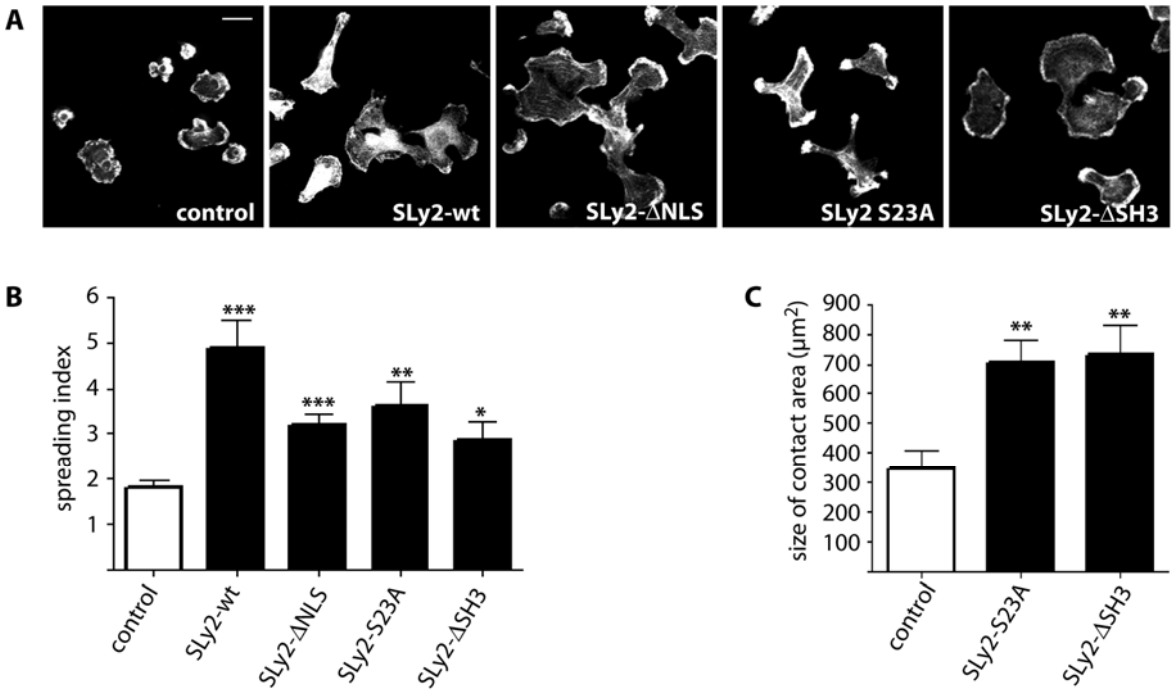

Figure 22: Enhanced spreading capacity of transgenic HeLa cells. (A) HeLa cells were transduced with the indicated constructs and seeded onto gelatine coated cover glasses. The cells were allowed to adhere for 45' and subsequently fixed and stained for F-actin (scalebar: 20 µm). (B) 10 cells were analysed for every species and the spreading index was determined as the ratio of length to width of each cell. (C) The size of the cell-substrate contact area was determined as the product of the length and the width of each cell (***, $p<0.0006$; **, $p<0.007$; *, $p<0.04$).

3.3.5. The overexpression of SLy2 leads to defective proliferation

While analysing the SLy2-HA expressing HeLa and Jurkat cell lines, it became apparent that the percentage of GFP^+ cells in the transduced populations declined over time. This effect emerged only in those cells that overexpressed SLy2 and its mutant derivatives but not in the control cells, expressing GFP alone (Figure 23, A). To assess if this was caused by a diminished rate of proliferation, BrdU pulse-chase experiments were conducted which indeed proved an anti-proliferative effect that correlated with the overexpression of SLy2 (Figure 23, B). As expected, HeLa populations expressing the different mutants did not display an equal decline of GFP^+ cells. Consistent with previous data, cells overexpressing the wildtype or the S23A protein showed the strongest defect, followed by ΔNLS, which inhibited cell growth at an intermediate level. Deletion of the SH3 domain almost led to a full restoration of a normal proliferation rate. The obvious parallels in the effect of the various deletions on actin dynamics and proliferation favoured the assumption that the inhibition of cell growth is connected to the massive alterations in the actin cytoskeleton observed in these cells.

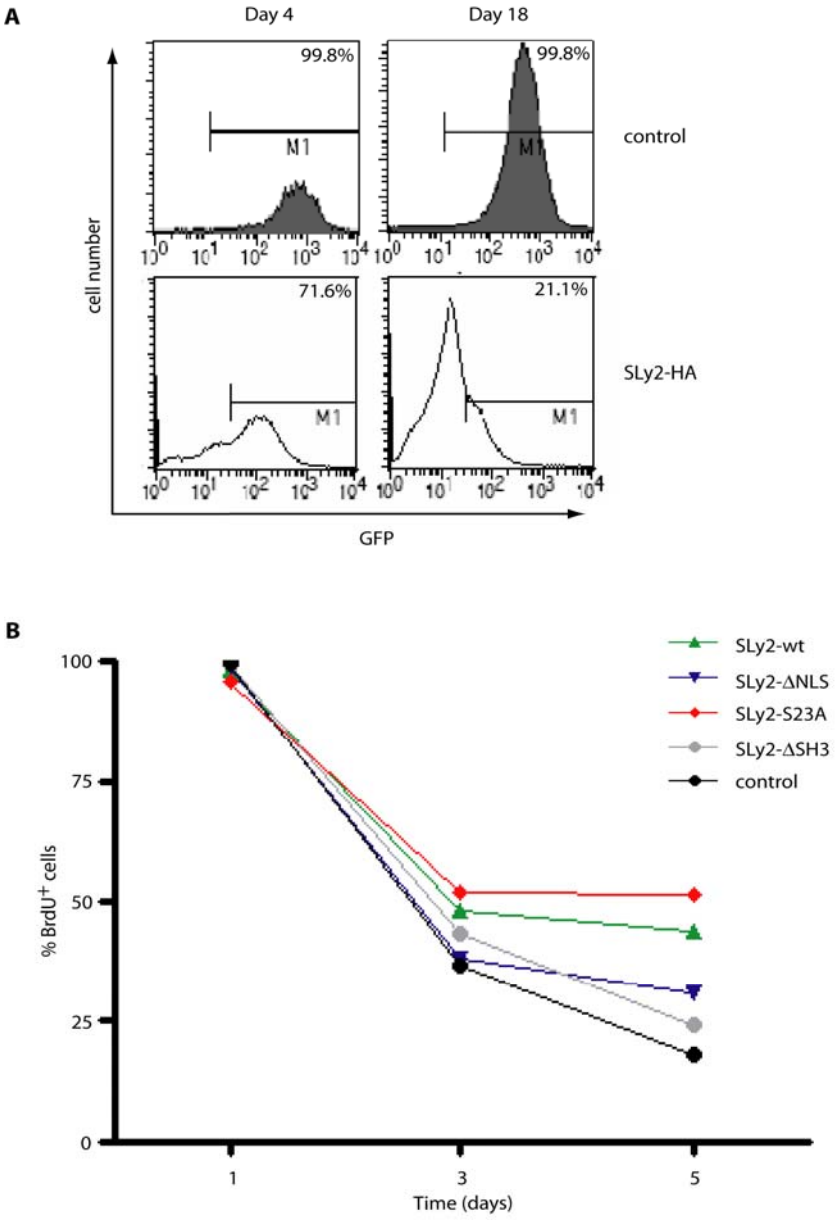

Figure 23: Overexpression of SLy2 inhibits proliferation. (A) Jurkat cells were transduced with SLy2-IRES GFP or GFP-only expression constructs. GFP expression served as marker for SLy2 expression and the amount of GFP^+ positive cells was determined on day 4 and day 18 after transduction. The percentage of GFP^+ (Gate M1) cells is depicted in each histogram. (B) Transgenic HeLa cells were pulsed with BrdU and the BrdU content of the cells was monitored for 5 days. Results are representative of at least 3 independent experiments.

3.3.6. Overexpression of SLy2 causes the formation of cytonemes

Interestingly, a strict dependency on actin polymerisation was reported for cytokinesis, the last step of cell division, in which the two daughter cells separate their cytoplasms after successful karyokinesis (Eggert et al., 2006). Interfering with cytokinesis stops the last step of cell division, leaving the two daughter cells connected by a thin cytoplasmic tube, a

cytoneme. As mentioned above, the overexpression of wildtype SLy2 and the S23A mutant induced the formation of such bridges between the cells. The detailed analysis of cells growing on gelatine coated cover glasses and stained for F-actin demonstrated that this induction of cytonemes almost exclusively occurred in cells expressing SLy2 wildtype or S23A (Figure 24).

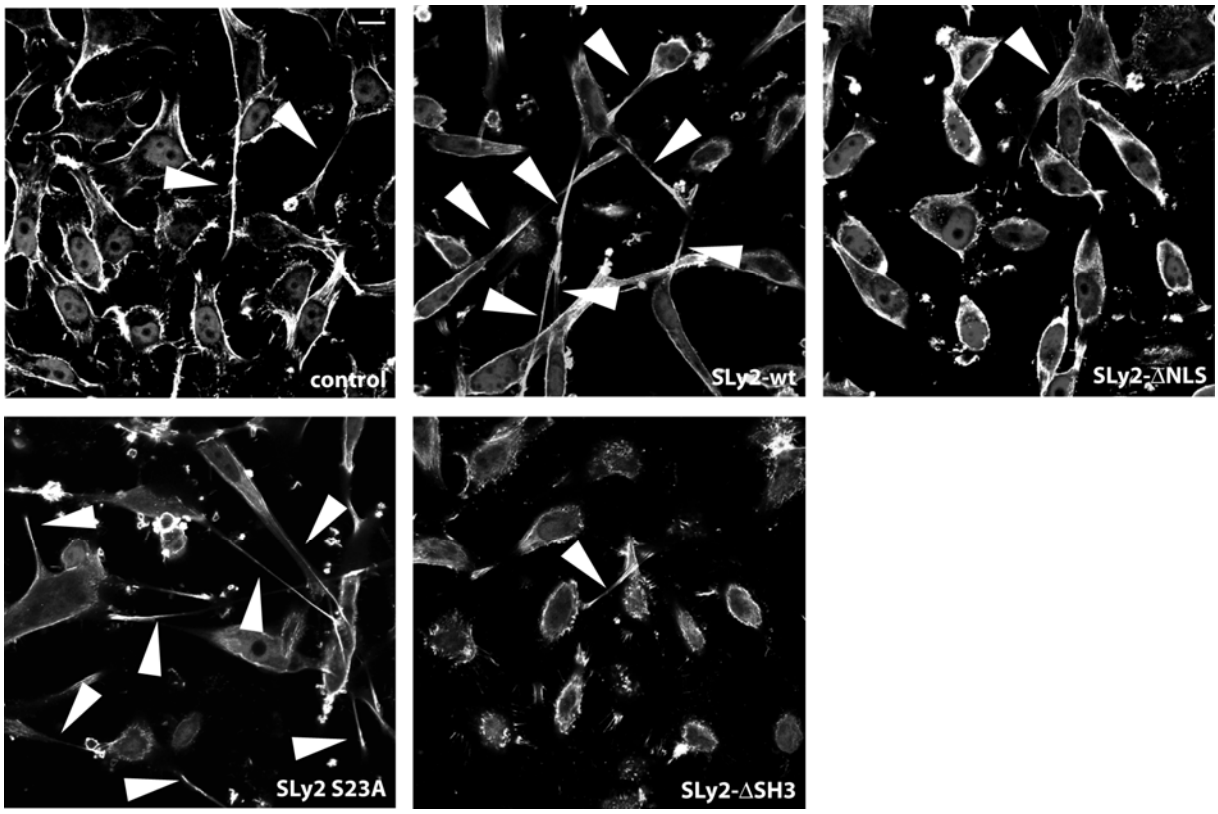

Figure 24: Overexpression of SLy2 induces the formation of cytoplasmic bridges between dividing cells. HeLa cells were transduced with expression constructs for various SLy2 species or control plasmids. Cells were seeded onto gelatine coated cover glasses, allowed to grow for 24h and stained for F-actin. Arrowheads indicate cytonemes (scalebar: 10 µm).

The notion that SLy2 overexpression interfered with cytokinesis received further support by the finding, that in SLy2 wildtype, and even more in S23A expressing cultures huge multinucleated cells accumulated, probably caused by aberrant cell division (Figure 25).

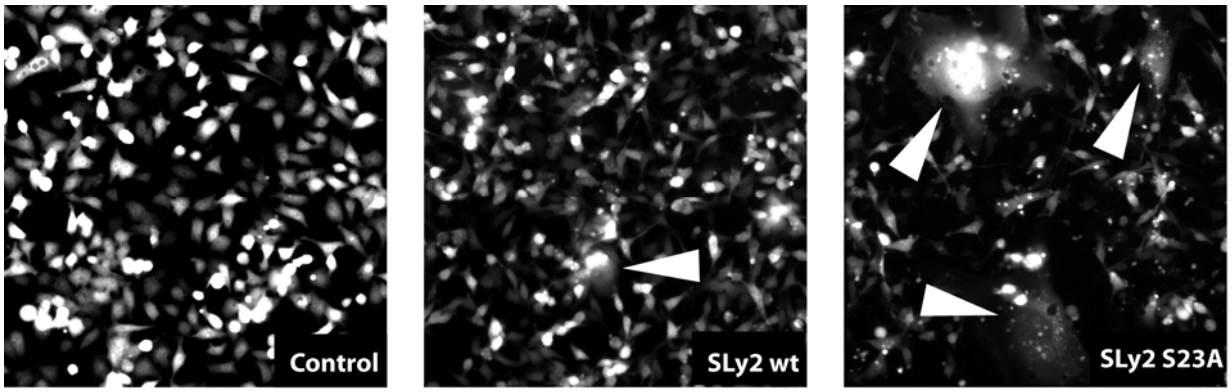

Figure 25: Overexpression of SLy2 in HeLa cells induces generation of giant cells. HeLa cells were transduced with SLy2 expression or control constructs and grown in 6-well dishes. Pictures were taken on day 5 after transduction. Arrowheads indicate giant, multinucleated cells.

3.4. SLy2 is involved in the activation of Rho-family GTPases

3.4.1. Dominant negative Rac1N17 counteracts the effects of SLy2

The Rho-family GTPases Rho, Rac and Cdc42 were shown to be of crucial importance for the regulation of a plethora of actin-cytoskeletal processes. Indeed, different actin-structures can be associated with the function of different Rho family members. The induction of stress fibres is connected to the GTPase activity of Rho, while lamellipodia and membrane ruffles are mediated mainly through the function of Rac1 and to a lesser extent also of Cdc42. In addition, the latter is responsible for the induction of filopodia (Hall, 1998). Due to the morphology of HeLa cells overexpressing SLy2, an investigation of the role of Rac1 in the generation of the phenotype was performed. To determine if the effect of SLy2 overexpression on the induction of ruffles and lamellipodia was mediated by Rac1, a dominant negative mutant of Rac1, Rac1N17 or a control construct were transfected into these cells. Transfectants expressing SLy2 and the control plasmid (indicated by the mCherry expression) showed the intense actin-cytoskeletal rearrangements described above (Figure 26, middle panels). Yet upon expression of Rac1N17, this phenotype was entirely reverted and the double expressing cells took on a wildtype appearance again (Figure 26, right panels). The cells displayed a strong staining of the cortical actin networks and also stress fibres were reappearing. The same held true for HeLa cells expressing the S23A mutant, whose effect was also annihilated by the simultaneous expression of Rac1N17. Expression of this dominant negative mutant in control cells without the expression of SLy2 showed a rather mild effect on cellular F-actin structures (Figure 26, left panels).

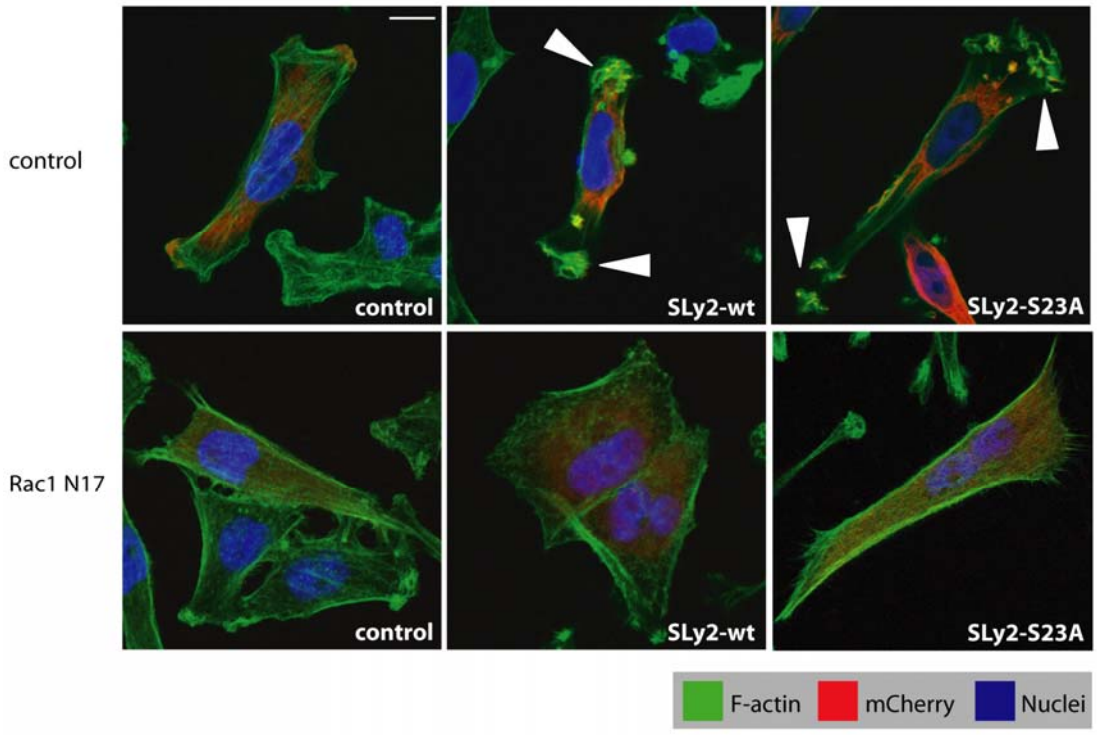

Figure 26: Point mutations in Rac interfere with the effect of SLy2 in HeLa cells (I). HeLa cells expressing SLy2-wt, SLy2-S23A or a control construct were transfected with a dominant negative Rac1N17 expression construct (lower panels) or the empty mCherry vector (upper panels). Transfectants are marked by the red colour. Cells were seeded onto gelatine coated cover glasses and stained for F-actin (green) and nuclei (blue). Arrowheads indicate SLy2 induced membrane ruffles (scalebar: 10 µm).

3.4.2.Constitutively active Rac1V12 and SLy2 act in concert

The dependency of the effect of SLy2 on Rac1 signalling was further supported by the phenotype of HeLa cells expressing the constitutively active Rac1 point mutant Rac1V12. The control cells, only expressing Rac1V12 displayed the marked induction of lamellipodia along the cell cortex. The overexpression of Rac1V12 and SLy2 or SLy2-S23A led to the strong induction of dorsal ruffles and to a more spiky confirmation of the cortical F-actin, both of which are not induced by the overexpression of SLy2 or RacV12 alone (compare to Figure 20 and Figure 27, left panel). A further finding pointing in the same direction was the marked poly-karyogeny displayed by HeLa cells co-expressing both SLy2 and Rac1V12 (Figure 27). This phenotype was not observed in cells expressing the small GTPase alone (left panel and (Ridley et al., 1992)) and, as described above, also in SLy2 expressing HeLa populations these giant cells only accumulated over a longer period (Figure 25).

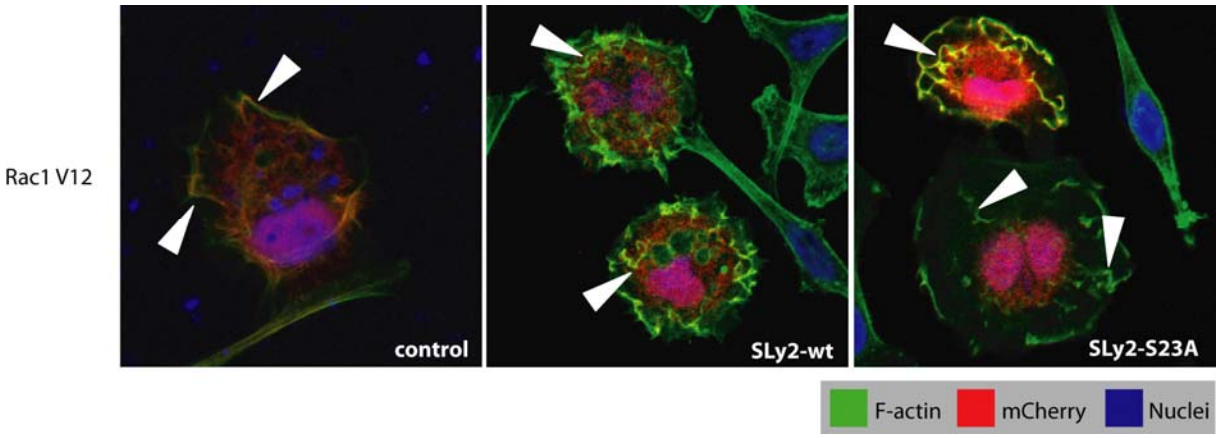

Figure 27: Point mutations in Rac interfere with the effect of SLy2 in HeLa cells (II). The same cells as in Figure 26 were transfected with an expression construct for constitutively active Rac1V12. Transfectants are marked by the red colour. Arrowheads indicate lamellipodia (left panel) or dorsal ruffles (middle and right panels). The cells were seeded onto gelatine coated cover glasses and stained for F-actin (green) and nuclei (blue).

3.5. A search for SLy2-interacting proteins at the cytoskeleton

The strong effects of ectopic SLy2 expression onto the cytoskeleton lead to the subsequent question, which of the plethora of pathways known to be involved in actin reorganisation would be employed by this novel adapter protein. In general, two different approaches were chosen to unravel binding partners of SLy2. The first one was of biochemical nature and consisted of the co-immunoprecipitation (Co-IP) of possible SLy2 binding partners from ^{35}S labelled cell lysates. The second approach was based on a database mediated similarity search for the interaction partners of proteins with SH3 domains homologous to that of SLy2.

3.5.1. Co-immunoprecipitation of SLy2 binding partners

Co-IP is a powerful method to analyse the entity of interaction partners of a given protein. To allow the later visualisation by autoradiography, cells expressing SLy2-HA or a control construct were metabolically labelled with ^{35}S. Subsequently, the cells were either treated with H_2O_2 and sodium-pervanadate or left untreated prior to lysis and immunoprecipitation with α-HA antibody. Figure 28 shows the autoradiographic analysis of Co-IPs from murine endothelial cells. Several proteins migrating at different sizes were co-immunoprecipitated with SLy2 and did not occur in the control lane. A background signal migrated at the same size as SLy2-HA, yet this was most probably unspecific, as the control cells did not express any HA-tagged protein. A second signal, which occurred in all

four samples, migrated at approximately 42 kDa and most likely represented actin. Most interesting, one protein migrating around 90kDa was only co-precipitated upon activation of the cells (Figure 28, uppermost arrowhead). This was of special interest as the previously mentioned regulator of actin dynamics, cortactin, has a size of approximately 85kDa.

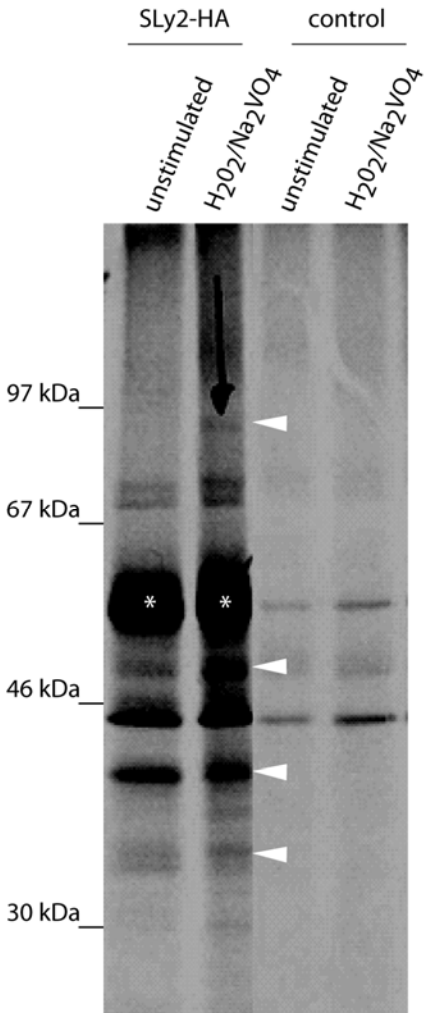

Figure 28: Coimmunoprecipitation of SLy2 interacting proteins from ^{35}S-labelled cell lysates. Transduced SVEC cells (murine endothelial cell line) expressing SLy2-HA or a control construct, were metabolically labelled over night with ^{35}S marked methionine/cysteine. Subsequently, the cells were stimulated, lysed and SLy2 was immunoprecipitated with α-HA. Precipitated proteins were separated on 10% polyacrylamide gels and radioactively labelled proteins were detected by autoradiography as described. The arrowheads indicate signals precipitated only in the SLy2-HA samples. The primary SLy2 IP signal is marked by an asterisk.

3.5.2. A homology based screen for interaction partners

SH3 domains have been known to be involved in protein-protein interactions for a long time and fulfil crucial functions in many proteins. They mediate protein-protein interactions by binding to evolutionary conserved proline rich domains. Facilitated by the great number of SH3 domain containing proteins with well described binding partners, a BLAST search was performed with the SH3 domain of SLy2. After all double hits and entirely unknown proteins were excluded from the primary list of homologous proteins, ten candidate proteins emerged. The left panel of figure 29 A shows these candidates, sorted by order of the percentage of identity of their SH3 domain to that of SLy2. A comprehensive publication database search identified the reported interaction partners that the previously identified proteins would bind through their SH3 domains (Figure 29 A, right panel). The cDNA for each of these fourteen candidate proteins was amplified by RT-PCR from mouse tissues and cloned into an expression construct, adding a C-terminal myc-tag to each open reading frame. The co-transfection of these expression-constructs together with a SLy2-HA expression plasmid into 293T cells and subsequent IP with α–HA produced a first set of potentially SLy2 interacting proteins (Figure 29, B). With Cbl-b, SLP-65 and SLP-76 and Gab-1, four out of these seven proteins represent important players of antigen receptor proximal signalling. Also connected to TCR signalling was the interaction with the intracellular domain of CD2 (LFA-2), which serves as an adhesion molecule in T cell-APC interaction. Finally, RN-tre and cortactin represent proteins that are essentially involved in regulation of the actin cytoskeleton. RN-tre has been found to bind actin, but being a GAP for the GTPases Rab-5 and Rab-43 it mainly exerts effects on endocytosis and membrane trafficking (Lanzetti et al., 2004; Haas et al., 2007). Accordingly, out of the seven primary candidates, only cortactin is known for being a master regulator of actin dynamics in membrane protrusions (Cosen-Binker and Kapus, 2006).

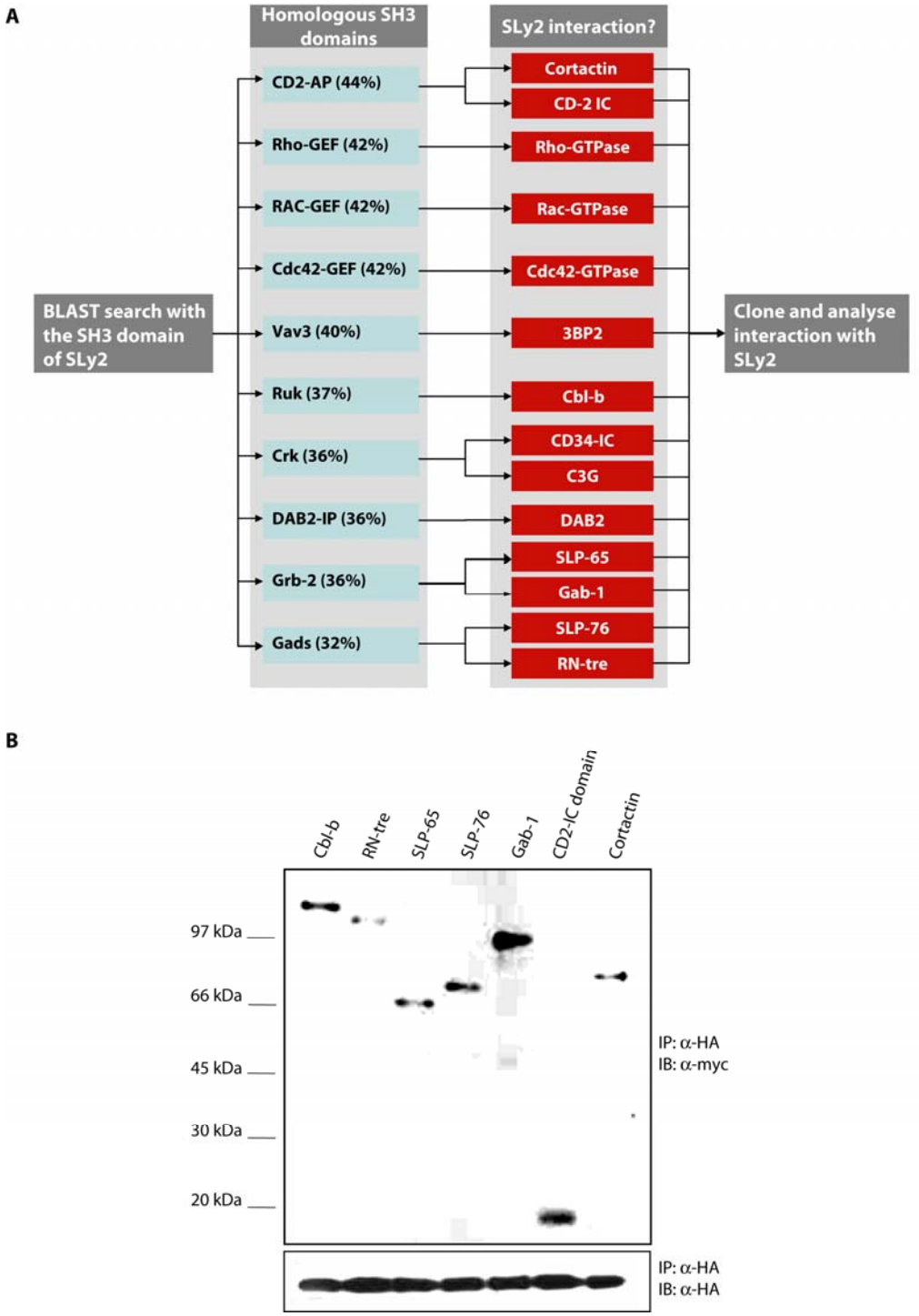

Figure 29: A homology based search for SLy2 interacting proteins. (A) A blast search with the SH3 domain of SLy2 was conducted in NCBI database. Step 1 was the identification of proteins with homologous SH3 domains, which are depicted in box 1 (The values describe the percentage of identity between the SH3 domain of SLy2 and that of the candidate protein). Subsequently Pubmed database was searched for proteins interacting with the former proteins through their SH3 domains (box 2). (B) The candidate binding partners identified in (A) were cloned into expression construct, adding a C-terminal myc tag. Constructs were cotransfected with a SLy2-HA expression plasmid into 293T cells and IPs with α-HA were performed. Shown are only those candidates that could be co-immunoprecipitated with SLy2, as determined by western blotting with α-myc.

3.5.3. SLy2 colocalises with cortactin in peripheral ruffles

Considering the pronounced effect on cortical actin dynamics observed in SLy2 overexpressing cells and the coimmunoprecipitation from 293T cells, cortactin was a promising candidate to mediate the observed cytoskeletal changes. This multi-domain adapter protein was shown, together with its close homologue HS1, to localise to the cell membrane upon stimulation, where it binds F-actin, Arp2/3 and WASP family proteins, thus leading to the enhanced formation and increased stability of branched actin structures (Cosen-Binker and Kapus, 2006).

To get a first hint about a possible interaction of SLy2 with cortactin, their respective localisation was analysed in SLy2-HA overexpressing HeLa cells, co-stained for both proteins. Consistent with the previous data, SLy2 and cortactin showed a specific colocalisation in the distal ruffles induced by overexpression of SLy2 (Figure 30, upper row). Subsequently, it was essential to determine the domain(s) of SLy2 involved in the colocalisation with cortactin. As expected, the S23A mutation did rather have an enhancing effect on the colocalisation. Consistent with the homology based screen for binding partners, the colocalisation signal was lost upon deletion of the SH3 domain. Unpredicted, but consistent with previous data, also the deletion of the NLS abolished the colocalisation of SLy2 with endogenous cortactin (Figure 30).

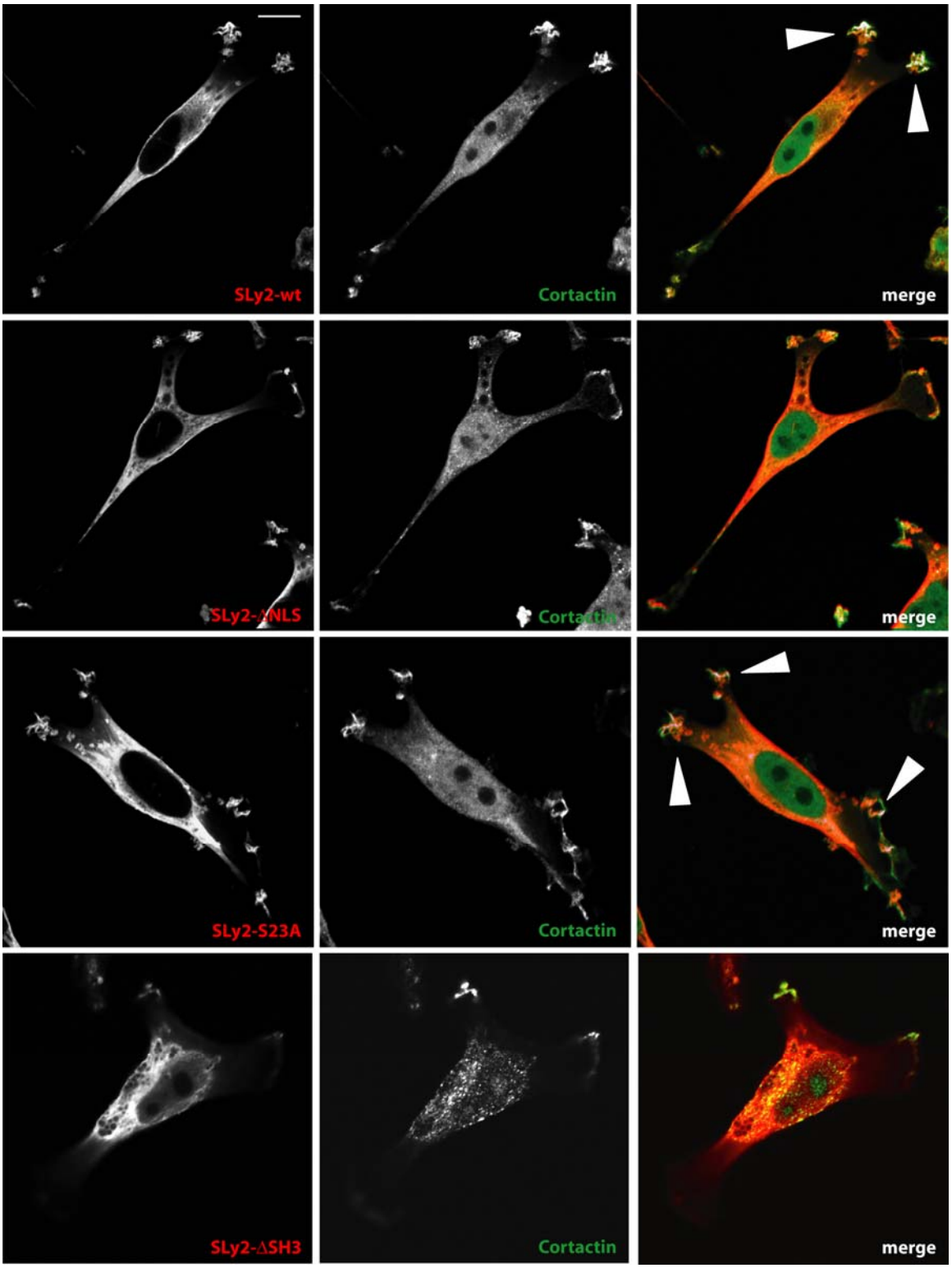

Figure 30: SLy2 colocalizes with cortactin in peripheral ruffles. HeLa cells were transduced with different SLy2 expression constructs, seeded onto gelatine coated cover glasses and subsequently stained for SLy2 and cortactin. The SLy2 staining is shown in the left, the cortactin staining in the middle panels. The merged images are shown on the right with SLy2 in red and cortactin in green. Pixels with colocalising stainings are marked white in the merged images, as indicated by the arrowheads. Images were analysed with ImageJ and the plug-in *colocalizationRGB* (scalebar: 10 µm).

3.5.4. SLy2 interacts with cortactin-family proteins

To analyse the physical interaction of SLy2 and cortactin, SLy2-HA was immunoprecipitated from HeLa lysates and the IPs were analysed by western blotting with an α-cortactin antibody. As shown in Figure 31 A, endogenous cortactin could be precipitated together with SLy2 from unstimulated HeLa cells, transduced with a SLy2-HA expression vector. Consistent with the immunofluorescent data, it turned out that the ΔNLS and the ΔSH3 mutants were not capable of binding to cortactin anymore (Figure 31 B, left western blot). Interestingly, stimulation of the cells with the phorbol ester PDBU prior to the IP, reconstituted the binding of SLy2 to cortactin in all SLy2 variants, independently of the deletion (Figure 31 B, right western blot). The S23A mutant was not included in this analysis since gathering the appropriate cell numbers for the IPs was hindered by the proliferational defects displayed by cells overexpressing SLy2-S23A.

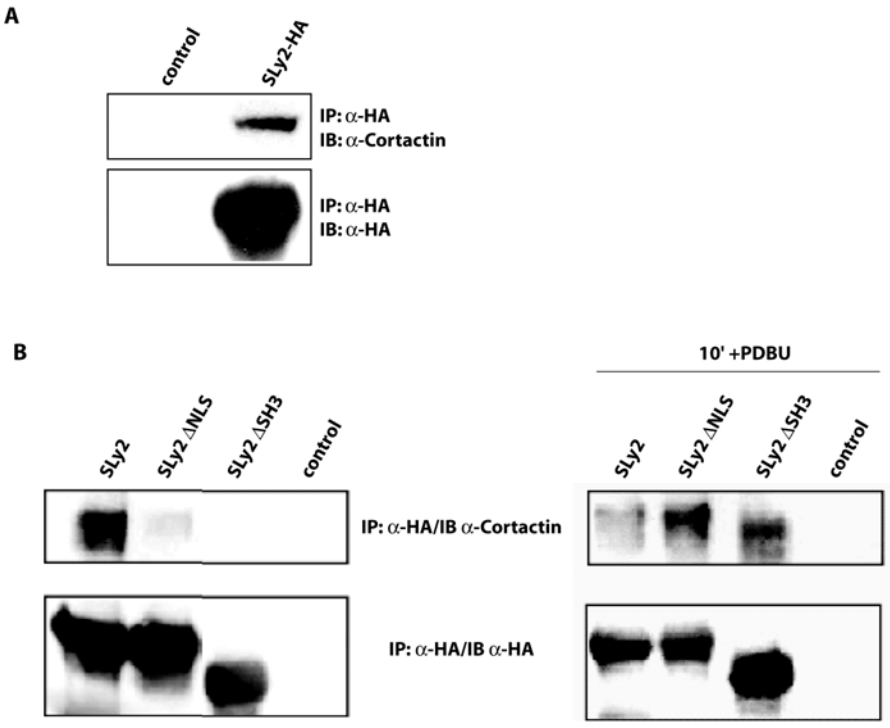

Figure 31: Co-immunoprecipitation of cortactin with SLy2. (A) HeLa cells were transduced with SLy2-HA or a control construct. SLy2 was precipitated with α-HA and IPs were analysed by western blotting with an α-cortactin antibody. (B) HeLa cells were transduced as described with expression vectors for various SLy2 mutants. The cells were left untreated or stimulated with PDBU for 15 min. Subsequently, SLy2 was precipitated with α-HA and coimmunoprecipitation was analysed by western blotting with α-cortactin and α-HA (IP-control).

The cortactin family comprises only two proteins, cortactin itself and HS1, a close homologue, which is exclusively expressed in lymphocytes (Weed and Parsons, 2001). As HS1 function was shown to be crucial in the formation of an intact immunological synapse (Gomez et al., 2006), it was a promising candidate to cause the aberrant spreading to antigen coated surfaces seen in SLy2-transgenic B cells. To analyse a possible interaction between SLy2 and HS1 in primary lymphocytes, murine splenocytes of wildtype or transgenic background were lysed and the transgenic SLy2-HA was precipitated. The IPs were analysed by western blotting with α-HS1 antibody and indeed demonstrated an interaction of the two proteins (Figure 32).

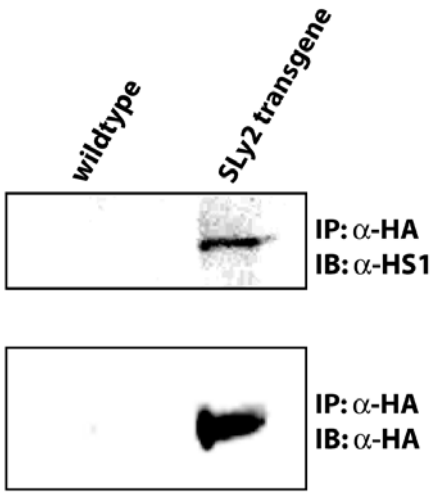

Figure 32: SLy2 also interacts with the cortactin lymphocyte homologue HS1. Murine splenocytes were isolated from wildtype or SLy2 transgenic spleens as described. SLy2 was precipitated from lysates with α-HA and IPs were analysed with α-HS1.

3.6. Generation of a SLy2 deficient mouse strain

The generation of genetic deficiencies by means of gene targeting is a powerful tool in the functional analysis of any given protein. Gene-targeting is based on the phenomenon of homologous recombination (Thomas and Capecchi, 1986; Thomas et al., 1986). This describes the interaction of two homologous stretches of DNA, one on the genomic side, the other on an external DNA fragment. Mediated by crossing-over events between these identical regions, genetic information is exchanged and thus introduced into the genomic DNA in a site specific, i.e. targeted manner. According to the conventional method, as introduced by Capecchi and colleagues (Thomas and Capecchi, 1987), an expression cassette for a neomycin resistance gene, which is flanked by DNA stretches identical to the

insertion site (so called arms of homology), is introduced into the coding region of the target gene by homologous recombination. This blocks transcription through insertion of a number of ectopic stop codons and simultaneously allows the positive selection of cells carrying the mutation. To maximise the inhibitory effect of the cassette, the latter is inserted in inverted orientation into the target gene, so that its own transcription interferes with that of the genomic locus. As homologous recombination is such an unlikely event, the vast majority of cells contain random integrations of the construct. Accordingly, a negative selection cassette, the thymidine kinase of *Herpes Simplex Virus* (*HSV-tk*), is also inserted into the targeting construct. This gene is positioned outside of the homology arms, and is thus only inserted upon random integration and not in the case of homologous recombination. Supplementation of the ES cell medium with the *HSV-tk* substrate ganciclovir leads to the generation and integration of the nucleotide analogon and thus to the counter selection of those ES cell clones with random integrations. After a ten day period of double selection, the surviving ES cell colonies are picked, propagated and checked for homologous integration of the targeting construct. ES cells carrying the desired mutation are subsequently injected into 3.5 day mouse blastocysts and implanted into mock-pregnant foster mothers, resulting in the chimeric animals founding a gene-targeted mouse strain.

3.6.1. First targeting strategy

To achieve the targeted deletion of the *sly2*-locus, the *neoR*-cassette was planned to be inserted into the first coding exon of SLy2 (exon1) only a few base pairs downstream of the start ATG. A targeting construct was cloned with one arm of homology on either side of the *neoR*, representing the regions flanking the insertion site. To minimise the alteration of the genomic locus, the selection cassette was inserted without the deletion of endogenous sequence, maintaining the original pattern of splice donors and acceptors. The homology arms were generated by PCR from E14 ES cell genomic DNA, to guarantee complete sequence identity. The short arm of homology located 5' of the *neoR* comprised 2.5kb of genomic sequence, whereas the long arm of homology consisted of the downstream adjacent 5.1kb of the SLy2 locus. Both arms of homology were cloned into pBluescript, 5' and 3' of the previously inserted *neoR*-cassette and followed by the *HSV-tk* gene. Integrity of the construct was determined by analysis of various restriction digests (data not shown).

The southern blot strategy to detect homologously recombined ES cell clones employed a 5' flanking probe, hybridisation of which would yield an 11.4kb and an 8.9kb fragment for the wildtype or the targeted locus, respectively (Figure 33).

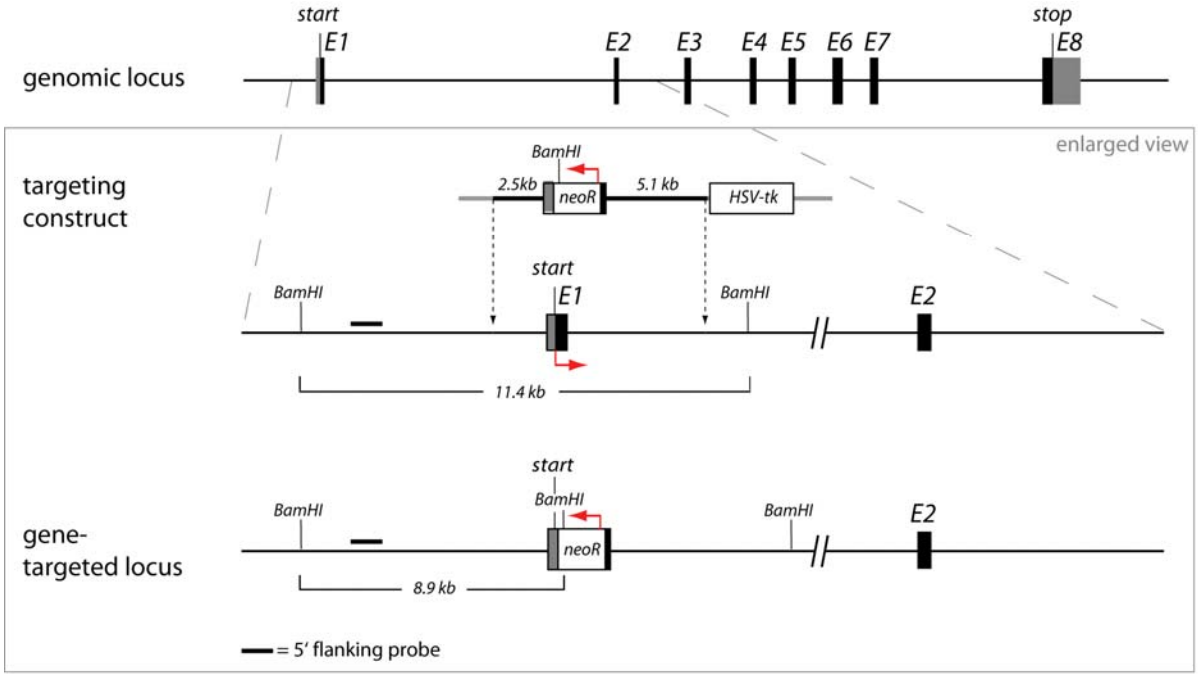

Figure 33: First strategy to genetically inactivate the *sly2*-locus. To achieve an inactivation of the *sly2*-locus, a *neomycin* resistance gene expression cassette (neoR) was inserted in inverted orientation with respect to the transcriptional start of the endogenous reading frame, directly downstream of the first ATG. To detect homologously recombined ES cell clones a southern blot strategy was designed, which employs a probe flanking the targeting construct on the 5' side. Hybridisation of this probe to *BamH*I digested genomic DNA would yield a signal migrating at 11.4 kb in the wildtype locus and one migrating at 8.9 kb in the targeted situation. UTRs are marked in grey, coding exons in black (not drawn to scale) (red arrows indicate the direction of transcription).

E14.1 ES cells were electroporated with the linearised targeting construct and double selected for 10 days with G418 (geneticin) and ganciclovir. 500 clones were analysed by southern blot, four of which were identified as homologously recombined (Figure 34 A). Two of these clones, C12 and G5, were injected into blastocysts and gave rise to two independently generated SLy2 gene-targeted mouse lines. Figure 34 B shows the southern blot analysis of mouse tail DNA from strain C12.

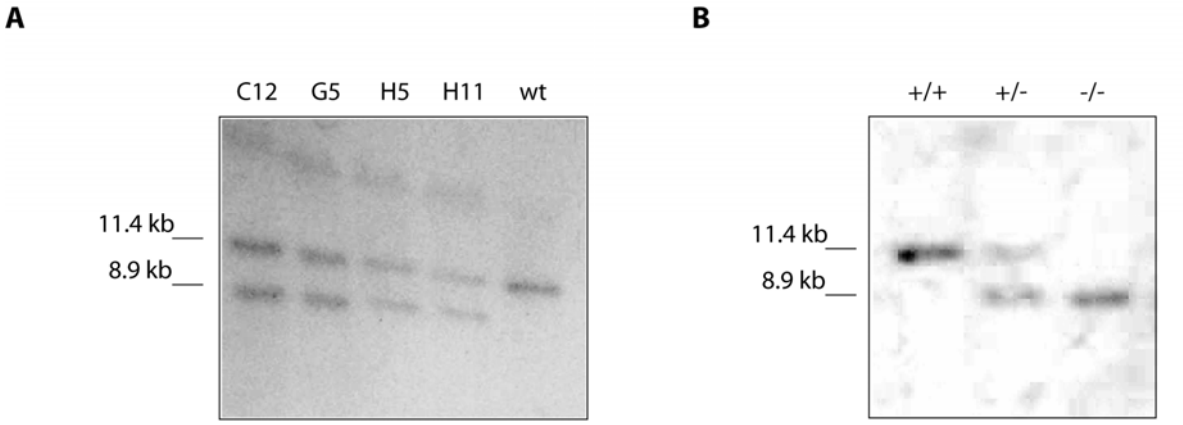

Figure 34: Targeted ES cell clones and mice. (A) The ES cell DNA was isolated and analysed by southern blot as described. The 5' flanking probe was hybridised to *BamH*I digested DNA. Shown are the four homologously recombined clones and a wildtype control. The clones C12 and G5 were injected into blastocysts to generate gene-targeted mouse strains. (B) Genomic DNA from mouse tail biopsies (strain C12) was isolated as described. The DNA was digested with *BamH*I and wildtype and targeted fragments were detected by hybridisation with the 5' flanking probe.

3.6.1.1. SLy2 gene-targeted mice express functional SLy2 protein

To confirm the inactivation of the *sly2*-locus in the gene-targeted mice, splenocytes of wildtype and gene-targeted mice were isolated and analysed by northern and western blotting for SLy2 expression. Northern blot analysis with a complete SLy2 cDNA probe clearly proves that there was still a substantial amount of SLy2 mRNA, although at diminished levels compared to wildtype (Figure 35 A). Western blot analysis with a polyclonal α-SLy2 serum indicated that, in contrast to the mRNA, the protein levels of SLy2 were equal in wildtype and gene-targeted mice (Figure 35 B). A further striking finding was the apparently unchanged size of the message and the corresponding protein in the wildtype and the targeted situation (Figure 35 A and B).

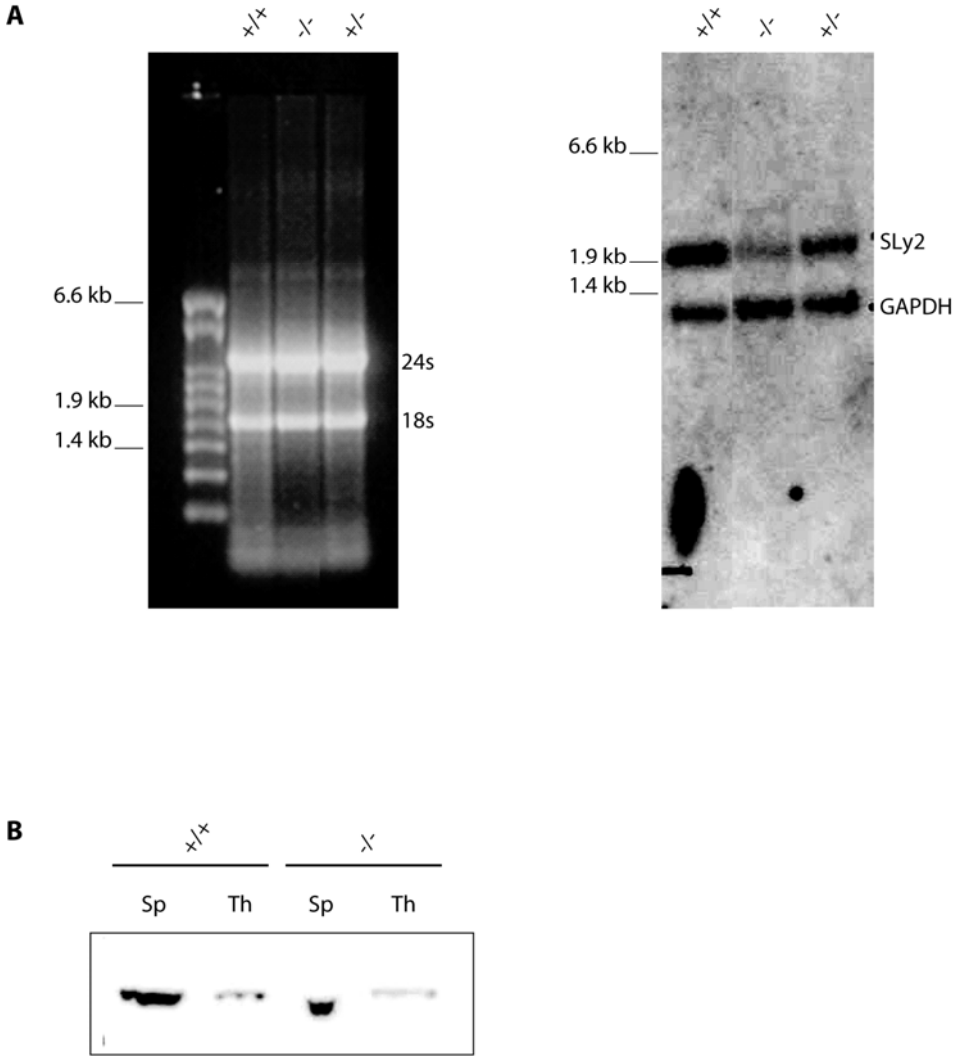

Figure 35: Expression of SLy2 in wildtype as well as in gene-targeted mice. (A) RNA was isolated from thymi of wildtype and gene-targeted mice as described. 20µg of total RNA from each sample were separated on a formaldehyde containing 1% agarose gel (left panel), blotted and hybridised with full length cDNA probes of SLy2 and GAPDH (right panel), the latter serving as loading control. (B) Splenocytes (Sp) and thymocytes (Th) from wildtype and gene-targeted mice were isolated and lysed as described. Lysates were separated on 10% polyacrylamide gels and immunoblotted with a peptide-purified α-SLy2 polyclonal serum.

3.6.1.2. Ectopic splicing and an alternative ATG lead to SLy2 expression in gene-targeted mice

To unravel the nature of the unexpected SLy2 expression in the gene-targeted mice, RACE PCR was employed. As the region of interest was located in the 5' part of the mRNA, the RACE PCR was performed with a gene specific reverse primer in exon 5. This led to the amplification of different fragments, depending on the genotype. The wildtype cDNA yielded the expected fragment of approximately 600bp, sequencing of which proved the annotated sequence and exon-intron structure (Figure 36 A left gel lane and B upper

drawing). Gel electrophoresis indicated that the RACE product from the gene-targeted cDNA migrated slightly higher than the wildtype fragment. Additionally, there was a second amplicon in the gene-targeted situation, migrating just below 2.0kb (arrowhead in A). Cloning and sequencing of both gene-targeted fragments showed the difference to the wildtype situation. The large amplificate comprised exons 1-5 and the complete *neoR* selection cassette inserted into exon 1. The smaller, more abundant fragment also contained a fragment of *neoR*, but only the 3' end of it (Figure 36 A right lane and B lower drawing).

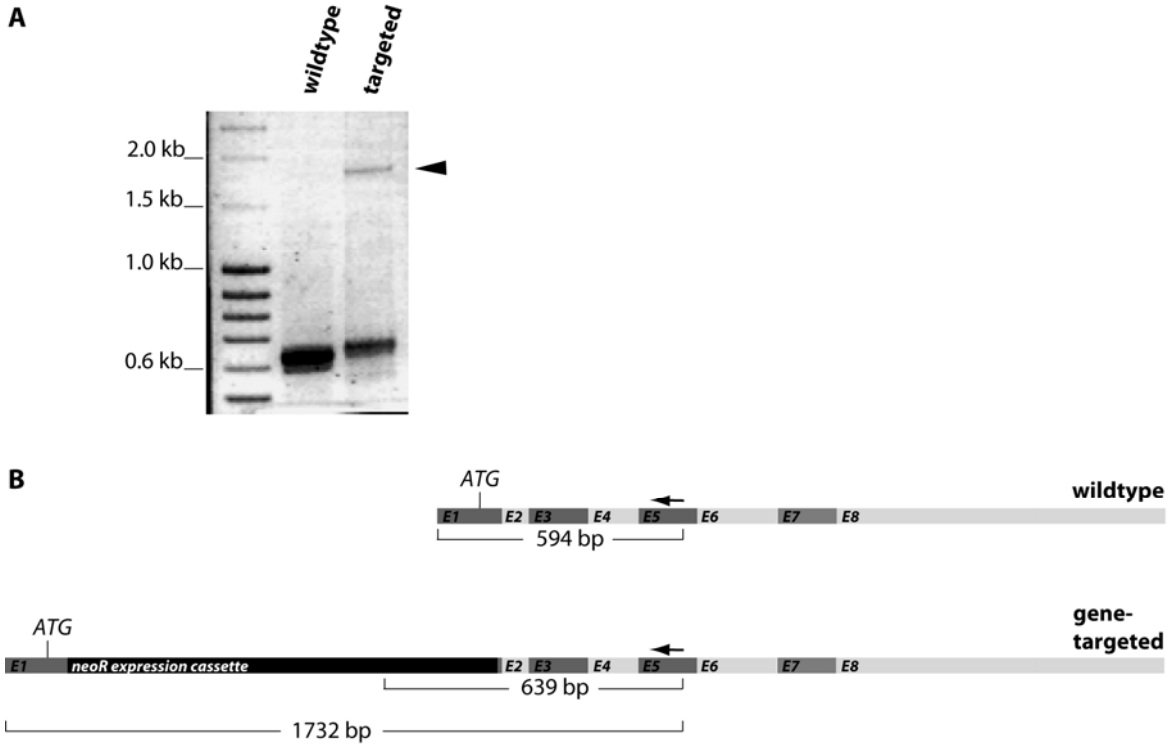

Figure 36: RACE PCR on wildtype and gene-targeted SLy2 cDNA yields different fragments. (A) RACE PCR was performed on cDNA from wildtype and gene-targeted splenocytes with a reverse primer in exon 5. The fragments are roughly 30 bp bigger than expected from the locus, due to additional nucleotides in the 5' RACE primer. The arrowhead indicates the large fragment amplified only from gene-targeted cDNA. (B) Schematic drawing of the wildtype and the gene-targeted cDNA species. The arrow indicates the gene specific reverse primer used for the 5' RACE reaction. Below the sequence, the length of the fragments yielded in the RACE PCR is depicted as confirmed by sequencing.

The analysis of the hybrid mRNA sequence (SLy2 + *neoR*) with a detection program for cryptic splice sites (*splicefinder*, H. Schaal, personal communication) suggested the existence of two fairly strong splice acceptors in the vicinity of the start codon of the *neoR*-gene. Subsequent sequence analysis of the now known hybrid fragment proved the

existence of more than one alternative start ATG, usage of which would yield an ORF* in frame with the original one (Figure 37). This new ORF would lead to a similarily sized protein only lacking the first nine amino acids, which would also include the first 6 residues of the N-terminal fraction of the bipartite NLS.

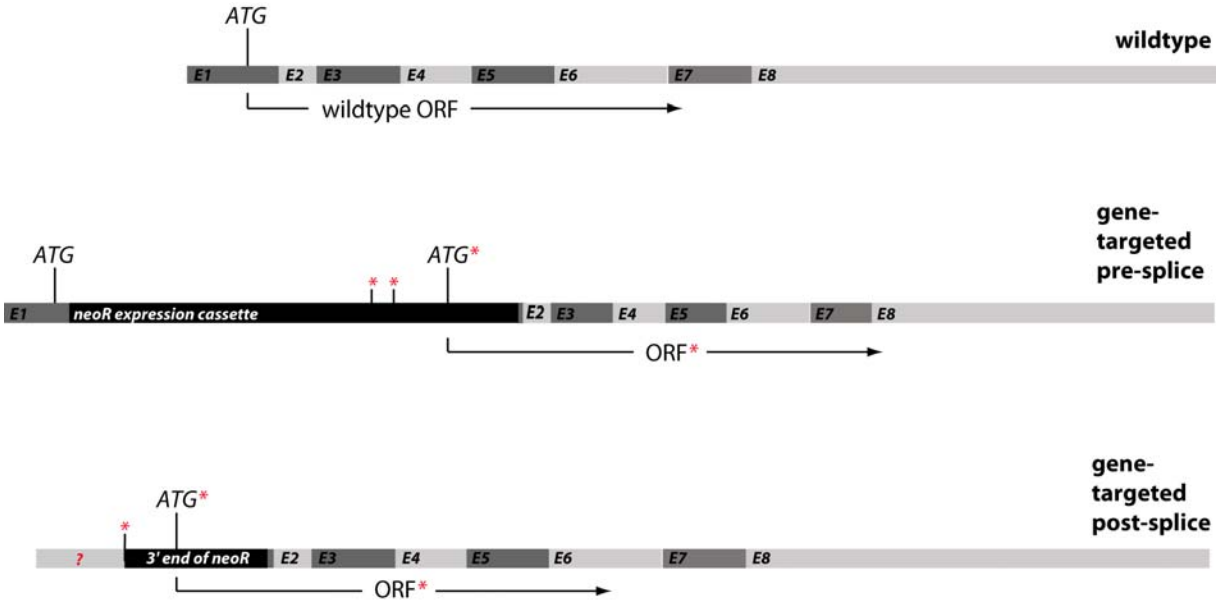

Figure 37: A theory to explain expression of a wildtype sized SLy2 from the targeted locus. Splicing of an hypothetical upstream exon onto one of two strong splice acceptors (red asterisks) in the *neoR* expression cassette and subsequent usage of an alternative ATG* in the 3' end of the cassette leads to the transcription of a new mRNA, ORF*, with the same reading frame as the wildtype message. The hypothetical upstream exon is indicated by a question mark.

3.6.2. Second targeting strategy

Sensitized by the outcome of the first attempt to generate SLy2 deficient mice, the second targeting strategy was designed to rule out the possibility of such ectopic expression. As the nature of the hypothetical upstream exon remained obscure, only deletion of the larger part of the genomic locus could insure its complete inactivation. Therefore, the *neoR* cassette was inserted such, that it replaced all of the genomic sequence between exons 2 through exon 6, thereby deleting approximately 15kb of genomic sequence (Figure 38).

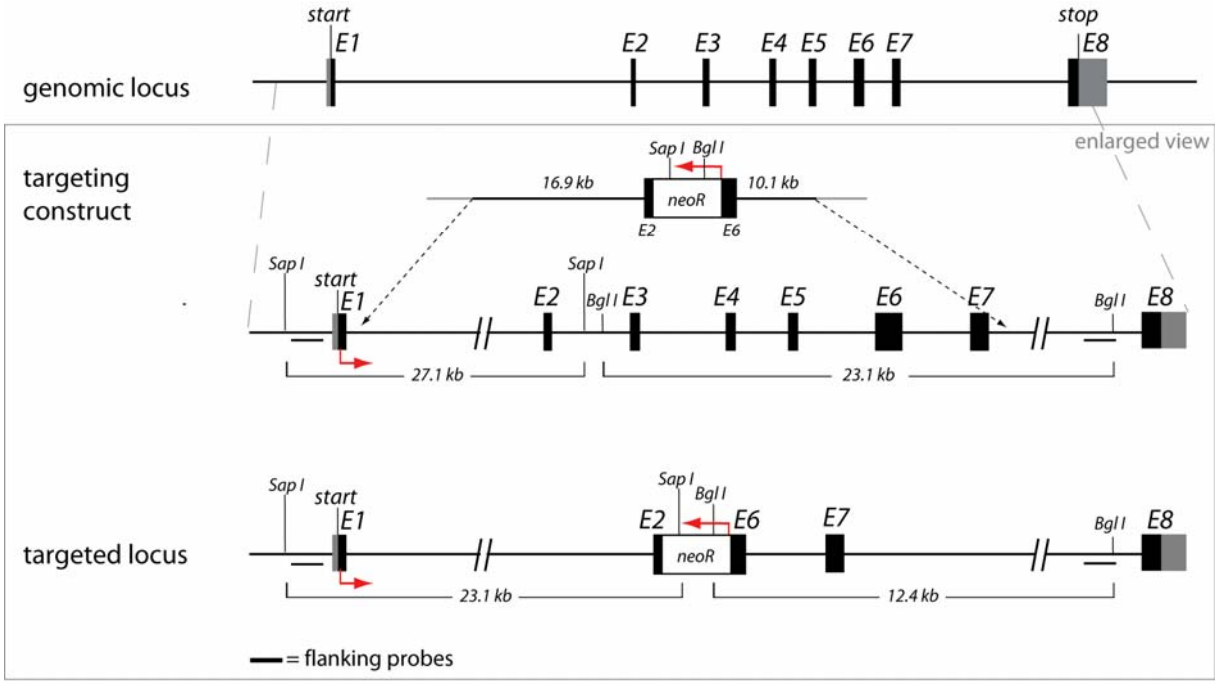

Figure 38: Second strategy to genetically inactivate the *sly2*-locus. To ensure the inactivation of the *sly2*-locus, the genomic region between exons 2-6 was replaced by the neomycin resistance cassette. The insertion left the 5' region of exon 2 and the 3' region of exon 6 intact, to facilitate correct splicing from exon 1 and to exon 7, respectively. The southern blot strategy to detect homologously recombined ES cell clones is comprised of an external 5' and a 3' probe. Hybridisation of the former to *Sap*I digested genomic DNA would yield a signal migrating at 27.1 kb in the wildtype locus and 23.1kb in the targeted situation. The 3' probe, together with a *Bgl*I digest would detect a fragment of 23.1kb in the wildtype and 12.4kb in the targeted locus (not drawn to scale) (red arrows indicate the direction of transcription).

Because the targeting efficiency negatively correlates with the size of the deletion, but positively with the length of the arms of homology, these had to be of adequate size. As a conventional cloning strategy limits this size to roughly 5kb, Red/ET cloning was applied as a new technique. This method makes use of fosmid or BAC vectors which contain 40kb up to 200kb of genomic sequence cloned into a vector, allowing propagation in *E.coli*. The *neoR*-cassette was not conventionally cloned, but rather recombined into these vectors. This intra-bacterial genetic modification was mediated by a recombinase from the λ-phage, expressed inducibly from an external plasmid. This enzyme mediates with high efficiency the recombination between homologous sequences as short as 50bp. Thus, both the *neoR* and the *HSV-tk* cassette were flanked by such miniature arms homologous to the target site and inserted into the fosmid, resulting in the final targeting construct. The integrity of the resulting fosmid was determined by restriction digests (Figure 39).

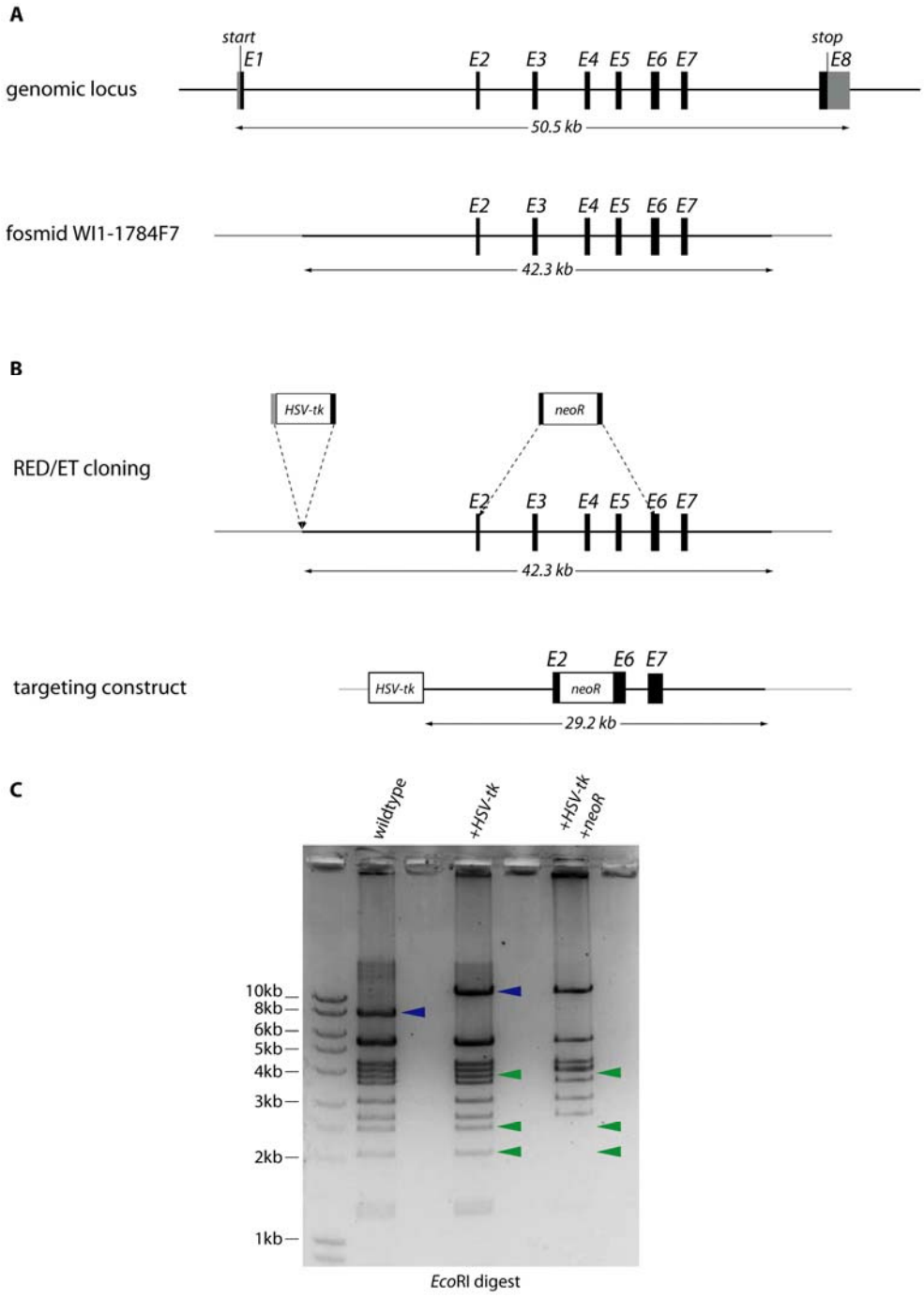

Figure 39: Generation of the second targeting construct. (A) The genomic locus of *sly2* and the corresponding fosmid-clone. (B) The second targeting construct was generated by Red/ET cloning in two consecutive steps. First the *HSV-tk* cassette was inserted at the border between the genomic sequence and the fosmid backbone. Subsequently, the *neoR* cassette was integrated, deleting approximately 15kb of genomic sequence from exon2 to 6. Shown above are the fosmid map and both cassettes with their respective arms of homology as generated by PCR prior to recombination. (C) Restriction digests showing the correct integration of both selection markers. Blue arrowheads indicate the fragments, which increases in size between the wildtype and the first recombination step due to the incorporation of the *HSV-tk* cassette. Green arrowheads mark the bands which disappear due to the replacement of the genomic sequence by the *neoR* cassette. The fosmid WI1-1784F7 was purchased through www.bacpac.chori.com.

E14.1 ES cells were electroporated with this construct and the southern blot analysis of 500 clones identified four homologously recombined clones according to the 3' flanking probe. Two clones, C5 and B6, also showed the recombination event on the 5' end of the locus (Figure 40). A *sly2* gene-targeted mouse strain has been generated by injection of ES cells of the clone C5 into C57BL/6 blastocysts and successful germline transmission of the mutated allele.

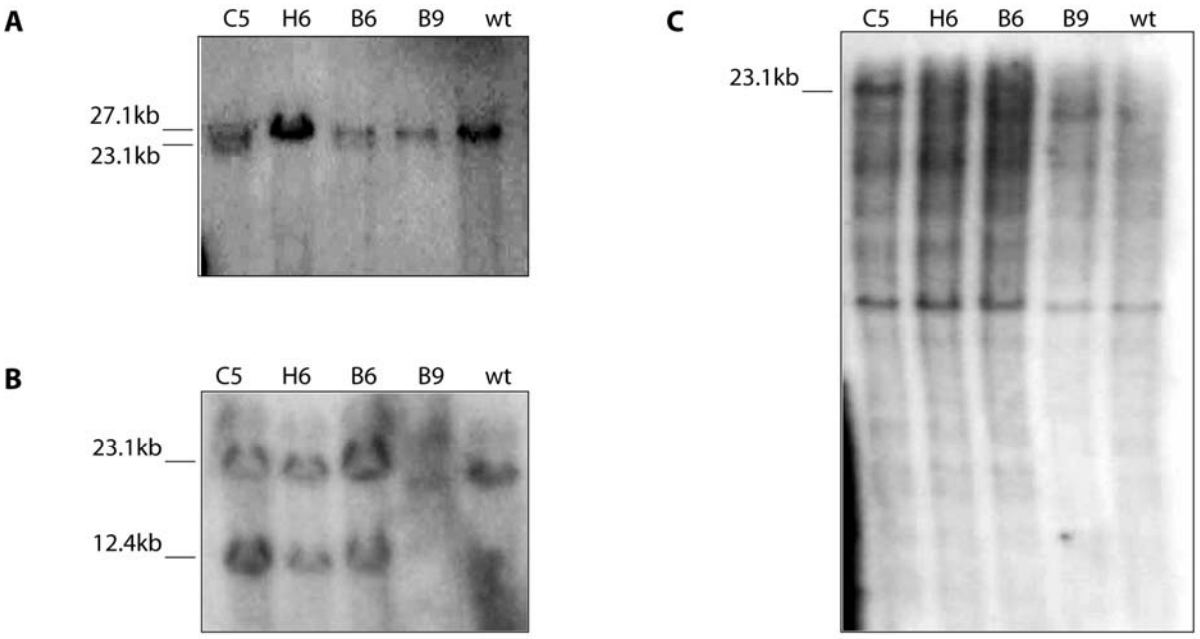

Figure 40: Targeted ES cell clones. (A+B) ES cell DNA was isolated and analysed by Southern blot as described. The 5' and the 3' flanking probe were hybridised to *Sap*I or *Bgl*I digested DNA, respectively. (C) Single integration of the targeting construct was shown with a probe detecting the neomycin resistance cassette. Hybridisation to a *Sap*I digested DNA yielded a single band migrating at 23.1kb. The additional signals are unspecific and also occur in the wildtype sample.

4. Discussion

4.1. The SLy family of putative adapter proteins

By definition, adapter proteins comprise various interaction domains, mediating either protein-protein binding or the interaction between proteins and other cellular components (e.g. membranes or lipids). In addition, they are marked by the absence of enzymatically active domains. Due to their modular structure they facilitate specific binding of different interaction partners at the same time and thus hold crucial functions in the spatial-temporal regulation of cellular signalling circuits and pathways.

When SLy was initially discovered, the structural analysis of its amino acid sequence instantly showed that both of these hallmark criteria of adapter proteins were met. The existence of an SH3 and a SAM domain in addition to the absence of any enzymatic domains led to the classification of this novel lymphocyte protein as an adapter molecule (Beer et al., 2001). The NLS in the N-terminus of all SLy proteins urges the question, if these molecules carry out regulatory functions by transporting or sequestering binding partners from or to the nucleus.

The novel family member SLy2 has been identified by two other groups independently, resulting in the names HACS1 and NASH1 (Claudio et al., 2001; Uchida et al., 2001). Aligning the amino acid sequences of SLy and SLy2 reveals that the overall identity between the two proteins is only 43.3%. Yet, there are several clusters of very high identity found along the complete sequence (Figure 1). In addition, analysis of the SLy2 amino-acid sequence by the proteomics database *Expasy.org* reveals, that both proteins show an identical molecular organisation with respect to the NLS, the SH3 and the SAM domain. Interestingly, the clusters of high identity correlate with the identified domains, indicating a high selection pressure onto these structures.

SASH1 was identified as the third protein of the SLy family. It differs greatly from SLy and SLy2 with respect to its size (110kDa (SASH1) vs. 55kDa (SLy) vs. 48kDa (SLy2)) and also shows a somewhat different molecular structure. Most identical to the two smaller proteins is the middle domain of SASH1, which is flanked by an additional coiled-coil motif in the N-terminus and a second SAM domain in the C-terminus. In spite of the different structure, the functional domains show up to 80% sequence identity between these proteins.

Surprisingly, the BLAST analysis of the SH3 domains of SLy and SLy2 indicates a very low level of sequence identity to the SH3 domains of other signalling molecules, the most identical being the SH3 of *CD2-associated protein*, CD2-AP with 42%. This positions the SLy

proteins in distance to other SH3 containing molecules and, supported by the striking similarity of the modular structure, suggests a close relationship of these three proteins and thus leads to the definition of the novel SLy-family of proteins.

4.1.1. Different expression patterns for SLy, SLy2 and SASH1

In evolutionary terms, SASH1 is the most ancient member of this family, as it occurs already in arthropods such as *D. melanogaster*, whereas SLy and SLy2 are restricted to bony fish and land borne vertebrate species. It is in agreement with this finding that the expression of SASH1 is ubiquitous, in contrast to the highly specific and thus further refined expression patterns of SLy and SLy2. Given the high degree of sequence and structural identity between both proteins, their expression pattern is surprisingly different. While SLy is exclusively expressed in the lymphoid cell lineage (Beer et al., 2001), SLy2 occurs in a broader range of tissues. The strong expression in the lymphoid organs (with the exception of the bone marrow) has been reported elsewhere (Claudio et al., 2001; Uchida et al., 2001). Also the expression of SLy2 in the brain was described (Claudio et al., 2001), albeit not at such high levels as encountered in hematopoietic tissues. Completely novel, and in marked contrast to published findings is the presence of remarkable SLy2 levels in skeletal and heart muscle (Figure 9). This is of special interest with respect to the newly identified role of SLy2 in actin dynamics as these play a pivotal role in muscle cell function. The analysis of SLy2 deficient mice will help to elucidate the function of this novel adapter also in the non-hematopoietic tissues.

The immunoblot analysis of different murine tissues gives rise to speculations on different splice variants of SLy2, as the signal is of clearly different size in different organs. This would be consistent with data found on www.ensembl.org and accordingly this matter was addressed extensively during this study. Yet, RT-PCR analysis with forward and reverse primers in different exons could not identify differentially spliced SLy2 species including exons 1-8. To verify the additional splice variants proposed in the ensembl database, also RT-PCR with primers in the suggested novel upstream exons was conducted, which did not yield any fragments at all (data not shown). Secondly, during the expression analysis of the first SLy2-gene-targeted mouse, intensive RACE PCR analysis of the 5′ part of the SLy2 mRNA was conducted. This never yielded any differentially sized PCR products, arguing against the alternative upstream exons suggested by www.ensembl.org. The only argument in favor of an additional upstream exon is the outcome of the first targeting strategy, where splicing from a hypothetical 5′ exon into the *neoR* cassette resulted in the rescued expression of SLy2 in the gene-targeted mice. Yet, the existence of this exon

remains speculative, as it could not be identified in the RACE PCR (Figures 35-37). Accordingly, the true nature of the differentially sized immunoblot signals remains elusive, as they might also be accounted for by posttranslational modifications. A first hint in that direction is the protein size of approximately 50kDa observed in the western blot analysis, which differs by 8kDa from the 42kDa, predicted according to the amino acid sequence (Figure 9). Worth mentioning in this respect is the markedly different migration behaviour of the ΔSAM deletion mutant (Figure 19), which only displays a size of 30kDa in western blot analyses. In contrast to this, the ΔSH3 mutant migrates at approximately 42kDa, although both mutants differ only by 8 aa in length. To completely rule out the possibility that this size-shift is due to proteolytic activity, it would be necessary to analyse the sequence of the expressed protein. Another interesting hypothesis would be that the deletion of the SAM domain interferes with a posttranslational modification of SLy2, which might be responsible for the size shift. Along these lines, SAM domains have repeatedly been shown to mediate interaction with *small ubiquitin related modifier* (SUMO)-conjugating enzymes (Chakrabarti et al., 1999; Chakrabarti et al., 2000; Zhang et al., 2004). As SUMO has a molecular weight of approximately 10kDa, this would nicely correspond to the size-shift occurring upon deletion of the SAM domain. This interesting possibility awaits further investigation.

4.1.2. Molecular properties of SLy2

In the two different first publications describing SLy2, there is great controversy with respect to the subcellular localisation of the protein. While Uchida *et al.* report an exclusively nuclear localisation of SLy2 (and thus termed it NASH), Claudio *et al.* detect only a minor fraction of SLy2 in the nucleus, while the bulk amount resides in the cytoplasm (Claudio et al., 2001; Uchida et al., 2001). This latter finding is also supported by the results obtained during this thesis (Figure 11). As both groups performed their analyses in overexpression systems using very similar cells, the only obvious difference between the experiments is the N-terminal GFP-tag used by Uchida *et al*. As this bulky tag is located close to the NLS it potentially interferes with the correct subcellular localisation of the protein. The HA-tag used by Claudio *et al.* and in this thesis probably infers less sterical inhibition. In support of that theory, C-terminally GFP-tagged SLy2 that was initially used in immunofluorescent studies during this work, showed no nuclear localisation at all (data not shown). Consistent with the predicted function of the NLS, the amount of SLy2 located in the nucleus is diminished upon deletion of the NLS domain, although it has to be noted that the nuclear localisation is not abolished. As only the second part of the bipartite NLS

was deleted in the mutant, the 5' part of the domain potentially accounts for this residual amount of nuclear SLy2 (Figure 10). Alternatively, one could argue that SLy2 translocates to the nucleus as a homodimer, which would raise the possibility that wildtype/ΔNLS heterodimers make up for the HA staining in the nuclear compartement. This question will be addressed in future studies by reexpressing the ΔNLS SLy2 deletion mutant in a $SLy2^{-/-}$ background.

Given the identification of SLy2 as a potentially tumour associated molecule it is worth mentioning that SLy2 is constitutively and prominently phosphorylated in different malignant cell lines (Figure 11 and data not shown). As this stands in marked contrast to the situation occurring in primary cells, it is tempting to speculate that the phosphorylation renders SLy2 more active. This is also suggested by the finding, that the phosphorylation status of this adapter protein is drastically increased upon activation of the cells. Further investigation about the responsible kinase(s) and the downstream effects of SLy2 phosphorylation will help to elucidate this matter. Since serine is the most abundant amino acid in SLy2, it will be difficult to determine exact sites of phosphorylation. Furthermore, a database analysis has identified several tyrosine residues as possible kinase targets. The NLS deficient SLy2 species further suggests a connection between impaired SLy2 phosphorylation and diminished functionality, since it displays the co-migration of an apparently less phosphorylated second band. It would be interesting to analyse if the reduced activity of SLy2-ΔNLS is caused by the reduced amount of fully phosphorylated SLy2. Of note, the deletion of the first section of the NLS together with the serine residue 27 completely abrogates SLy function, as shown by phenotypical comparison of $SLy^{\Delta/\Delta}$ and $SLy^{-/-}$ mice (B. Reis personal communication and (Beer et al., 2005)). Accordingly, subsequent analyses will have to show if this is also the case for SLy2.

4.1.3. A notorious locus in different pathogenic conditions

In the human genome, the *sly2* gene is located on chromosome 21 in the region *21q11.2*, which is frequently targeted by translocation events in hematopoietic malignancies (Mitelman et al., 1997). Along the same lines, SLy2 was reported to be upregulated in different leukemic cell lines and primary human tumours (Claudio et al., 2001; Williams et al., 2003). This notion receives further support by studies conducted in the laboratory of Prof. Bernhard Holzmann at the Technical University of Munich, which also showed an upregulation of the SLy2 mRNA in different human tumour tissues, including colon, pancreas and liver (Dr. Klaus-Peter Janssen, personal communication). However, it has to be noted that a recent publication reports the region *21q11.2* to be often affected by loss-

of-heterozygosity events in human lung cancer. Consistently, Yamada and colleagues find SLy2 to be downregulated in different cell lines derived from human lung cancer, thus rather suggesting a tumour suppressor activity, which was also reported for SASH1 (Zeller et al., 2003; Yamada et al., 2008). This controversy is further intensified by the finding presented in this study, that the overexpression of SLy2 induces aberrant cytokinesis and accordingly causes a proliferation defect in different human cancer cell lines (Figure 23).

The most obvious disease genetically related to chromosome 21 is Down syndrome, caused by a trisomy due to defective meiosis. As the aetiology of this disorder is commonly attributed to gene dosage effects, the expression of various genes located on chromosome 21 has been analysed in wildtype and trisomic situations. Cheon and co-workers compared the levels of six different proteins and could show that the expression of SLy2 was significantly downregulated in the cerebral cortex of Down syndrome fetuses. This stands in marked contrast to what was expected from the multiplicity of the locus (Cheon et al., 2003). However, the completely descriptional character of this study does not allow any speculations about the connection between the decreased SLy2 protein levels and the disease phenotype. Another interesting finding is that region *21q11.2* has been connected to the abnormal myelopoiesis and frequent occurrence of leukaemia in Down syndrome patients, representing one of the main reasons for the limited life span especially in Down syndrome children (Izraeli et al., 2007).

A neuro-pathologic condition connected to this chromosomal region is Alzheimer's disease (Groet et al., 1998), whose incidence is also significantly increased in Down syndrome patients (Zigman and Lott, 2007). Amongst other genes in this region, also SLy2 has been identified as a marker correlating with a predisposition to Alzheimer's (Kimura et al., 2007). Remarkable in this respect is the finding that SLy2 is highly and specifically expressed in the hippocampus (Lein et al., 2007). This region of the brain has been implicated with long term memory and is amongst the first structures to be affected by the β-amyloid-plaques. The importance of F-Actin reorganisation in hippocampal neuron synapse formation, which is important in the formation of long-term memory, implies a possible role for SLy2 in these processes (Wegner et al., 2008).

Taken together, these findings suggest that the chromosomal region around SLy2 represents a true "Hot-Spot" for neuro-pathology and cancer related genes.

4.2. SLy2 transgenic mice

SLy2 expression is upregulated in B cells upon stimulation with various maturation and proliferation inducing stimuli (Figure 9). Zhu *et al*. expanded this finding to a functional level by transducing primary splenic B cells with a SLy2 expression construct. In agreement with the upregulated expression after stimulation with CD40L and IgM, the SLy2 overexpression induced the differentiation of B cells towards a plasma cell fate (Zhu et al., 2004). To determine this maturation inducing effect in a physiological setting *in vivo*, we generated transgenic mice with a constitutively elevated expression level of SLy2 in B and T cells (Figure 14). To our surprise, the different T and B cell populations did not show any alterations, as defined by FACS analysis. Also, we could not confirm the elevated levels of CD138 or the decrease in CD23 expression reported in the work of Zhu and coworkers (Figure 15). Although the plasma cell levels ($B220^+$, $CD138^+$) appear slightly elevated in the transgenic mice, this phenomenon is not significant ($p>0.2$) (Figure 15, lowest panels). Consistent with this, also the serum antibody levels were unaltered compared to wildtype mice (K. Buchholz, personal communication). The differing results might be explained by a more drastic overexpression in the transduction system compared to the transgenic cells. Also, the *in vitro* nature of the transduction experiments might lead to an artificial situation that is not comparable to the *in vivo* studies, especially since the B cells had to be stimulated prior to retroviral transduction (Zhu et al., 2004). It remains to be determined how B and T cells of transgenic mice behave in an infectious setting or after immunisation of the mice with T-dependent or T-independent antigens.

4.3. Form follows function – the F-actin cytoskeleton

Actin is the hallmark protein of one of the three pillars of cytoskeletal structures, which also comprise the microtubular network and the intermediate filament system. By polymerising of actin monomers (globular, G-actin) into multimers of a helical, filamentous structure (F-actin), the foundation for a plethora of different functions is laid. In general, two different forms of F-actin are known, stretched linear filaments and branched networks. Depending on the required morphology either of them is employed specifically, e.g. in the formation of protrusive structures. The former accounts for long, finger-like protrusions such as filopodia, used to probe the surrounding area. The latter is found in broad, sheet like lamellipodia and ruffles, involved in the organisation of the leading edge in a migrating cell. Additionally, both structures are assembled to higher ordered complexes (Chhabra and Higgs, 2007). With its high degree of flexibility and the plethora of possible structures

it is not surprising that the F-actin cytoskeleton is involved in almost each aspect of cellular biology.

4.3.1. A new player in the field?

It has emerged in the recent years how important the reorganisation of the F-actin cytoskeleton is during the intial events of lymphocyte activation (Vicente-Manzanares and Sanchez-Madrid, 2004; Billadeau and Burkhardt, 2006; Harwood and Batista, 2008). During the first minutes after the encounter of an antigen presenting cell or antigen coated surface, T and B cells undergo drastic rearrangements of their actin cytoskeleton (Fleire et al., 2006; Barral et al., 2008). Quickly after the engagement of the antigen receptors, the whole actin network focuses towards the cell-antigen contact area and serves as scaffold for an IS. In addition to this structural function, the actin polymers also actively transport integrin-molecules into the p-SMAC (*p*eripheral *s*upra *m*olecular *a*ctivation *c*luster), which are attached to actin via the protein talin (Vicente-Manzanares and Sanchez-Madrid, 2004; Harwood and Batista, 2008). Besides these intracellular reorganisation events, especially B cells have been shown to literally perform a choreography of spreading and contraction, thereby gathering the maximum of possible antigen binding to their B cell receptors (Fleire et al., 2006). It is of great interest in this respect that transgenic B cells overexpressing SLy2 show marked difficulties in the initial spreading on an α-IgM coated surface (Figure 16). In wildtype B cells the F-actin structures at the contact plane between cell and surface show a clear spreading during the first 15 minutes. The same structures in the transgenic cells remain largely unchanged during the first two minutes and also then only partially increase their size. Approximately 5 minutes after cell-substrate contact, the transgenic cells reach their peak with respect to the relative size of the contact area, identically to the wildtype cells, although still at decreased levels. The wildtype cells maintain a stable size of the contact area for approximately 10 minutes, after which they begin to contract again, reaching the initial size in the following 15 minutes. In contrast, the size of the F-actin structures at the synapse of transgenic B cells immediately starts to decline after having reached the peak size, indicating that these cells are unable to maintain a stable contact with the antigen coated surface. This effect was not due to decreased surface expression of IgM on these cells, as shown in Figure 15, third row of panels. Accordingly, the aberrant spreading must be accounted for by an inability to correctly reorganise the F-actin network beneath the cell membrane at the contact site between the cell and the substrate (Figure 16). Further experiments will have to show at which point and in which pathway SLy2 exerts its effects on F-actin reorganisation. It will

be revealing to analyse the intracellular Ca^{2+}-signals upon activation in the transgenic cells, as those have been shown to be impaired by interfering with actin polymerisation (Varma et al., 2006). It is a remarkable finding that the transgenic B cells are not only impaired in their spreading, but potentially also in the maintenance of a mature synapse. This hints towards an additional defect in the microtubule system, which was shown to be responsible for the stabilisation of the IS (Bunnell et al., 2001). Yet, given the intensive crosstalk between the actin and the tubulin network, it can not be ruled out at this point, that the stabilisation defect is also due to defective F-actin assembly at the contact zone between the cell and the antigen coated surface.

4.3.2. Aberrant induction of branched F-actin networks

As the actin structure underlying the IS is homologous to a lamellipodium (Billadeau and Burkhardt, 2006) and SLy2 was shown to be expressed in HeLa cells (data not shown), we used this well characterised cell line to further define the role of this novel adapter in the regulation of the actin cytoskeleton. The expression of SLy2 under the control of the *EF2α*-promoter in these cells induced a drastic reorganisation of F-actin structures. The most prominent feature was the extreme skewing of most of the cellular F-actin towards the distal poles of the cells, where it formed sheet like lamellipodia and peripheral ruffles (Figure 17, right panels). Concurrently, the previously highly abundant stress fibres dissolved, as did the cortical F-actin, located underneath the membrane in wildtype cells (Figure 17, left panel). The simultaneously occurring induction of one F-actin structure with the disassembly of another is a highly interesting finding, as different F-actin structures are based on the action of different signalling networks (Chhabra and Higgs, 2007). Small GTPases of the Rho-family proved to be of pivotal importance in this respect (Hall, 1998). The activity of RhoA enhances cell contractility through the formation of stress fibres, intracellular "cables" assembled from anti-parallel bundles of linear F-actin. At each end they are attached to focal adhesions (FA), integrin-rich complexes that mediate a firm interaction between a cell and its substratum, the formation of which is also induced by the activity of RhoA (Ridley and Hall, 1992). On the other hand, the activity of two other prominent members of the Rho-family, Rac and Cdc42 lead to the extension and migration of the cell, primarily by the formation of lamellipodia and filopodia at the leading edge, assembled from a network of branched actin filaments. Secondly, Rac and Cdc42 activate the effector PAK, which induces the disassembly of stress fibres and FA, thereby enabling the cell to migrate by decreasing the contractility and loosening the adhesion, respectively (Manser et al., 1997; Hall, 1998). It is in agreement with the disassembly of intracellular

stress fibres that the SLy2 overexpressing cells take on a markedly spread morphology, often displaying several long and thin protrusions (Figure 17, middle panels) (Schoenwaelder and Burridge, 1999). In line with the previous findings, SLy2 was never found to colocalise with FA in HeLa cells (data not shown).

4.3.2.1. Different domains of SLy2 account for its localisation to F-actin structures and their induction

Double stainings clearly show the colocalisation of SLy2 with the F-actin structures induced by its overexpression (Figure 18). It was a surprising finding, when analysing the HeLa cells expressing the different SLy2 mutant proteins, that the localisation to and the induction of the peripheral ruffles can be uncoupled (Figure 20 B). The deletion of the second part of the NLS clearly impairs the ability of SLy2 to induce peripheral ruffles, although not abolishing it. Equally unexpected was the missing enrichment in F-actin structures. With respect to the decreased nuclear localisation of SLy2 upon deletion of the NLS it is mandatory to analyse what causes the impaired induction of membrane ruffles. Given the less pronounced colocalisation of this deletion mutant with F-actin structures, it will be interesting to define the molecular functions of this domain apart from nuclear transport. The deletion of the SH3 domain yields quite the contrary result: now the induction of ruffled membranes is lost, but the protein still colocalises, at least to some extent, with the F-actin. This suggests that SLy2 interacts with a cytosolic protein via its SH3 domain and that this interaction does not have to occur in the immediate proximity to the place where the ruffles are subsequently induced. On the other hand, the localised accumulation alone obviously does not suffice to induce membrane ruffling (Figure 20 B). This finding received further support from biochemical separations of HeLa cell lysates into G-actin and F-actin rich fractions. Whereas wildtype SLy2 and the S23A point mutant exclusively co-purified to the F-actin fraction, ΔNLS and ΔSH3 displayed a different distribution. After the deletion of the NLS, at least half of the SLy2 molecules occur in the G-actin fraction, while this fraction was markedly decreased upon deletion of the SH3 domain (Figure 21). Also, the phenotype of the NLS deletion mutant elicits speculations about the specific function of this domain, as it is apparently not only mediating the nuclear localisation of SLy2 (compare to Figure 10). Considering the compromised functionality of the NLS or the SH3 deleted SLy2 mutants it is interesting that both migrate as a double band. Furthermore, the treatment of the cells with the phosphatase inhibitor calyculin shifts the distribution of SLy2-ΔNLS towards the upper band, suggesting that the size difference is due to differential phosphorylation (Figure 21, right panel). Given the

constitutive phosphorylation of the wildtype SLy2 protein in different cell lines (Figure 11 and data not shown) it is tempting to speculate that phosphorylation of SLy2 is needed to exert its full effect on F-actin dynamics. However, the amino acid residues that are modified by phosphorylation have to be identified before this hypothesis can be verified in an experimental setting.

Concerning the phenotype of the deletion of the SAM domain, future experiments analysing the overall stability of the protein have to show if the complete loss of function effect is protein intrinsic. Yet, this is suggested by the immunofluorescent analysis of the few cells expressing it at levels comparable to the other SLy2 species (Figure 20 A and B). It would be interesting to treat the ΔSAM expressing cells with proteasome inhibitors and investigate if the cells take on a similar morphology as the SLy2 wildtype expressing cells. However, the pleiotropic effects of such inhibitors have to be taken into account. Subsequently, assessing the impact of the SAM domain alone by expressing it ectopically in HeLa cells would yield further information about its function. Of note, ongoing experiments suggest that the deletion of the SAM domain leads to a loss of function phenotype in SLy without interfering with the cellular levels of the protein (D. Finkenstädt, personal communication).

4.3.2.2. A potentially regulatory function of serine residue 23 in SLy2

Overexpression of a serine to alanine point mutant in aa position 23 of SLy2 induces even more ruffles in the HeLa cells and also leads to an increasingly condensed morphology of the cells, compared to overexpression of the wildtype protein or the NLS deletion. Consistently, the intracellular localisation of the mutant protein seems to be skewed towards the membrane (Figure 20 A and B). It is worth mentioning that the amino acids up- and downstream of Ser23 are highly conserved between SLy and SLy2 (Figure 1). Database analysis indicates that this sequence represents the consensus motif of protein kinase D (PKD) target substrates (Doppler et al., 2005), and it was shown for SLy that the corresponding Ser27 is phosphorylated *in vitro* by this kinase (B. Reis, personal communication). Of note, the phosphorylation of Ser27 in SLy leads to the generation of a 14-3-3 binding site and mutation of this residue to alanine abolishes the binding of different 14-3-3 proteins to SLy (S. Brandt and B. Reis, personal communication). Since also SLy2 is interacting with various 14-3-3 family proteins (S. Brandt, personal communication), it is tempting to speculate that the mutation of serine to alanine in position 23 also yields defective binding of SLy2 to 14-3-3 proteins and that this results in the enhanced activity of this mutant to induce peripheral ruffles.

4.3.3. Enhanced spreading of SLy2 overexpressing HeLa cells

The molecular machineries that are involved in lamellipodia formation also control cell spreading and migration (Pollard et al., 2000; Ridley et al., 2003; Chhabra and Higgs, 2007). Thus, it is consistent with the strong induction of peripheral membrane ruffles and lamellipodia by SLy2, that the transgenic HeLa cells also exhibited increased spreading on gelatine coated surfaces. In agreement with previous findings, HeLa cells overexpressing SLy2 displayed pronounced membrane protrusions and multiple lamellipodia, as opposed to the rather round and evenly shaped control cells (Figure 22). A surprise was the strong spreading of the ΔSH3 expressing cells, although these cells did not display multiple lamellipodia but rather produced one big ring-like structure of F-actin surrounding the cell. Potentially, this is caused by a less locally restricted induction of F-actin.

The outcome of the spreading analysis appears to stand in contradiction to the results from the transgenic B cells, which clearly exhibited impaired spreading on antigen coated surfaces (Figure 16). A possible explanation for this diverging behaviour could be that the overexpression of SLy2 leads to the induction of lamellipodia without a defined spatio-temporal regulation. This probably does not impose an obstacle to HeLa spreading on gelatine as it seems somewhat erratic in its direction. Yet, such a locally restricted regulation of the F-actin network is mandatory for the antigen induced spreading preceeding the establishment of a mature IS at the contact plane between the cell and the surface (Bunnell et al., 2001; Vicente-Manzanares and Sanchez-Madrid, 2004; Harwood and Batista, 2008). This suggests that the high abundance of SLy2 molecules in the transgenic B cells apparently rather disturbs than promotes spreading.

4.3.4. Defective cytokinesis through ectopic SLy2 expression

Cytokinesis represents the last step in mitosis and describes the final separation of one mother into two daughter cells, after successful karyokinesis. Again, the F-actin cytoskeleton is involved in this process at multiple levels (reviewed in (Eggert et al., 2006)). Accordingly, it is of interest that the overexpression of SLy2 causes a proliferational defect in all cell lines analysed (Jurkat, HeLa, SVEC) (Figure 23 and data not shown). Especially HeLa cells expressing SLy2 wildtype or the S23A mutant exhibited extensive difficulties in the last steps of cell division as indicated by the accumulation of cytoplasmic bridges between the daughter cells (Figure 24). Probably as a result of the impaired cytokinesis, giant and multinucleated cells accumulated in long time cultures especially of SLy2-S23A overexpressing HeLa cells (Figure 25). Considering the deleterious effects of SLy2 overexpression on other RhoA mediated structures such as stress fibres, it is worth

mentioning that Bement and colleagues could show the specific enrichment of active RhoA at the cleavage plain between dividing cells shortly before cell division is accomplished (Bement et al., 2005). Also, different regulators of RhoA activity accumulate at the cleavage plain (Kimura et al., 2000; Hirose et al., 2001) and the deepening of the cleavage furrow is mediated by actin and myosin II, the activity of which is also controlled by RhoA (Uyeda et al., 2004). Cytokinesis ends with the abscission of the two daughter cells, preceeded by the ingression of the cleavage furrow, which leads to the formation of a thin cytoplasmic bridge of 1-1.5 µm strength. The diameter of this bridge reduces to approximately 0.2 µm during maturation (Mullins and Biesele, 1977; Piel et al., 2001). Concurrently, the maintenance of the bridge becomes insensitive to actin depolymerising agents like Latrunculin B, indicating that it is no longer dependent on F-actin reorganisation (Echard et al., 2004). This suggests an involvement of SLy2 into this process at an earlier time point. Consistently, many of the cytonemes found between SLy2 expressing cells are considerably thicker than the described 0.2–1.5 µm (Figure 24). In addition, given the pivotal role of RhoA in cytokinesis, this small GTPase seems to be a potential target of SLy2 activity worthwhile of further investigation. An additional phenotypical hint towards an implication of SLy2 in cytokinesis is the finding that U2OS cells depleted for the protein Bruce display the same cytonemes as seen in SLy2 overexpressing cells (Pohl and Jentsch, 2008). Interestingly, this knock down of Bruce leads to a defect in the last stages of cytokinesis. Another theory to explain the cytokinesis defect of SLy2 overexpressing cells could be a possible impairment of the spatio-temporal induction of F-actin, thus leading to a defect in the localised actin reorganisation at the cleavage plain, elicited by an excess of SLy2 throughout the cell.

4.3.5. Rac1 is involved in the effect of SLy2 on the actin cytoskeleton

As mentioned above, the role of different Rho-family members in the formation of diverse F-actin structures is well established (Ridley, 2001; Ladwein and Rottner, 2008). As SLy2 overexpression clearly induces the generation of lamellipodia and membrane ruffles, Rac proteins were the first candidates to be tested as the potential mediators of the effects of SLy2 on the actin cytoskeleton. To analyse the Rac-dependency of the phenotype of SLy2 overexpression, cells were transfected with expression vectors for a dominant-negative point mutant of Rac1, Rac1N17 (Ridley et al., 1992). Indeed, the formation of membrane ruffles in SLy2 overexpressing cells was strongly Rac1 dependent, as the expression of Rac1N17 completely abolished the phenotype elicited by SLy2 (Figure 26). An additional hint was the phenotype displayed by HeLa cells stably expressing SLy2, which were

transfected with an expression vector for constitutively active Rac1V12 (Figure 27). In contrast to the smooth lamellipodia induced by Rac1 activity alone (left panel), the double expressors took on a spiky appearance due to the characteristic topology of the cortical F-actin. Further suggesting a combined activity of SLy2 and Rac1 was the massive occurrence of dorsal ruffles (middle and right panels), which was not accounted for by Rac1V12 activity alone (left panel). Furthermore, most of the double transfected cells contained several nuclei, a phenotype that was not seen in cells overexpressing only Rac1V12 (Figure 27 and (Ridley et al., 1992)). This obvious defect in cell-division was apparently caused by the synergistic action of SLy2 and Rac1V12. In addition, Ridley and colleagues also report that the microinjection of Rac1V12 into Swiss 3T3 mouse fibroblasts induces the accumulation of vesicles in these cells, which originate from pinocytosis (see Figure 27 middle panel, ring-like F-actin structures and (Ridley et al., 1992)). Of note, these vesicles are also sometimes witnessed in HeLa cell overexpressing SLy2 wildtype or SLy2 S23A (data not shown). In conclusion, it is clear that the generation of the peripheral ruffles and other ectopic F-actin structures induced by SLy2 is dependent on Rac. Albeit it remains elusive until now, which nucleation promoting factor (NPF) is involved here, as either NPFs I (N-WASP, WAVE1, WAVE2) or NPFs II (cortactin/HS1) are reported to mediate lamellipodia and ruffle formation and both classes of proteins depend on the activation through Rac proteins (Cosen-Binker and Kapus, 2006; Takenawa and Suetsugu, 2007; Ladwein and Rottner, 2008).

4.3.6. SLy2 interacts with proteins of the cortactin family

Actin polymerisation starts with the formation of actin-oligomers, which further assemble into filaments. Since the generation of these actin di- and trimers is energetically unfavored, the equilibrium in these first steps is clearly skewed towards the monomeric molecule (Chhabra and Higgs, 2007). The two groups of NPFs are involved in the nucleation of monomeric actin into F-actin, in a separate as well as a synergistic fashion. Both cortactin/HS1 and WAVE1-3 are involved in the generation of lamellipodial structures and membrane ruffles (Cosen-Binker and Kapus, 2006; Takenawa and Suetsugu, 2007). Even more, both HS1 and WAVE were shown to be essential for the formation of IS and the subsequent activation of T cells (Gomez et al., 2006; Nolz et al., 2006).

To identify the downstream effectors of SLy2 that mediate the formation of lamellipodia, two different approaches were chosen. IPs of SLy2 from metabolically labelled cell lysates yielded a first hint at the “interactome” of SLy2. A protein band migrating at 85-90kDa especially raised our interest, as it only seemed to co-precipitate with SLy2 after

stimulation of the cells with sodium ortho-vanadate and hydrogen peroxide (Figure 28) and because a member of the second class of NPFs, cortactin, migrates at that size. The treatment of cells with both oxidising agents leads to the persistent inactivation of cellular phosphatases, as important residues in their active centre are irreversibly oxidised. This results in the accumulation of phosphorylated signalling proteins and thus an enhanced activation status of the cell (Wienands et al., 1996). Remarkably, stimulation of cells with PDGF, LPA or bradykinine, which are well known activators of Rac1, RhoA or Cdc42 and their respective F-actin structures, induces intracellular peroxide production (Rhee et al., 2000; Reth, 2002).

The second approach to find SLy2 interacting proteins was a database search for proteins interacting with molecules containing SH3 domains homologous to that of SLy2. This led to the identification of 14 candidate proteins, which potentially interact with SLy2 (Figure 29). Interestingly, many of the hits yielded by this functionally unbiased approach are well-known regulators of the actin-cytoskeleton, such as the Rho-family GTPases and cortactin. However, only the interaction with cortactin was confirmed in the subsequent immunoprecipitation studies. As cortactin is a well known regulator of branched actin networks, it is a likely candidate to mediate the effects of SLy2 on the actin cytoskeleton. This hypothesis received further support by the finding that the inability of different SLy2 deletion mutants to colocalise with the F-actin rich ruffles correlates with their inability to colocalise and to coimmunoprecipitate with cortactin (Figure 30 and 31). Although the latter finding underlines the specificity of the SLy2-cortactin interaction, future experiments in a completely endogenous situation will have to be performed for final confirmation.

As mentioned above, cortactin is involved in the generation of lamellipodia through the concomitant binding of Arp2/3 complex, F-actin and WASP proteins. To facilitate cellular migration, the induction of lamellipodia has to coincide with the establishment of new focal contacts to the substratum, in order to generate the needed traction. Their absence results in the uplifting and back folding of the induced lamellipodia, resulting in extensive membrane ruffling (Weaver et al., 2001; Ammer and Weed, 2008). This is supported by findings from SLy2 overexpressing cells that show remarkable ruffling, but fail to exhibit enhanced migratory capacities (data not shown). It remains elusive, if the interaction of SLy2 and cortactin leads to the activation or the inhibition of the latter. This matter is further complicated due to conflicting data on the effect of cortactin downregulation on the spreading and migratory capacity of the cell. Illes and colleagues show on the one hand that RNAi mediated cortactin knock down leads to impaired spreading of COS-7 cells

on fibronectin (Illes et al., 2006). On the other hand, Kempiak *et al.* show that cortactin knock down in rat adeno-carcinoma cells leads to enhanced formation of lamellipodia and van Rossum *et al.* suggest that downregulated expression of cortactin leads to enhanced spreading and adhesion, but diminishes the migratory behaviour of breast epithelial cells (Kempiak et al., 2005; van Rossum et al., 2006). It remains to be elucidated how the interaction of SLy2 and cortactin can account for the marked changes in F-actin organisation in SLy2 overexpressing cells.

With respect to the high basal expression of SLy2 in brain and the specific expression in the hippocampus it is of great interest that the hippocampal expression of cortactin is highly regulated and appears to affect the plasticity of hippocampal neurons during REM sleep phases (Davis et al., 2006).

As mentioned above, the F-actin structure underlying the IS is homologous to a lamellipodium. In agreement with this, HS1, a protein from the cortactin family, is of pivotal importance in the generation and maintenance of this specific structure and the subsequent activation of T and NK cells. In addition, HS1 deficient mice display defective B cell proliferation after IgM stimulation and decreased T-independent immunoglobulin production (Taniuchi et al., 1995; Gomez et al., 2006; Butler et al., 2008). Considering the defect in antigen induced spreading in SLy2 overexpressing B cells, it is thus remarkable that SLy2 also interacts with HS1 in primary splenocytes (Figure 32). This makes HS1 a likely candidate to mediate the effects of SLy2 on the intact formation of the F-actin cytoskeleton at the IS, especially as the protein was shown to affect NK cell spreading in response to ICAM-1 coated surfaces (Butler et al., 2008).

4.4. Targeting SLy2

With the aim to abrogate expression from the *sly2* locus but to reduce the impact on adjacent loci to a minimum, the first targeting strategy only encompassed the insertion of a *neoR* cassette into the first coding exon in the reverse direction with respect to the reading frame of the endogenous locus (Figure 33). The strong transcriptional activity of the *PGK*-promoter in the inserted sequence should thus mediate an additional inhibiting effect on the SLy2 expression. Unexpectedly, unaltered SLy2 mRNA and protein levels were detected in the gene-targeted mice (Figure 35). As the RACE analysis clearly proved a correct insertion of the *neoR* cassette at the intended location, an aberrant targeting event could be excluded as the reason (Figure 36). Given the existence of splice acceptors in the 3' end of the *neoR* cassette, these results suggest an ectopic splicing event. Since the cassette is located in the first coding exon, this unexpected splicing accounts for the

transcripts of identical size in the wildtype and the gene-targeted situation. This hypothesis received additional support by the identically sized SLy2 mRNAs in the wildtype and the gene-targeted situation, in spite of the inserted *neoR* cassette in the first exon. The markedly reduced amount of the hybrid mRNA species containing the complete resistance cassette compared to the spliced variant is further stressing the efficiency of this splice event. Yet it has to be noted that the postulated existence of an unknown upstream exon, needed to provide the splice donors, could not be proven. These findings elicit further discussion concerning the additional upstream exons and splice variants resulting thereof. An alternative explanation would be the formation of a new promoter inside the *neoR* cassette. Since the cassette is positioned within the SLy2 locus in an inverted orientation its strong promoter is located in the 3' part. Potentially, this would yield an as yet hypothetical promoter that could mediate the recruitment of the transcriptional machinery and subsequent production of the alternative mRNA. However, such an ectopic promoter function would most probably have been already described elsewhere, given the frequent usage of the *PGK-neoR* cassette in various gene-targeted mouse strains.
It can only be speculated wether the alternative gene product expressed from the targeted locus could exert full function, yet this seems very likely, given the lack of only six residues of the N-terminal part of the NLS and the presence of all other functional domains including the serine residue 23.

4.5.Conclusion and outlook

The thesis presented here provides essential evidence that SLy2 is a new factor in actin dynamics and represents the first molecular characterisation of this novel adapter protein. So far, published knowledge about SLy2 rather concentrated on the expression levels in different diseases and especially malignancies and the control of SLy2 expression in primary B cells. Biochemical and immunohistological analyses strongly suggest that SLy2 exerts its effects on the actin cytoskeleton by interaction with the NPF II cortactin. In addition, the Rac1 dependency of the SLy2 effect was demonstrated by the coexpression of SLy2 and dominant negative Rac1 protein. Albeit, given the involvement of Rac1 in actin reorganisation up- and downstream of cortactin, no conclusion can be drawn towards the operating level of SLy2. Consistent with the interaction with the cortactin homologue HS1, SLy2 was shown to be involved in the complex spreading and contraction choreography displayed by B cells encountering membrane bound antigen. How this inhibitory effect of SLy2 overexpression influences the activation-specific and proliferative capacities of primary B cells still has to be determined. Also, in spite of the novel data presented here,

the complete working mechanism of this newly identified adapter still remains elusive. In addition, the effects of abrogated SLy2 expression on the activation of hematopoietic cells will have to be unravelled. With the *sly2*-gene-targeted mouse strain generated during this thesis the foundation for such analyses is laid.

Until now, when analysing the role of SLy2, the main focus was always on its function in hematopoietic cells. This is mainly due to the reported upregulation of the expression of this protein in malignant cells of hematopoietic origin. Thus, it is necessary to determine its role in other tissues such as smooth and skeletal muscle or brain, in all of which SLy2 is highly expressed. Notably, actin reorganisation is of pivotal importance in the central functions of all of the tissues mentioned. Given the involvement of SLy2 in such profound cellular functions as cell spreading and proliferation, it will be highly interesting to analyse the phenotype of the gene-targeted SLy2 deficient mice.

5. Summary

This thesis represents the first molecular characterisation of SLy2, a novel member of the recently described SLy family of adapter proteins. SLy2 was previously identified as HACS1 on the basis of its deregulated expression in different hematopoietic cancer cell lines (Claudio et al., 2001). Database analysis defined an identical modular organisation of SLy and SLy2, with an N-terminal NLS-, a central SH3- and a C-terminal SAM domain.

Western blot analysis using a polyclonal anti-serum demonstrated SLy2 expression throughout the hematopoietic tissues, but also in muscle, heart, brain and colon. *In vivo* overexpression in B cells of a transgenic mouse line established a role for SLy2 in the initial spreading and contraction of B cells in response to contact with antigen containing membranes. *In vitro* overexpression of wildtype SLy2 protein in HeLa cells resulted in the prominent and robust induction of branched F-actin structures like lamellipodia and peripheral ruffles, to which SLy2 also specifically localised. This primary effect was accompanied by markedly enhanced spreading and correlated with diminished proliferation, most probably due to defective cytokinesis in SLy2 overexpressing cells. Of note, it could be shown that the deletion of the various functional domains affected this impact on F-actin reorganisation to different degrees: The removal of the NLS domain impaired ruffle formation only mildly, although the specific colocalisation with F-actin was abrogated. In contrast to this, the SH3 domain proved to be of pivotal importance for the F-actin reorganising effect of SLy2, with the mutant protein retaining some ability to recruit to peripheral branched F-actin structures. This functional dichotomy awaits further elucidation. Finally, the loss of the SAM domain led to a complete loss of function, yet the diminished protein levels of this mutant might potentially lead to an overinterpretation of this effect. Furthermore, the molecular cause for the characteristic size-shift of the ΔSAM mutant remains to be defined. The mutation of a conserved serine residue in the N-terminus (serine 23) resulted in an even enhanced phenotype of the overexpressing cells, thus proposing a regulatory function for this amino acid. Interestingly, SLy was shown to be phosphorylated at this residue upon T cell receptor ligation (Astoul et al., 2003).

Overexpression studies with different point mutants of Rac1 suggested a direct role for this small GTPase in the SLy2 induced F-actin structures. Dominant negative Rac1N17 abrogated the F-actin inducing effects of SLy2, while constitutively active Rac1V12 even enhanced this phenotype.

Ultimately, two complementary approaches towards the identification of downstream SLy2 effectors proved the interaction with the members of the cortactin family of

nucleation promoting factors, cortactin and its lymphocyte homologue HS1. As their role in the induction of lamellipodia and immunological synapses has been clearly established before, they are highly likely to be the mediators of the actin regulatory effects of SLy2.

With the generation of gene targeted SLy2 deficient mice, an in depth analysis of this novel regulator of branched F-actin structures *in vivo* is now possible.

5.1. Zusammenfassung

Die vorliegende Dissertation beinhaltet die erste molekulare Charakterisierung des Proteins SLy2. Auf Grund des hohen Expressionslevels in Zellen des hämatopoietischen Systems und seiner markanten Domänenstruktur ist SLy2 ursprünglich als *hematopoietic adapter protein containing SH3 and SAM domains 1* (HACS1) beschrieben worden (Claudio et al., 2001). Eine Analyse der molekularen Struktur auf Grund von Datenbankvergleichen ergab einen zu SLy hochidentischen Aufbau, bestimmt durch eine N-terminale Kern-Lokalisationssequenz (NLS), eine zentrale SH3 und eine C-terminale SAM Domäne.
Es konnte gezeigt werden, dass SLy2 sowohl in allen hämatopoietischen Geweben, als auch in Muskel, Herz, Gehirn, Dünndarm und Pankreas exprimiert wird. *In vivo* führte eine verstärkte Expression von SLy2 in transgenen murinen B Lymphozyten zu einer Störung der Zellausdehnung und –kontraktion während der frühen Antwort auf oberflächen-fixierte Antigene. *In vitro* bedingte eine Überexpression von SLy2 in HeLa Zellen die Bildung von Membrankrausen und Lamellipodien, beides von verzweigtem F-Aktin geprägte zelluläre Strukturen. Es wurde außerdem eine spezifische Lokalisation von SLy2 in diesen Strukturen beschrieben. Als sekundärer Effekt wurde eine deutlich beschleunigte Ausbreitung dieser Zellen auf mit Gelatine beschichteten Oberflächen gezeigt. Auffällig war außerdem die verminderte Zellteilungsaktivität der transgenen Zellen, die wahrscheinlich auf einer gestörten Zytokinese beruht, was durch das verstärkte Auftreten von Zytoplasma-Brücken, sog. Zytonemen zwischen den SLy2-transgenen HeLa Zellen nahegelegt wurde.
Interessanterweise tragen die verschiedenen Domänen von SLy2 zu unterschiedlichem Ausmaß zu diesem Phänotyp bei. Während eine SLy2-Mutante ohne die NLS nur mehr einen eingeschränkten Einfluss auf die genannten zellulären Strukturen nahm, bedeutete die Beseitigung der SH3 Domäne beinahe einen kompletten Verlust der Lamellipodien-induzierenden Aktivität. Der Effekt der SAM Domäne konnte nicht abschließend evaluiert werden, da eine Mutante ohne diese Domäne nur zu einem deutlich verminderten

Ausmaß exprimiert wurde. Allerdings zeigen auch Zellen mit hoher Expression dieser Mutante einen weitgehend wildtypischen Phänotyp. Die Punktmutation eines konservierten Serin-Restes im N-Terminus (Serin 23) zu Alanin resultierte in einer Verstärkung des beschriebenen Effekts auf Membrankrausen und Lamellipodien. Stimmigerweise zeigten Zellen mit dieser Mutante auch die stärksten Zellteilungsdefekte. Dies ist vor allem vor dem Hintergrund interessant, dass das analoge Serin 27 in SLy als Ziel der PKD ausgemacht wurde. Beide Ergebnisse legen eine regulatorische Funktion dieser Aminosäure nahe (Astoul et al., 2003).

Durch die Überexpression von verschiedenen Rac1 Punktmutanten konnte eine Einflussnahme dieser kleinen GTPase auf die von SLy2 bedingten F-Aktin Strukturen gezeigt werden. Die dominant negative Mutante Rac1N17 verhinderte bei gleichzeitiger Expression mit SLy2 die Bildung der auffälligen Membranstrukturen. Dem gegenüber bedingte die Expression der allzeit aktivierten Variante Rac1V12 noch eine zusätzliche Verstärkung des SLy2 Effektes.

Schlussendlich konnten die beiden Proteine der Cortactin Familie, Cortactin und das lymphozyten-spezifische HS1 als Interaktionspartner identifiziert werden. Da die Rolle dieser beiden Adaptoren in der Bildung von verzweigten F-Aktin Strukturen bereits klar definiert wurde, stellen sie vielversprechende Effektoren für die von SLy2 ausgelösten F-Aktin Zytoskelett Veränderungen dar.

Die in dieser Arbeit generierte SLy2-defiziente Mauslinie wird in Zukunft eine tiefgreifende *in vivo* Analyse der Effekte dieses Proteins auf das Aktin Zytoskelett ermöglichen.

6. References

1. Ammer,A.G. and Weed,S.A. (2008). Cortactin branches out: Roles in regulating protrusive actin dynamics. Cell Motil. Cytoskeleton.

2. Arana,E., Vehlow,A., Harwood,N.E., Vigorito,E., Henderson,R., Turner,M., Tybulewicz,V.L., and Batista,F.D. (2008). Activation of the small GTPase Rac2 via the B cell receptor regulates B cell adhesion and immunological-synapse formation. Immunity. *28*, 88-99.

3. Astoul,E., Laurence,A.D., Totty,N., Beer,S., Alexander,D.R., and Cantrell,D.A. (2003). Approaches to define antigen receptor-induced serine kinase signal transduction pathways. J. Biol. Chem. *278*, 9267-9275.

4. Bailly,M., Ichetovkin,I., Grant,W., Zebda,N., Machesky,L.M., Segall,J.E., and Condeelis,J. (2001). The F-actin side binding activity of the Arp2/3 complex is essential for actin nucleation and lamellipod extension. Curr. Biol. *11*, 620-625.

5. Barral,P., Eckl-Dorna,J., Harwood,N.E., De Santo,C., Salio,M., Illarionov,P., Besra,G.S., Cerundolo,V., and Batista,F.D. (2008). B cell receptor-mediated uptake of CD1d-restricted antigen augments antibody responses by recruiting invariant NKT cell help in vivo. Proc. Natl. Acad. Sci. U. S. A *105*, 8345-8350.

6. Baum,B. and Kunda,P. (2005). Actin nucleation: spire - actin nucleator in a class of its own. Curr. Biol. *15*, R305-R308.

7. Beer,S., Scheikl,T., Reis,B., Huser,N., Pfeffer,K., and Holzmann,B. (2005). Impaired immune responses and prolonged allograft survival in Sly1 mutant mice. Molecular and Cellular Biology *25*, 9646-9660.

8. Beer,S., Simins,A.B., Schuster,A., and Holzmann,B. (2001). Molecular cloning and characterization of a novel SH3 protein (SLY) preferentially expressed in lymphoid cells. Biochim. Biophys. Acta *1520*, 89-93.

9. Bement,W.M., Benink,H.A., and von Dassow,G. (2005). A microtubule-dependent zone of active RhoA during cleavage plane specification. J. Cell Biol. *170*, 91-101.

10. Bender,A. and Pringle,J.R. (1989). Multicopy suppression of the cdc24 budding defect in yeast by CDC42 and three newly identified genes including the ras-related gene RSR1. Proc. Natl. Acad. Sci. U. S. A *86*, 9976-9980.

11. Billadeau,D.D. and Burkhardt,J.K. (2006). Regulation of cytoskeletal dynamics at the immune synapse: new stars join the actin troupe. Traffic. *7*, 1451-1460.

12. Birnboim,H.C. and Doly,J. (1979). Rapid Alkaline Extraction Procedure for Screening Recombinant Plasmid Dna. Nucleic Acids Research *7*, 1513-1523.

13. Blanchoin,L., Amann,K.J., Higgs,H.N., Marchand,J.B., Kaiser,D.A., and Pollard,T.D. (2000). Direct observation of dendritic actin filament networks nucleated by Arp2/3 complex and WASP/Scar proteins. Nature *404*, 1007-1011.

14. Block,J., Stradal,T.E., Hanisch,J., Geffers,R., Kostler,S.A., Urban,E., Small,J.V., Rottner,K., and Faix,J. (2008). Filopodia formation induced by active mDia2/Drf3. J. Microsc. *231*, 506-517.

15. Bowden,E.T., Barth,M., Thomas,D., Glazer,R.I., and Mueller,S.C. (1999). An invasion-related complex of cortactin, paxillin and PKCmu associates with invadopodia at sites of extracellular matrix degradation. Oncogene *18*, 4440-4449.

16. Bryce,N.S., Clark,E.S., Leysath,J.L., Currie,J.D., Webb,D.J., and Weaver,A.M. (2005). Cortactin promotes cell motility by enhancing lamellipodial persistence. Curr. Biol. *15*, 1276-1285.

17. Bunnell,S.C., Kapoor,V., Trible,R.P., Zhang,W., and Samelson,L.E. (2001). Dynamic actin polymerization drives T cell receptor-induced spreading: a role for the signal transduction adaptor LAT. Immunity. *14*, 315-329.

18. Butler,B., Gao,C., Mersich,A.T., and Blystone,S.D. (2006). Purified integrin adhesion complexes exhibit actin-polymerization activity. Curr. Biol. *16*, 242-251.

19. Butler,B., Kastendieck,D.H., and Cooper,J.A. (2008). Differently phosphorylated forms of the cortactin homolog HS1 mediate distinct functions in natural killer cells. Nat. Immunol. *9*, 887-897.

20. Campbell,I.D. (2008). Studies of focal adhesion assembly. Biochem. Soc. Trans. *36*, 263-266.

21. Cannon,J.L. and Burkhardt,J.K. (2004). Differential roles for Wiskott-Aldrich syndrome protein in immune synapse formation and IL-2 production. J. Immunol. *173*, 1658-1662.

22. Cantrell,D.A. (2003). GTPases and T cell activation. Immunol. Rev. *192*, 122-130.

23. Cao,H., Orth,J.D., Chen,J., Weller,S.G., Heuser,J.E., and McNiven,M.A. (2003). Cortactin is a component of clathrin-coated pits and participates in receptor-mediated endocytosis. Mol. Cell Biol. *23*, 2162-2170.

24. Carrasco,Y.R., Fleire,S.J., Cameron,T., Dustin,M.L., and Batista,F.D. (2004). LFA-1/ICAM-1 interaction lowers the threshold of B cell activation by facilitating B cell adhesion and synapse formation. Immunity. *20*, 589-599.

25. Cassimeris,L., Safer,D., Nachmias,V.T., and Zigmond,S.H. (1992). Thymosin beta 4 sequesters the majority of G-actin in resting human polymorphonuclear leukocytes. J. Cell Biol. *119*, 1261-1270.

26. Chakrabarti,S.R., Sood,R., Ganguly,S., Bohlander,S., Shen,Z., and Nucifora,G. (1999). Modulation of TEL transcription activity by interaction with the ubiquitin-conjugating enzyme UBC9. Proc. Natl. Acad. Sci. U. S. A *96*, 7467-7472.

27. Chakrabarti,S.R., Sood,R., Nandi,S., and Nucifora,G. (2000). Posttranslational modification of TEL and TEL/AML1 by SUMO-1 and cell-cycle-dependent assembly into nuclear bodies. Proc. Natl. Acad. Sci. U. S. A *97*, 13281-13285.

28. Cheon,M.S., Bajo,M., Kim,S.H., Claudio,J.O., Stewart,A.K., Patterson,D., Kruger,W.D., Kondoh,H., and Lubec,G. (2003). Protein levels of genes encoded on chromosome 21 in fetal Down syndrome brain: challenging the gene dosage effect hypothesis (Part II). Amino. Acids *24*, 119-125.

29. Chhabra,E.S. and Higgs,H.N. (2007). The many faces of actin: matching assembly factors with cellular structures. Nat. Cell Biol. *9*, 1110-1121.

30. Claudio,J.O., Zhu,Y.X., Benn,S.J., Shukla,A.H., McGlade,C.J., Falcioni,N., and Stewart,A.K. (2001). HACS1 encodes a novel SH3-SAM adaptor protein differentially expressed in normal and malignant hematopoietic cells. Oncogene *20*, 5373-5377.

31. Cohen,S.N., Chang,A.C.Y., and Hsu,L. (1972). Nonchromosomal Antibiotic Resistance in Bacteria - Genetic Transformation of Escherichia-Coli by R-Factor Dna. Proceedings of the National Academy of Sciences of the United States of America *69*, 2110-&.

32. Cory,G.O., Garg,R., Cramer,R., and Ridley,A.J. (2002). Phosphorylation of tyrosine 291 enhances the ability of WASp to stimulate actin polymerization and filopodium formation. Wiskott-Aldrich Syndrome protein. J. Biol. Chem. *277*, 45115-45121.

33. Cosen-Binker,L.I. and Kapus,A. (2006). Cortactin: the gray eminence of the cytoskeleton. Physiology. (Bethesda.) *21*, 352-361.

34. Cuschieri,L., Nguyen,T., and Vogel,J. (2007). Control at the cell center: the role of spindle poles in cytoskeletal organization and cell cycle regulation. Cell Cycle *6*, 2788-2794.

35. Davis,C.J., Meighan,P.C., Taishi,P., Krueger,J.M., Harding,J.W., and Wright,J.W. (2006). REM sleep deprivation attenuates actin-binding protein cortactin: a link between sleep and hippocampal plasticity. Neurosci. Lett. *400*, 191-196.

36. de la Fuente,M.A., Sasahara,Y., Calamito,M., Anton,I.M., Elkhal,A., Gallego,M.D., Suresh,K., Siminovitch,K., Ochs,H.D., Anderson,K.C., Rosen,F.S., Geha,R.S., and Ramesh,N. (2007). WIP is a chaperone for Wiskott-Aldrich syndrome protein (WASP). Proc. Natl. Acad. Sci. U. S. A *104*, 926-931.

37. Derry,J.M., Ochs,H.D., and Francke,U. (1994). Isolation of a novel gene mutated in Wiskott-Aldrich syndrome. Cell *79*, following.

38. Didsbury,J., Weber,R.F., Bokoch,G.M., Evans,T., and Snyderman,R. (1989). rac, a novel ras-related family of proteins that are botulinum toxin substrates. J. Biol. Chem. *264*, 16378-16382.

39. Doppler,H., Storz,P., Li,J., Comb,M.J., and Toker,A. (2005). A phosphorylation state-specific antibody recognizes Hsp27, a novel substrate of protein kinase D. J. Biol. Chem. *280*, 15013-15019.

40. Dustin,M.L. (2008). T-cell activation through immunological synapses and kinapses. Immunol. Rev. *221*, 77-89.

41. Echard,A., Hickson,G.R., Foley,E., and O'Farrell,P.H. (2004). Terminal cytokinesis events uncovered after an RNAi screen. Curr. Biol. *14*, 1685-1693.

42. Eggert,U.S., Mitchison,T.J., and Field,C.M. (2006). Animal cytokinesis: from parts list to mechanisms. Annu. Rev. Biochem. *75*, 543-566.

43. Fan,L., Ciano-Oliveira,C., Weed,S.A., Craig,A.W., Greer,P.A., Rotstein,O.D., and Kapus,A. (2004). Actin depolymerization-induced tyrosine phosphorylation of cortactin: the role of Fer kinase. Biochem. J. *380*, 581-591.

44. Feinberg,A.P. and Vogelstein,B. (1983). A Technique for Radiolabeling Dna Restriction Endonuclease Fragments to High Specific Activity. Analytical Biochemistry *132*, 6-13.

45. Feng,S., Chen,J.K., Yu,H., Simon,J.A., and Schreiber,S.L. (1994). Two binding orientations for peptides to the Src SH3 domain: development of a general model for SH3-ligand interactions. Science *266*, 1241-1247.

46. Fleire,S.J., Goldman,J.P., Carrasco,Y.R., Weber,M., Bray,D., and Batista,F.D. (2006). B cell ligand discrimination through a spreading and contraction response. Science *312*, 738-741.

47. Geiger,B., Rosen,D., and Berke,G. (1982). Spatial relationships of microtubule-organizing centers and the contact area of cytotoxic T lymphocytes and target cells. J. Cell Biol. *95*, 137-143.

48. Goldman,R.D., Grin,B., Mendez,M.G., and Kuczmarski,E.R. (2008). Intermediate filaments: versatile building blocks of cell structure. Curr. Opin. Cell Biol. *20*, 28-34.

49. Goldschmidt-Clermont,P.J., Furman,M.I., Wachsstock,D., Safer,D., Nachmias,V.T., and Pollard,T.D. (1992). The control of actin nucleotide exchange by thymosin beta 4 and profilin. A potential regulatory mechanism for actin polymerization in cells. Mol. Biol. Cell *3*, 1015-1024.

50. Gomez,M., Kioussis,D., and Cantrell,D.A. (2001). The GTPase Rac-1 controls cell fate in the thymus by diverting thymocytes from positive to negative selection. Immunity. *15*, 703-713.

51. Gomez,T.S., McCarney,S.D., Carrizosa,E., Labno,C.M., Comiskey,E.O., Nolz,J.C., Zhu,P., Freedman,B.D., Clark,M.R., Rawlings,D.J., Billadeau,D.D., and Burkhardt,J.K. (2006). HS1 functions as an essential actin-regulatory adaptor protein at the immune synapse. Immunity. *24*, 741-752.

52. Goode,B.L. and Eck,M.J. (2007). Mechanism and function of formins in the control of actin assembly. Annu. Rev. Biochem. *76*, 593-627.

53. Groet,J., Ives,J.H., South,A.P., Baptista,P.R., Jones,T.A., Yaspo,M.L., Lehrach,H., Potier,M.C., Van Broeckhoven,C., and Nizetic,D. (1998). Bacterial contig map of the 21q11 region associated with Alzheimer's disease and abnormal myelopoiesis in Down syndrome. Genome Res. *8*, 385-398.

54. Haas,A.K., Yoshimura,S., Stephens,D.J., Preisinger,C., Fuchs,E., and Barr,F.A. (2007). Analysis of GTPase-activating proteins: Rab1 and Rab43 are key Rabs required to maintain a functional Golgi complex in human cells. J. Cell Sci. *120*, 2997-3010.

55. Hall,A. (1998). Rho GTPases and the actin cytoskeleton. Science *279*, 509-514.

56. Hanahan,D. (1983). Studies on Transformation of Escherichia-Coli with Plasmids. Journal of Molecular Biology *166*, 557-580.

57. Harwood,N.E. and Batista,F.D. (2008). New insights into the early molecular events underlying B cell activation. Immunity. *28*, 609-619.

58. He,Y., Hicke,L., and Radhakrishnan,I. (2007). Structural basis for ubiquitin recognition by SH3 domains. J. Mol. Biol. *373*, 190-196.

59. Helfand,B.T., Chang,L., and Goldman,R.D. (2004). Intermediate filaments are dynamic and motile elements of cellular architecture. J. Cell Sci. *117*, 133-141.

60. Hidaka,M., Homma,Y., and Takenawa,T. (1991). Highly conserved eight amino acid sequence in SH2 is important for recognition of phosphotyrosine site. Biochem. Biophys. Res. Commun. *180*, 1490-1497.

61. Higgs,H.N. (2005). Formin proteins: a domain-based approach. Trends Biochem. Sci. *30*, 342-353.

62. Hirose,K., Kawashima,T., Iwamoto,I., Nosaka,T., and Kitamura,T. (2001). MgcRacGAP is involved in cytokinesis through associating with mitotic spindle and midbody. J. Biol. Chem. *276*, 5821-5828.

63. Hotulainen,P. and Lappalainen,P. (2006). Stress fibers are generated by two distinct actin assembly mechanisms in motile cells. J. Cell Biol. *173*, 383-394.

64. Huang,Y., Comiskey,E.O., Dupree,R.S., Li,S., Koleske,A.J., and Burkhardt,J.K. (2008). The c-Abl tyrosine kinase regulates actin remodeling at the immune synapse. Blood *112*, 111-119.

65. Huse,M., Quann,E.J., and Davis,M.M. (2008). Shouts, whispers and the kiss of death: directional secretion in T cells. Nat. Immunol. *9*, 1105-1111.

66. Illes,A., Enyedi,B., Tamas,P., Balazs,A., Bogel,G., Melinda, Lukacs, and Buday,L. (2006). Cortactin is required for integrin-mediated cell spreading. Immunol. Lett. *104*, 124-130.

67. Innocenti,M., Zucconi,A., Disanza,A., Frittoli,E., Areces,L.B., Steffen,A., Stradal,T.E., Di Fiore,P.P., Carlier,M.F., and Scita,G. (2004). Abi1 is essential for the formation and activation of a WAVE2 signalling complex. Nat. Cell Biol. *6*, 319-327.

68. Iritani,B.M., Forbush,K.A., Farrar,M.A., and Perlmutter,R.M. (1997). Control of B cell development by Ras-mediated activation of Raf. EMBO J. *16*, 7019-7031.

69. Izraeli,S., Rainis,L., Hertzberg,L., Smooha,G., and Birger,Y. (2007). Trisomy of chromosome 21 in leukemogenesis. Blood Cells Mol. Dis. *39*, 156-159.

70. Johnson,D.I. and Pringle,J.R. (1990). Molecular characterization of CDC42, a Saccharomyces cerevisiae gene involved in the development of cell polarity. J. Cell Biol. *111*, 143-152.

71. Kanner,S.B., Reynolds,A.B., Vines,R.R., and Parsons,J.T. (1990). Monoclonal antibodies to individual tyrosine-phosphorylated protein substrates of oncogene-encoded tyrosine kinases. Proc. Natl. Acad. Sci. U. S. A *87*, 3328-3332.

72. Kempiak,S.J., Yamaguchi,H., Sarmiento,C., Sidani,M., Ghosh,M., Eddy,R.J., Desmarais,V., Way,M., Condeelis,J., and Segall,J.E. (2005). A neural Wiskott-Aldrich Syndrome protein-mediated pathway for localized activation of actin polymerization that is regulated by cortactin. J. Biol. Chem. *280*, 5836-5842.

73. Kimura,K., Tsuji,T., Takada,Y., Miki,T., and Narumiya,S. (2000). Accumulation of GTP-bound RhoA during cytokinesis and a critical role of ECT2 in this accumulation. J. Biol. Chem. *275*, 17233-17236.

74. Kimura,R., Kamino,K., Yamamoto,M., Nuripa,A., Kida,T., Kazui,H., Hashimoto,R., Tanaka,T., Kudo,T., Yamagata,H., Tabara,Y., Miki,T., Akatsu,H., Kosaka,K., Funakoshi,E., Nishitomi,K., Sakaguchi,G., Kato,A., Hattori,H., Uema,T., and Takeda,M. (2007). The DYRK1A gene, encoded in chromosome 21 Down syndrome critical region, bridges between beta-amyloid production and tau phosphorylation in Alzheimer disease. Hum. Mol. Genet. *16*, 15-23.

75. Kinley,A.W., Weed,S.A., Weaver,A.M., Karginov,A.V., Bissonette,E., Cooper,J.A., and Parsons,J.T. (2003). Cortactin interacts with WIP in regulating Arp2/3 activation and membrane protrusion. Curr. Biol. *13*, 384-393.

76. Kinnunen,T., Kaksonen,M., Saarinen,J., Kalkkinen,N., Peng,H.B., and Rauvala,H. (1998). Cortactin-Src kinase signaling pathway is involved in N-syndecan-dependent neurite outgrowth. J. Biol. Chem. *273*, 10702-10708.

77. Kitamura,D., Kaneko,H., Miyagoe,Y., Ariyasu,T., and Watanabe,T. (1989). Isolation and characterization of a novel human gene expressed specifically in the cells of hematopoietic lineage. Nucleic Acids Res. *17*, 9367-9379.

78. Klages,N., Zufferey,R., and Trono,D. (2000). A stable system for the high-titer production of multiply attenuated lentiviral vectors. Molecular Therapy *2*, 170-176.

79. Koch,C.A., Anderson,D., Moran,M.F., Ellis,C., and Pawson,T. (1991). SH2 and SH3 domains: elements that control interactions of cytoplasmic signaling proteins. Science *252*, 668-674.

80. Kovar,D.R. (2006). Molecular details of formin-mediated actin assembly. Curr. Opin. Cell Biol. *18*, 11-17.

81. Kuhn,R., Rajewsky,K., and Muller,W. (1991). Generation and analysis of interleukin-4 deficient mice. Science *254*, 707-710.

82. Kupfer,A. and Dennert,G. (1984). Reorientation of the microtubule-organizing center and the Golgi apparatus in cloned cytotoxic lymphocytes triggered by binding to lysable target cells. J. Immunol. *133*, 2762-2766.

83. Kupfer,A. and Singer,S.J. (1988). Molecular dynamics in the membranes of helper T cells. Proc. Natl. Acad. Sci. U. S. A *85*, 8216-8220.

84. Ladwein,M. and Rottner,K. (2008). On the Rho'd: the regulation of membrane protrusions by Rho-GTPases. FEBS Lett. *582*, 2066-2074.

85. Lakamper,S. and Meyhofer,E. (2006). Back on track - on the role of the microtubule for kinesin motility and cellular function. J. Muscle Res. Cell Motil. *27*, 161-171.

86. Lanzetti,L., Palamidessi,A., Areces,L., Scita,G., and Di Fiore,P.P. (2004). Rab5 is a signalling GTPase involved in actin remodelling by receptor tyrosine kinases. Nature *429*, 309-314.

87. Lein,E.S., Hawrylycz,M.J., Ao,N., Ayres,M., Bensinger,A., Bernard,A., Boe,A.F., Boguski,M.S., Brockway,K.S., Byrnes,E.J., Chen,L., Chen,L., Chen,T.M., Chin,M.C., Chong,J., Crook,B.E., Czaplinska,A., Dang,C.N., Datta,S., Dee,N.R., Desaki,A.L., Desta,T., Diep,E., Dolbeare,T.A., Donelan,M.J., Dong,H.W., Dougherty,J.G., Duncan,B.J., Ebbert,A.J., Eichele,G., Estin,L.K., Faber,C., Facer,B.A., Fields,R., Fischer,S.R., Fliss,T.P., Frensley,C., Gates,S.N., Glattfelder,K.J., Halverson,K.R., Hart,M.R., Hohmann,J.G., Howell,M.P., Jeung,D.P., Johnson,R.A., Karr,P.T., Kawal,R., Kidney,J.M., Knapik,R.H., Kuan,C.L., Lake,J.H., Laramee,A.R., Larsen,K.D., Lau,C., Lemon,T.A., Liang,A.J., Liu,Y., Luong,L.T., Michaels,J., Morgan,J.J., Morgan,R.J., Mortrud,M.T., Mosqueda,N.F., Ng,L.L., Ng,R., Orta,G.J., Overly,C.C., Pak,T.H., Parry,S.E., Pathak,S.D., Pearson,O.C., Puchalski,R.B., Riley,Z.L., Rockett,H.R., Rowland,S.A., Royall,J.J., Ruiz,M.J., Sarno,N.R., Schaffnit,K., Shapovalova,N.V., Sivisay,T., Slaughterbeck,C.R., Smith,S.C., Smith,K.A., Smith,B.I., Sodt,A.J., Stewart,N.N., Stumpf,K.R., Sunkin,S.M., Sutram,M., Tam,A., Teemer,C.D., Thaller,C., Thompson,C.L., Varnam,L.R., Visel,A., Whitlock,R.M., Wohnoutka,P.E., Wolkey,C.K., Wong,V.Y., Wood,M., Yaylaoglu,M.B., Young,R.C., Youngstrom,B.L., Yuan,X.F., Zhang,B., Zwingman,T.A., and Jones,A.R. (2007). Genome-wide atlas of gene expression in the adult mouse brain. Nature *445*, 168-176.

88. Leung,T., Chen,X.Q., Manser,E., and Lim,L. (1996). The p160 RhoA-binding kinase ROK alpha is a member of a kinase family and is involved in the reorganization of the cytoskeleton. Mol. Cell Biol. *16*, 5313-5327.

89. Lin,K.B., Freeman,S.A., Zabetian,S., Brugger,H., Weber,M., Lei,V., Dang-Lawson,M., Tse,K.W., Santamaria,R., Batista,F.D., and Gold,M.R. (2008). The rap GTPases regulate B cell morphology, immune-synapse formation, and signaling by particulate B cell receptor ligands. Immunity. *28*, 75-87.

90. Lommel,S., Benesch,S., Rottner,K., Franz,T., Wehland,J., and Kuhn,R. (2001). Actin pedestal formation by enteropathogenic Escherichia coli and intracellular motility of Shigella flexneri are abolished in N-WASP-defective cells. EMBO Rep. *2*, 850-857.

91. Luders,J. and Stearns,T. (2007). Microtubule-organizing centres: a re-evaluation. Nat. Rev. Mol. Cell Biol. *8*, 161-167.

92. Madaule,P. and Axel,R. (1985). A novel ras-related gene family. Cell *41*, 31-40.

93. Manser,E., Huang,H.Y., Loo,T.H., Chen,X.Q., Dong,J.M., Leung,T., and Lim,L. (1997). Expression of constitutively active alpha-PAK reveals effects of the kinase on actin and focal complexes. Mol. Cell Biol. *17*, 1129-1143.

94. Martinez-Quiles,N., Ho,H.Y., Kirschner,M.W., Ramesh,N., and Geha,R.S. (2004). Erk/Src phosphorylation of cortactin acts as a switch on-switch off mechanism that controls its ability to activate N-WASP. Mol. Cell Biol. *24*, 5269-5280.

95. Miki,H., Sasaki,T., Takai,Y., and Takenawa,T. (1998). Induction of filopodium formation by a WASP-related actin-depolymerizing protein N-WASP. Nature *391*, 93-96.

96. Miki,H., Yamaguchi,H., Suetsugu,S., and Takenawa,T. (2000). IRSp53 is an essential intermediate between Rac and WAVE in the regulation of membrane ruffling. Nature *408*, 732-735.

97. Mitelman,F., Mertens,F., and Johansson,B. (1997). A breakpoint map of recurrent chromosomal rearrangements in human neoplasia. Nat. Genet. *15 Spec No*, 417-474.

98. Mizutani,K., Miki,H., He,H., Maruta,H., and Takenawa,T. (2002). Essential role of neural Wiskott-Aldrich syndrome protein in podosome formation and degradation of extracellular matrix in src-transformed fibroblasts. Cancer Res. *62*, 669-674.

99. Molina,I.J., Sancho,J., Terhorst,C., Rosen,F.S., and Remold-O'Donnell,E. (1993). T cells of patients with the Wiskott-Aldrich syndrome have a restricted defect in proliferative responses. J. Immunol. *151*, 4383-4390.

100. Moon,S.Y. and Zheng,Y. (2003). Rho GTPase-activating proteins in cell regulation. Trends Cell Biol. *13*, 13-22.

101. Mullins,J.M. and Biesele,J.J. (1977). Terminal phase of cytokinesis in D-98s cells. J. Cell Biol. *73*, 672-684.

102. Mullins,R.D., Heuser,J.A., and Pollard,T.D. (1998). The interaction of Arp2/3 complex with actin: nucleation, high affinity pointed end capping, and formation of branching networks of filaments. Proc. Natl. Acad. Sci. U. S. A *95*, 6181-6186.

103. Mullis,K., Faloona,F., Scharf,S., Saiki,R., Horn,G., and Erlich,H. (1986). Specific enzymatic amplification of DNA in vitro: the polymerase chain reaction. Cold Spring Harb. Symp. Quant. Biol. *51 Pt 1*, 263-273.

104. Naldini,L., Blomer,U., Gage,F.H., Trono,D., and Verma,I.M. (1996). Efficient transfer, integration, and sustained long-term expression of the transgene in adult rat brains injected with a lentiviral vector. Proc. Natl. Acad. Sci. U. S. A *93*, 11382-11388.

105. Nobes,C.D. and Hall,A. (1995). Rho, rac, and cdc42 GTPases regulate the assembly of multimolecular focal complexes associated with actin stress fibers, lamellipodia, and filopodia. Cell *81*, 53-62.

106. Nolz,J.C., Gomez,T.S., Zhu,P., Li,S., Medeiros,R.B., Shimizu,Y., Burkhardt,J.K., Freedman,B.D., and Billadeau,D.D. (2006). The WAVE2 complex regulates actin cytoskeletal reorganization and CRAC-mediated calcium entry during T cell activation. Curr. Biol. *16*, 24-34.

107. Notarangelo,L.D., Miao,C.H., and Ochs,H.D. (2008). Wiskott-Aldrich syndrome. Curr. Opin. Hematol. *15*, 30-36.

108. Ono,S. (2007). Mechanism of depolymerization and severing of actin filaments and its significance in cytoskeletal dynamics. Int. Rev. Cytol. *258*, 1-82.

109. Pantaloni,D. and Carlier,M.F. (1993). How profilin promotes actin filament assembly in the presence of thymosin beta 4. Cell *75*, 1007-1014.

110. Peng,J., Wallar,B.J., Flanders,A., Swiatek,P.J., and Alberts,A.S. (2003). Disruption of the Diaphanous-related formin Drf1 gene encoding mDia1 reveals a role for Drf3 as an effector for Cdc42. Curr. Biol. *13*, 534-545.

111. Perelroizen,I., Didry,D., Christensen,H., Chua,N.H., and Carlier,M.F. (1996). Role of nucleotide exchange and hydrolysis in the function of profilin in action assembly. J. Biol. Chem. *271*, 12302-12309.

112. Perelroizen,I., Marchand,J.B., Blanchoin,L., Didry,D., and Carlier,M.F. (1994). Interaction of profilin with G-actin and poly(L-proline). Biochemistry *33*, 8472-8478.

113. Piel,M., Nordberg,J., Euteneuer,U., and Bornens,M. (2001). Centrosome-dependent exit of cytokinesis in animal cells. Science *291*, 1550-1553.

114. Pohl,C. and Jentsch,S. (2008). Final stages of cytokinesis and midbody ring formation are controlled by BRUCE. Cell *132*, 832-845.

115. Pollard,T.D. (1983). Measurement of rate constants for actin filament elongation in solution. Anal. Biochem. *134*, 406-412.

116. Pollard,T.D. (1986). Rate constants for the reactions of ATP- and ADP-actin with the ends of actin filaments. J. Cell Biol. *103*, 2747-2754.

117. Pollard,T.D. (2007). Regulation of actin filament assembly by Arp2/3 complex and formins. Annu. Rev. Biophys. Biomol. Struct. *36*, 451-477.

118. Pollard,T.D., Blanchoin,L., and Mullins,R.D. (2000). Molecular mechanisms controlling actin filament dynamics in nonmuscle cells. Annu. Rev. Biophys. Biomol. Struct. *29*, 545-576.

119. Pruyne,D., Evangelista,M., Yang,C., Bi,E., Zigmond,S., Bretscher,A., and Boone,C. (2002). Role of formins in actin assembly: nucleation and barbed-end association. Science *297*, 612-615.

120. Qiao,F. and Bowie,J.U. (2005). The many faces of SAM. Sci. STKE. *2005*, re7.

121. Quinlan,M.E., Heuser,J.E., Kerkhoff,E., and Mullins,R.D. (2005). Drosophila Spire is an actin nucleation factor. Nature *433*, 382-388.

122. Reth,M. (2002). Hydrogen peroxide as second messenger in lymphocyte activation. Nat. Immunol. *3*, 1129-1134.

123. Rhee,S.G., Bae,Y.S., Lee,S.R., and Kwon,J. (2000). Hydrogen peroxide: a key messenger that modulates protein phosphorylation through cysteine oxidation. Sci. STKE. *2000*, E1.

124. Ridley,A.J. (2001). Rho family proteins: coordinating cell responses. Trends Cell Biol. *11*, 471-477.

125. Ridley,A.J. and Hall,A. (1992). The small GTP-binding protein rho regulates the assembly of focal adhesions and actin stress fibers in response to growth factors. Cell *70*, 389-399.

126. Ridley,A.J., Paterson,H.F., Johnston,C.L., Diekmann,D., and Hall,A. (1992). The small GTP-binding protein rac regulates growth factor-induced membrane ruffling. Cell *70*, 401-410.

127. Ridley,A.J., Schwartz,M.A., Burridge,K., Firtel,R.A., Ginsberg,M.H., Borisy,G., Parsons,J.T., and Horwitz,A.R. (2003). Cell migration: integrating signals from front to back. Science *302*, 1704-1709.

128. Rimkus,C., Martini,M., Friederichs,J., Rosenberg,R., Doll,D., Siewert,J.R., Holzmann,B., and Janssen,K.P. (2006). Prognostic significance of downregulated expression of the candidate tumour suppressor gene SASH1 in colon cancer. Br. J. Cancer *95*, 1419-1423.

129. Rohatgi,R., Ma,L., Miki,H., Lopez,M., Kirchhausen,T., Takenawa,T., and Kirschner,M.W. (1999). The interaction between N-WASP and the Arp2/3 complex links Cdc42-dependent signals to actin assembly. Cell *97*, 221-231.

130. Rong,S.B. and Vihinen,M. (2000). Structural basis of Wiskott-Aldrich syndrome causing mutations in the WH1 domain. J. Mol. Med. *78*, 530-537.

131. Rossman,K.L., Der,C.J., and Sondek,J. (2005). GEF means go: turning on RHO GTPases with guanine nucleotide-exchange factors. Nat. Rev. Mol. Cell Biol. *6*, 167-180.

132. Sakata,D., Taniguchi,H., Yasuda,S., Adachi-Morishima,A., Hamazaki,Y., Nakayama,R., Miki,T., Minato,N., and Narumiya,S. (2007). Impaired T lymphocyte trafficking in mice deficient in an actin-nucleating protein, mDia1. J. Exp. Med. *204*, 2031-2038.

133. Schafer,D.A., Jennings,P.B., and Cooper,J.A. (1996). Dynamics of capping protein and actin assembly in vitro: uncapping barbed ends by polyphosphoinositides. J. Cell Biol. *135*, 169-179.

134. Scheikl,T., Reis,B., Pfeffer,K., Holzmann,B., and Beer,S. (2008). Reduced notch activity is associated with an impaired marginal zone B cell development and function in Sly1 mutant mice. Mol. Immunol.

135. Schoenwaelder,S.M. and Burridge,K. (1999). Bidirectional signaling between the cytoskeleton and integrins. Curr. Opin. Cell Biol. *11*, 274-286.

136. Sells,M.A., Knaus,U.G., Bagrodia,S., Ambrose,D.M., Bokoch,G.M., and Chernoff,J. (1997). Human p21-activated kinase (Pak1) regulates actin organization in mammalian cells. Curr. Biol. *7*, 202-210.

137. Small,J.V. and Resch,G.P. (2005). The comings and goings of actin: coupling protrusion and retraction in cell motility. Curr. Opin. Cell Biol. *17*, 517-523.

138. Southern,E.M. (1975). Detection of Specific Sequences Among Dna Fragments Separated by Gel-Electrophoresis. Journal of Molecular Biology *98*, 503-&.

139. Steffen,A., Faix,J., Resch,G.P., Linkner,J., Wehland,J., Small,J.V., Rottner,K., and Stradal,T.E. (2006). Filopodia formation in the absence of functional WAVE- and Arp2/3 complexes. Mol. Biol. Cell *17*, 2581-2591.

140. Steffen,A., Rottner,K., Ehinger,J., Innocenti,M., Scita,G., Wehland,J., and Stradal,T.E. (2004). Sra-1 and Nap1 link Rac to actin assembly driving lamellipodia formation. EMBO J. *23*, 749-759.

141. Suetsugu,S., Yamazaki,D., Kurisu,S., and Takenawa,T. (2003). Differential roles of WAVE1 and WAVE2 in dorsal and peripheral ruffle formation for fibroblast cell migration. Dev. Cell *5*, 595-609.

142. Sugihara,K., Nakatsuji,N., Nakamura,K., Nakao,K., Hashimoto,R., Otani,H., Sakagami,H., Kondo,H., Nozawa,S., Aiba,A., and Katsuki,M. (1998). Rac1 is required for the formation of three germ layers during gastrulation. Oncogene *17*, 3427-3433.

143. Takenawa,T. and Miki,H. (2001). WASP and WAVE family proteins: key molecules for rapid rearrangement of cortical actin filaments and cell movement. J. Cell Sci. *114*, 1801-1809.

144. Takenawa,T. and Suetsugu,S. (2007). The WASP-WAVE protein network: connecting the membrane to the cytoskeleton. Nat. Rev. Mol. Cell Biol. *8*, 37-48.

145. Taniuchi,I., Kitamura,D., Maekawa,Y., Fukuda,T., Kishi,H., and Watanabe,T. (1995). Antigen-receptor induced clonal expansion and deletion of lymphocytes are impaired in mice lacking HS1 protein, a substrate of the antigen-receptor-coupled tyrosine kinases. EMBO J. *14*, 3664-3678.

146. Thomas,K.R. and Capecchi,M.R. (1986). Introduction of homologous DNA sequences into mammalian cells induces mutations in the cognate gene. Nature *324*, 34-38.

147. Thomas,K.R. and Capecchi,M.R. (1987). Site-directed mutagenesis by gene targeting in mouse embryo-derived stem cells. Cell *51*, 503-512.

148. Thomas,K.R., Folger,K.R., and Capecchi,M.R. (1986). High frequency targeting of genes to specific sites in the mammalian genome. Cell *44*, 419-428.

149. Uchida,T., Nakao,A., Nakano,N., Kuramasu,A., Saito,H., Okumura,K., Ra,C., and Ogawa,H. (2001). Identification of Nash1, a novel protein containing a nuclear localization signal, a sterile alpha motif, and an SH3 domain preferentially expressed in mast cells. Biochem. Biophys. Res. Commun. *288*, 137-141.

150. Underhill,D.M. and Goodridge,H.S. (2007). The many faces of ITAMs. Trends Immunol. *28*, 66-73.

151. Uruno,T., Liu,J., Zhang,P., Fan,Y., Egile,C., Li,R., Mueller,S.C., and Zhan,X. (2001). Activation of Arp2/3 complex-mediated actin polymerization by cortactin. Nat. Cell Biol. *3*, 259-266.

152. Uruno,T., Zhang,P., Liu,J., Hao,J.J., and Zhan,X. (2003). Haematopoietic lineage cell-specific protein 1 (HS1) promotes actin-related protein (Arp) 2/3 complex-mediated actin polymerization. Biochem. J. *371*, 485-493.

153. Uyeda,T.Q., Nagasaki,A., and Yumura,S. (2004). Multiple parallelisms in animal cytokinesis. Int. Rev. Cytol. *240*, 377-432.

154. van Rossum,A.G., Moolenaar,W.H., and Schuuring,E. (2006). Cortactin affects cell migration by regulating intercellular adhesion and cell spreading. Exp. Cell Res. *312*, 1658-1670.

155. Varma,R., Campi,G., Yokosuka,T., Saito,T., and Dustin,M.L. (2006). T cell receptor-proximal signals are sustained in peripheral microclusters and terminated in the central supramolecular activation cluster. Immunity. *25*, 117-127.

156. Venter,J.C., Adams,M.D., Myers,E.W., Li,P.W., Mural,R.J., Sutton,G.G., Smith,H.O., Yandell,M., Evans,C.A., Holt,R.A., Gocayne,J.D., Amanatides,P., Ballew,R.M., Huson,D.H., Wortman,J.R., Zhang,Q., Kodira,C.D., Zheng,X.H., Chen,L., Skupski,M., Subramanian,G., Thomas,P.D., Zhang,J., Gabor Miklos,G.L., Nelson,C., Broder,S., Clark,A.G., Nadeau,J., McKusick,V.A., Zinder,N., Levine,A.J., Roberts,R.J., Simon,M., Slayman,C., Hunkapiller,M., Bolanos,R., Delcher,A., Dew,I., Fasulo,D., Flanigan,M., Florea,L., Halpern,A., Hannenhalli,S., Kravitz,S., Levy,S., Mobarry,C., Reinert,K., Remington,K., Abu-Threideh,J., Beasley,E., Biddick,K., Bonazzi,V., Brandon,R., Cargill,M., Chandramouliswaran,I., Charlab,R., Chaturvedi,K., Deng,Z.,

Di,F., V, Dunn,P., Eilbeck,K., Evangelista,C., Gabrielian,A.E., Gan,W., Ge,W., Gong,F., Gu,Z., Guan,P., Heiman,T.J., Higgins,M.E., Ji,R.R., Ke,Z., Ketchum,K.A., Lai,Z., Lei,Y., Li,Z., Li,J., Liang,Y., Lin,X., Lu,F., Merkulov,G.V., Milshina,N., Moore,H.M., Naik,A.K., Narayan,V.A., Neelam,B., Nusskern,D., Rusch,D.B., Salzberg,S., Shao,W., Shue,B., Sun,J., Wang,Z., Wang,A., Wang,X., Wang,J., Wei,M., Wides,R., Xiao,C., Yan,C., Yao,A., Ye,J., Zhan,M., Zhang,W., Zhang,H., Zhao,Q., Zheng,L., Zhong,F., Zhong,W., Zhu,S., Zhao,S., Gilbert,D., Baumhueter,S., Spier,G., Carter,C., Cravchik,A., Woodage,T., Ali,F., An,H., Awe,A., Baldwin,D., Baden,H., Barnstead,M., Barrow,I., Beeson,K., Busam,D., Carver,A., Center,A., Cheng,M.L., Curry,L., Danaher,S., Davenport,L., Desilets,R., Dietz,S., Dodson,K., Doup,L., Ferriera,S., Garg,N., Gluecksmann,A., Hart,B., Haynes,J., Haynes,C., Heiner,C., Hladun,S., Hostin,D., Houck,J., Howland,T., Ibegwam,C., Johnson,J., Kalush,F., Kline,L., Koduru,S., Love,A., Mann,F., May,D., McCawley,S., McIntosh,T., McMullen,I., Moy,M., Moy,L., Murphy,B., Nelson,K., Pfannkoch,C., Pratts,E., Puri,V., Qureshi,H., Reardon,M., Rodriguez,R., Rogers,Y.H., Romblad,D., Ruhfel,B., Scott,R., Sitter,C., Smallwood,M., Stewart,E., Strong,R., Suh,E., Thomas,R., Tint,N.N., Tse,S., Vech,C., Wang,G., Wetter,J., Williams,S., Williams,M., Windsor,S., Winn-Deen,E., Wolfe,K., Zaveri,J., Zaveri,K., Abril,J.F., Guigo,R., Campbell,M.J., Sjolander,K.V., Karlak,B., Kejariwal,A., Mi,H., Lazareva,B., Hatton,T., Narechania,A., Diemer,K., Muruganujan,A., Guo,N., Sato,S., Bafna,V., Istrail,S., Lippert,R., Schwartz,R., Walenz,B., Yooseph,S., Allen,D., Basu,A., Baxendale,J., Blick,L., Caminha,M., Carnes-Stine,J., Caulk,P., Chiang,Y.H., Coyne,M., Dahlke,C., Mays,A., Dombroski,M., Donnelly,M., Ely,D., Esparham,S., Fosler,C., Gire,H., Glanowski,S., Glasser,K., Glodek,A., Gorokhov,M., Graham,K., Gropman,B., Harris,M., Heil,J., Henderson,S., Hoover,J., Jennings,D., Jordan,C., Jordan,J., Kasha,J., Kagan,L., Kraft,C., Levitsky,A., Lewis,M., Liu,X., Lopez,J., Ma,D., Majoros,W., McDaniel,J., Murphy,S., Newman,M., Nguyen,T., Nguyen,N., and Nodell,M. (2001). The sequence of the human genome. Science *291*, 1304-1351.

157. Vicente-Manzanares,M. and Sanchez-Madrid,F. (2004). Role of the cytoskeleton during leukocyte responses. Nat. Rev. Immunol. *4*, 110-122.

158. Vidal,C., Geny,B., Melle,J., Jandrot-Perrus,M., and Fontenay-Roupie,M. (2002). Cdc42/Rac1-dependent activation of the p21-activated kinase (PAK) regulates human platelet lamellipodia spreading: implication of the cortical-actin binding protein cortactin. Blood *100*, 4462-4469.

159. Watanabe,N., Madaule,P., Reid,T., Ishizaki,T., Watanabe,G., Kakizuka,A., Saito,Y., Nakao,K., Jockusch,B.M., and Narumiya,S. (1997). p140mDia, a mammalian homolog of Drosophila diaphanous, is a target protein for Rho small GTPase and is a ligand for profilin. EMBO J. *16*, 3044-3056.

160. Watanabe,T., Noritake,J., and Kaibuchi,K. (2005). Regulation of microtubules in cell migration. Trends Cell Biol. *15*, 76-83.

161. Weaver,A.M. (2008). Cortactin in tumor invasiveness. Cancer Lett. *265*, 157-166.

162. Weaver,A.M., Karginov,A.V., Kinley,A.W., Weed,S.A., Li,Y., Parsons,J.T., and Cooper,J.A. (2001). Cortactin promotes and stabilizes Arp2/3-induced actin filament network formation. Curr. Biol. *11*, 370-374.

163. Weed,S.A., Karginov,A.V., Schafer,D.A., Weaver,A.M., Kinley,A.W., Cooper,J.A., and Parsons,J.T. (2000). Cortactin localization to sites of actin assembly in lamellipodia requires interactions with F-actin and the Arp2/3 complex. J. Cell Biol. *151*, 29-40.

164. Weed,S.A. and Parsons,J.T. (2001). Cortactin: coupling membrane dynamics to cortical actin assembly. Oncogene *20*, 6418-6434.

165. Wegner,A.M., Nebhan,C.A., Hu,L., Majumdar,D., Meier,K.M., Weaver,A.M., and Webb,D.J. (2008). N-wasp and the arp2/3 complex are critical regulators of actin in the development of dendritic spines and synapses. J. Biol. Chem. *283*, 15912-15920.

166. Welch,M.D. and Mullins,R.D. (2002). Cellular control of actin nucleation. Annu. Rev. Cell Dev. Biol. *18*, 247-288.

167. Wienands,J., Larbolette,O., and Reth,M. (1996). Evidence for a preformed transducer complex organized by the B cell antigen receptor. Proc. Natl. Acad. Sci. U. S. A *93*, 7865-7870.

168. Williams,N.S., Gaynor,R.B., Scoggin,S., Verma,U., Gokaslan,T., Simmang,C., Fleming,J., Tavana,D., Frenkel,E., and Becerra,C. (2003). Identification and validation of genes involved in the pathogenesis of colorectal cancer using cDNA microarrays and RNA interference. Clin. Cancer Res. *9*, 931-946.

169. Wu,H., Reynolds,A.B., Kanner,S.B., Vines,R.R., and Parsons,J.T. (1991). Identification and characterization of a novel cytoskeleton-associated pp60src substrate. Mol. Cell Biol. *11*, 5113-5124.

170. Yamada,H., Yanagisawa,K., Tokumaru,S., Taguchi,A., Nimura,Y., Osada,H., Nagino,M., and Takahashi,T. (2008). Detailed characterization of a homozygously deleted region corresponding to a candidate tumor suppressor locus at 21q11-21 in human lung cancer. Genes Chromosomes. Cancer *47*, 810-818.

171. Yamanashi,Y., Fukuda,T., Nishizumi,H., Inazu,T., Higashi,K., Kitamura,D., Ishida,T., Yamamura,H., Watanabe,T., and Yamamoto,T. (1997). Role of tyrosine phosphorylation of HS1 in B cell antigen receptor-mediated apoptosis. J. Exp. Med. *185*, 1387-1392.

172. Yan,C., Martinez-Quiles,N., Eden,S., Shibata,T., Takeshima,F., Shinkura,R., Fujiwara,Y., Bronson,R., Snapper,S.B., Kirschner,M.W., Geha,R., Rosen,F.S., and Alt,F.W. (2003). WAVE2 deficiency reveals distinct roles in embryogenesis and Rac-mediated actin-based motility. EMBO J. *22*, 3602-3612.

173. Yang,C., Czech,L., Gerboth,S., Kojima,S., Scita,G., and Svitkina,T. (2007). Novel roles of formin mDia2 in lamellipodia and filopodia formation in motile cells. PLoS. Biol. *5*, e317.

174. Zeller,C., Hinzmann,B., Seitz,S., Prokoph,H., Burkhard-Goettges,E., Fischer,J., Jandrig,B., Schwarz,L.E., Rosenthal,A., and Scherneck,S. (2003). SASH1: a candidate tumor suppressor gene on chromosome 6q24.3 is downregulated in breast cancer. Oncogene *22*, 2972-2983.

175. Zhang,H., Smolen,G.A., Palmer,R., Christoforou,A., van den,H.S., and Haber,D.A. (2004). SUMO modification is required for in vivo Hox gene regulation by the Caenorhabditis elegans Polycomb group protein SOP-2. Nat. Genet. *36*, 507-511.

176. Zhang,J., Shehabeldin,A., da Cruz,L.A., Butler,J., Somani,A.K., McGavin,M., Kozieradzki,I., dos Santos,A.O., Nagy,A., Grinstein,S., Penninger,J.M., and Siminovitch,K.A. (1999). Antigen receptor-induced activation and cytoskeletal rearrangement are impaired in Wiskott-Aldrich syndrome protein-deficient lymphocytes. J. Exp. Med. *190*, 1329-1342.

177. Zhu,Y.X., Benn,S., Li,Z.H., Wei,E., Masih-Khan,E., Trieu,Y., Bali,M., McGlade,C.J., Claudio,J.O., and Stewart,A.K. (2004). The SH3-SAM adaptor HACS1 is up-regulated in B cell activation signaling cascades. J. Exp. Med. *200*, 737-747.

178. Zigman,W.B. and Lott,I.T. (2007). Alzheimer's disease in Down syndrome: neurobiology and risk. Ment. Retard. Dev. Disabil. Res. Rev. *13*, 237-246.

179. Zufferey,R., Dull,T., Mandel,R.J., Bukovsky,A., Quiroz,D., Naldini,L., and Trono,D. (1998). Self-inactivating lentivirus vector for safe and efficient in vivo gene delivery. Journal of Virology *72*, 9873-9880.

7. Acknowledgments

Herewith I want to thank the many people, who proved indispensable for this thesis to take a happy ending:

First of all, I want to especially thank Dr. Sandra Beer for endowing me with this interesting topic and the constant and excellent supervision she provided. She truly turned a working into a delighting environment.

Furthermore, I want to thank Prof. Klaus Pfeffer, who facilitated all of this work. His enduring generosity and support have always granted the essential space for my ambition and creativity.

I thank Prof. Jens Brüning for being my official supervisor and first evaluator of this thesis.

I want to thank to Prof. Siegfried Roth for representing the head of my thesis committee.

I am thankful to Karin Buchholz for the reliable technical and organisatorial support.

The generation and the maintenance of the different mouse strains were excellently taken care of by Nicole Küpper.

I want to honestly thank all my colleagues in the work groups Beer, Pfeffer and Scheu, who, with their permanent supply of help and diversion, have made working in this institute so pleasurable. This thank also extends to many members of Hartmut Hengels group in the institute for virology. Especially, I want to thank Simone Brandt for the fruitful discussions and cooperative work on SLy2.

Thomas Wunderlich, Linda Koch and André Kleinridders from the Brüning lab introduced me into the BAC recombination technique that later proved so valuable.

Anne Mausberg granted inestimable help by solving technical difficulties and by being a true ally.

I especially want to mention Bernhard Reis, as the work on this thesis would not have been the same without his support and friendship.

Stefanie Scheu proved indispensable for the solution of a plethora of both scientific and mundane issues with her thoughtful and sincere advice. Furthermore, traffic jams have never been more enjoyable.

I want to thank Antje Gohla and Klaus-Peter Janssen for very helpful scientific discussions and constant support with all kinds of reagents and protocols.

I am deeply grateful to my family, Katrin, Kai and Lena v. Holleben, who have always accompanied and supported me along my way.

Finally, I am forever indebted to Neele Leana Vollmar for all her love and encouragement, which carried me the entire way and for catching me everytime I was stumbling.

8. Erklärung

Ich versichere, dass ich die von mir vorgelegte Dissertation selbständig angefertigt, die benutzten Quellen und Hilfsmittel vollständig angegeben und die Stellen der Arbeit - einschliesslich Tabellen, Karten und Abbildungen -, die anderen Werken im Wortlaut oder dem Sinn nach entnommen sind, in jedem Einzelfall als Entlehnung kenntlich gemacht habe; dass diese Dissertation noch keiner anderen Fakultät oder Universität zur Prüfung vorgelegen hat; dass sie – abgesehen von unten angegebenen Teilpublikationen - noch nicht veröffentlicht worden ist sowie, dass ich eine solche Veröffentlichung vor Abschluß des Promotionsverfahrens nicht vornehmen werde. Die Bestimmungen dieser Promotionsordnung sind mir bekannt. Die von mir vorgelegte Dissertation ist von Prof. Dr. Jens C. Brüning und Prof. Dr. Klaus Pfeffer betreut worden.

Köln, Dezember 2008 Max v. Holleben